Psychedelic-Inspired Medium-Throughput Assays for the Development of Next-Generation Neurotherapeutics

By

CALVIN LY

DISSERTATION

Submitted in partial satisfaction of the requirement for the degree of

DOCTOR OF PHILOSOPHY

In

Chemistry

in the

OFFICE OF GRADUATE STUDIES

of the

UNIVERSITY OF CALIFORNIA

DAVIS

Approved:

_____

Dr. David E. Olson, Chair

_____

Dr. Peter A. Beal

_____

Dr. Kit S. Lam

Committee in Charge

2021

Abstract

Major depressive disorder (MDD) affects more than 264 million people worldwide. A wide range of antidepressants are available to treat the disease including, but are not limited to, Prozac™, Elavil™, and Nardil™. Unfortunately, 1 in 3 patients prescribed these traditional antidepressants do not show significant mood improvement in response to the first regimen, and those who do require upwards of 2–4 weeks of treatment before observing any therapeutic effects. This delay of therapeutic onset with currently prescribed medications further highlights the necessity of novel faster-acting antidepressants. Recently, the Food and Drug Administration (FDA) approved esketamine—a ketamine enantiomer with rapid therapeutic effects (hours to days)—for treatment-resistant depression (TRD). It is hypothesized that ketamine produces its therapeutic effects by rectifying the atrophy of neurites, the reduction of the number of dendritic spines, and the loss of synapses in the prefrontal cortex (PFC) observed in postmortem brains of patients who suffered from MDD and rodent models of depression. However, ketamine has serious side effects, including the potential for abuse. Therefore, we are interested in developing, identifying, and optimizing novel chemical scaffolds with unique mechanisms of action that are better tolerated. One series of scaffolds that we are interested in is the classic psychedelics. Recently, the classic psychedelics have undergone a renaissance and have begun to be explored as next-generation therapeutics for the treatment of depression with psilocybin, lysergic acid diethylamide (LSD), and 5-methoxy-N, N-dimethyltryptamine (5-MeO-DMT) leading the way in clinical trials. Thus, we postulate that the scaffolds of the classic psychedelics would prove to be promising targets for next-generation antidepressants.

Here, I discuss efforts to develop next-generation therapeutics starting from classic psychedelics. First, I explored the similarities between ketamine and classic psychedelics with respect to their effects on structural neural plasticity. We categorized molecules that promoted plasticity as psychoplastogens, small molecules that can induce structural changes in the brain. Next, I investigated the mechanism of actions of the classic psychedelics and discovered the importance of tropomyosin receptor kinase B (TrkB), brain-derived neurotrophic factor (BDNF), the mammalian target of rapamycin (mTOR), serotonin 2A (5-HT2A), and α-amino-3-hydroxy-5-methyl-4-isoxazole-propionate (AMPA) receptors in psychoplastogen-induced plasticity. Furthermore, I examined transient stimulation versus chronic stimulation with the psychoplastogens and observed their effects in promoting long-lasting structural plasticity. Finally, to better

facilitate drug discovery of fast-acting antidepressants, I developed two orthogonal assays. First, I established phenotypic assays to examine the efficacy of small molecules in promoting neuritogenesis, spinogenesis, and synaptogenesis. I clustered known fast-acting antidepressants, traditional antidepressants, and non-antidepressant compounds by combining these structural plasticity phenotypes using principal component analysis (PCA). Second, we developed and characterized the first cellular assay to determine the hallucinogenic potential of small molecules using an engineered 5-HT2AR fluorescent biosensor. We identified two novel hallucinogens and several non-hallucinogens through this platform. We then validated their effects in the head-twitch response—a behavioral assay that correlates well with the hallucinogenic potential of small molecules in mice. Lastly, we combined the structural plasticity assays with the 5-HT2AR hallucinogenic potential counter-screen to identify a novel non-hallucinogenic small molecule, AAZ-A-154 (AAZ), with therapeutic potential. We then confirmed these findings using behavioral assays. Overall, this work describes mechanistic studies aimed at understanding the actions of psychedelics, the identification of new potential antidepressants through phenotypic assays, and a novel counter-screen for hallucinogenic potential. These studies will facilitate drug discovery efforts aimed at better-tolerated, fast-acting, next-generation antidepressants.

Acknowledgements

First, I would like to thank my family for their love and immense support through this long journey. Without my parents and younger sister, this journey would have been for nothing. Mom, I am sorry I have been gone for over a decade. I appreciate the food and love that you extend to me. Dad, thank you for teaching me how to stand up and continue to step forward even when it seems like I was not able to make it. Your strength and courage rubs off on me.

Next, I want to thank the Olson Lab and all my peers in the lab. You all are amazing people and it is always great to hear the chats that go on in lab. Lee and Guoliang, my family away from my family. You two are amazing older brothers. I love the spontaneous times we go out to get food or head to the Bay Area midday on a Saturday afternoon. The chats that we all have had, the QEs we all fought through, I greatly appreciate you both sharing your joys and excitement with me.

David E. Olson. There are not many words I can use to describe the amazing and awesome mentor and the father figure you are to me. I am deeply indebted to you for all the support, all the time, and all the excitement you give every day. I know you will keep that energy up the entire time and keep moving forward. You will always be a second father to me.

Department of Chemistry at UC Davis. While I did not get a chance to meet you all, I definitely made amazing connections with the individuals here, regardless of lecturer, graduate student, professor, administrator.

I want to thank my significant other Vicky. I am sorry this has taken so long, and I thank you immensely for being so patient with me while I complete my PhD. I love you and will continue to keep pushing forward as we strive to our next goals.

Finally, for anyone else I have forgotten. Thank you. I extend my thanks to you all.

Calvin Ly

Contents

List of Figures

Abbreviations

SEM = standard error of mean

MDD = major depressive disorder

NMDAR = N-methyl-D-aspartate receptor

FDA = Food and Drug Administration

TRD = treatment-resistant depression

GABA = gamma-aminobutyric acid

AMPAR = α-amino-3-hydroxy-5-methyl-4-isoxazolepropionic acid receptors

BDNF = brain-derived neurotrophic factor

TrkB = tropomyosin receptor kinase B

mTOR = mechanistic target of rapamycin

PFC = prefrontal cortex

NGF = nerve growth factor

dPC-12 = differentiated PC-12

TrkA = tropomyosin receptor kinase A

NeuN = hexaribonucleotide binding protein-3

DCX = doublecortin

SSRI = selective serotonin reuptake inhibitor

RA = retinoic acid

MAP2 = microtubule-associated protein-2

SAP-97 = synaptic associated protein-97

NSE = neuron-specific enolase

TH = tyrosine hydroxylase

DAT = dopamine transporter

D2R = dopamine receptor subtype 2

D3R = dopamine receptor subtype 3

NET = norepinephrine transporter

VMAT = vesicular monoamine transporter

nAChR = acetylcholine receptors

dSH-SY5Y = differentiated SH-SY5Y

E16 = embryonic days 16

E20 = embryonic days 20

DIV = days in vitro

DiI = 1,1'-dioctadecyl-3,3,3',3'-tetramethylindocarbocyanine perchlorate

GFP = green fluorescent protein

RFP = red fluorescent protein

SIM = structure illuminating microscopy

VGLUT1 = vesicular glutamate transporter 1

PSD-95 = postsynaptic density-95

DMSO = dimethyl sulfoxide

5-HT2AR = serotonin 2A receptor

Nmax = maximum number of crossings

AUC = area under the curve

LSD = lysergic acid diethylamide

DOI = 2,5-dimethoxy-4-iodoamphetamine

DMT = N,N-dimethyltryptamine

KET = ketamine

PSI = psilocin

MDMA = 3,4-methylenedioxymethamphetamine

7,8-DHF = 7,8-dihydroxyflavone

D-AMP = d-amphetamine

5HT = serotonin

ng/mL = nanograms per milliliter

pg/mL = picograms per milliliter

mRNA = messenger RNA

ddPCR = droplet digital PCR

ELISA = enzyme-linked immunosorbent assay

μM = micromolar

EC50 = half maximal effective concentration

μm = micrometer

VEH = vehicle

RAPA = rapamycin

DNQX = 6,7-dinitroquinoxaline-2,3-dione

NBQX = 2,3-Dioxo-6-nitro-1,2,3,4-tetrahydrobenzo[f]quinoxaline-7-sulfonamide

5-HT1AR = serotonin 1A receptor

8-OH-DPAT = 7-(dipropylamino)-5,6,7,8-tetrahydronaphthalen-1-ol

KCl = potassium chloride

MTT = 3-(4,5-dimethylthiazol-2-yl)-2,5-diphenyltetrazolium bromide

H_2O_2 = hydrogen peroxide

Glyx-13 = Rapastinel

FAD = fast-acting antidepressants = psychoplastogens

SAD = slow-acting antidepressants = traditional antidepressants

NAD = non-antidepressants

ND = not determined

Ara-C = 1-β-D-arabinofuranosylcytosine = cytosine arabinoside

PCA = principal component analysis

HBSS = Hank’s buffered saline solution

dPBS = Dulbecco's phosphate-buffered saline

HEPES = 4-(2-hydroxyethyl)-1-piperazineethanesulfonic acid

P/S = penicillin-streptomycin

TC = tissue culture

PFA = paraformaldehyde

BSA = bovine serum albumin

FBS = fetal bovine serum

PDL = poly-D-lysine

$MgCl_2$ = magnesium chloride

$CaCl_2$ = calcium chloride

NaCl = sodium chloride

CO_2 = carbon dioxide

GPCR = G-protein coupled receptors

IP3 = inositol trisphosphate

cAMP = cyclic adenosine monophosphate

BRET = bioluminescence resonance energy transfer

FRET = Förster resonance energy transfer

5-MeO-DMT = 5-MeO = 5-methoxy-N,N-dimethyltryptamine

6-MeO-DMT = 6-methoxy-N,N-dimethyltryptamine

HTR = head-twitch response

DD = drug discrimination

LIS = lisuride

BOL-148 = 2-bromo-lysergic acid diethylamide

6-F-DMT = 6-fluoro-N,N-dimethyltryptamine

6-F-DET = 6-fluoro-N,N-diethyltryptamine

5-F-DMT = 5-fluoro-N,N-dimethyltryptamine

5-Cl-DMT= 5-chloro-N,N-dimethyltryptamine

5-Br-DMT= 5-bromo-N,N-dimethyltryptamine

BUFO = bufotenine

N-5-HT = N-methyl-serotonin

TRY = trypamine

NMT = N-methyltryptamine

FST = forced swim test

R-Dimeth-AMPH = R-dimethylamphetamine

S-Dimeth-AMPH = S-dimethylamphetamine

2C-I = 2-(4-Iodo-2,5-dimethoxyphenyl)ethan-1-amine

S-Meth-AMPH = S-methamphetamine

LED = Lee E. Dunlap, notebook pages

AAZ = Arya Azinfar, notebook pages

PCP = phencyclidine

S-MDDMA = S-3,4-Methylenedioxy-N, N-dimethylamphetamine

R-MDDMA = R-3,4-Methylenedioxy-N, N-dimethylamphetamine

3-IAA = indole-3-acetic acid

S-MDA = S-3,4-Methylenedioxyamphetamine

R-MDA = R-3,4-Methylenedioxyamphetamine

cpGFP = circularly permuted green fluorescent protein

IL3 = third intracellular loop

HEK293T = human embryonic kidney 293T

SERT = serotonin transporter

ER = endoplasmic reticulum

HCl = hydrochloric acid

NaOH = sodium hydroxide

MDL = MDL 100,907 = volinanserin

KTSN = KETSN = ketanserin

Cmpd = compound

Emax = maximal response

GTPγS binding = GTPγS, guanosine 5'-O-[gamma-thio]triphosphate

PI = phosphatidylinositol

Ca^{2+} = calcium ion

AAV = adeno-associated viruses

ΔF/F = change in fluorescence over baseline fluorescence

mPFC = media prefrontal cortex

ANOVA = analysis of variance

Chapter 1

Chapter 1.1 Introduction

Major depressive disorder (MDD) affects more than 264 million people worldwide.[1] Long-lasting depression with moderate to severe intensity may progress into a serious health condition and at its worse, suicide. In 2019, 47,511 deaths in the United States were attributable to suicide despite the wide range of antidepressants available.[2] Furthermore, at least 1 in 3 patients do not show significant mood improvement in response to the first antidepressant regimen and those who do require upwards of 2–4 weeks of treatment prior to therapeutic effects.[3,4] This delay of therapeutic onset with currently available medications further highlights the necessity of novel fast-acting antidepressants with more efficacious antidepressant potential.[4]

One molecule that has garnered attention as a potent neurotherapeutic is ketamine, an N-methyl-D-aspartate receptor (NMDAR) antagonist. Ketamine **(Fig. 1.1)** has been approved by the Food and Drug Administration (FDA) for use in patients with treatment-resistant depression (TRD). A single infusion of ketamine, via low sub-anesthetic doses, in patients with MDD and/or TRD produces rapid antidepressant effects within hours.[5] Preclinical data suggest the mechanism of action of ketamine involves enhanced release of glutamate through the inhibition of NMDARs on gamma-aminobutyric acid (GABA)-ergic interneurons. The increase in glutamate results in the activation of glutamatergic pyramidal neurons.[6] Next, glutamate release is known to activate α-amino-3-hydroxy-5-methyl-4-isoxazolepropionic acid receptors (AMPARs), which when activated, lead to the synthesis and release brain-derived neurotrophic factor (BDNF).[7] BDNF then drives protein synthesis and growth of dendrites and the soma of pyramidal neurons through the phosphorylation of tropomyosin receptor kinase B (TrkB). Finally, TrkB phosphorylation leads

1. GBD 2017 Disease and Injury Incidence and Prevalence Collaborators. Global, regional, and national incidence, prevalence, and years lived with disability for 354 diseases and injuries for 195 countries and territories, 1990–2017: a systematic analysis for the Global Burden of Disease Study 2017. *Lancet* **2018**, *392*, 1789–1858.
2. Centers for Disease Control and Prevention 2021.
3. Kessler, R.C.; Berglund, P.; Demler, O.; Jin, R.; Koretz, D.; Merikangas, K.R.; Rush, A.J.; Walters, E.E.; Wang, P.S. The epidemiology of major depressive disorder: Results from the national comorbidity Survey Replication (NCS-R). *JAMA*, **2003**, *289*, 3095–3105.
4. Rush, A.J.; Trivedi, M.H.; Wisniewski, S.R.; Nierenberg, A.A.; Stewart, J.W.; Warden, D.; Niederehe, G.; Thase, M.E.; Lavori, P.W.; Lebowitz, B.D.; McGrath, P.J.; Rosenbaum, J.F.; Sackeim, H.A.; Kupfer, D.J.; Luther, J.; Fava, M. Acute and longer-term outcomes in depressed outpatients requiring one or several treatment steps: a STAR*D report. *Am. J. Psychiatry*, **2006**, *163*, 1905–1917.
5. Zarate, C.A. Jr; Singh, J.B.; Carlson, P.J.; Brutsche, N.E.; Ameli, R.; Luckenbaugh, D.A.; Charney, D.S.; Manji, H.K. A randomized trial of an N-methyl-D-aspartate antagonist in treatment-resistant major depression. *Arch. Gen. Psychiatry*. **2006**, *63*, 856–864.
6. Duman, R.S.; Aghajanian, G.K.; Sanacora, G.; Krystal, J.H. Synaptic plasticity and depression: new insights from stress and rapid-acting antidepressants. *Nat Med.*, **2016**, *22*, 238–249.
7. Autry, A.E.; Adachi, M.; Nosyreva, E.; Na, E.S.; Los, M.F.; Cheng, P.F.; Kavalali, E.T.; Monteggia, L.M. NMDA receptor blockade at rest triggers rapid behavioural antidepressant responses. *Nature* **2011**, *475*, 91–95.

downstream to the activation of the mechanistic target of rapamycin (mTOR) pathways and ultimately, the therapeutic response. Unfortunately, ketamine's clinical success is mired by its acute psychotomimetic and dissociative side effects, as well as its potential for abuse.[8] Therefore, efforts into identifying better-tolerated, fast-acting antidepressants with similar efficacy to ketamine without the side effects would assist in treating patients suffering from depression.

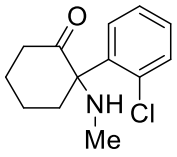

Ketamine

Figure. 1.1. Structure of ketamine.

To facilitate drug discovery campaigns of novel therapeutics, primary assays are necessary. Generally, drug discovery campaigns often approach therapeutic screens through the molecular medicine approach. This approach starts with the disease, identifies its cause, and determines how this cause is affecting the pathophysiological precipitation of the disease through basic research. Ultimately, this results in an approach that identifies a mechanistically inspired molecular target. Furthermore, through the optimization of lead molecules and previously established disease mechanisms based on target engagement, "me too" compounds, or small molecules that have similar pharmacological mechanisms of actions accompanied by fewer side effects, are prioritized.[9] To further complicate the drug discovery pipeline, the pharmacological targets associated with depression are tangled within a complex network of circuits, biochemical pathways, and structural plasticity involving multiple regions in the brain.[10] This highlights that specifically targeting pathways of interest may not identify novel mechanisms of action for next generation therapeutics. However, accumulating evidence in rodent studies have indicated the

8. Abdallah, C.G.; Sanacora, G.; Duman, R.S.; Krystal, J.H. Ketamine and rapid-acting antidepressants: a window into a new neurobiology for mood disorder therapeutics. *Annu Rev Med*. **2015**, *66*, 509–523.
9. (a) Rizzo, S.J.; Edgerton, J.R.; Hughes, Z.A.; Brandon, N.J. Future viable models of psychiatry drug discovery in pharma. *J Biomol Screen*. **2013**, *18*, 509–521.
(b) Gagny, J. J.; Choudhry, N. K. How Many "Me-Too" Drugs Is Too Many? *JAMA* **2011**, *305*, 711–712.
(c) Schwartz, T. L. Metabolites: Novel Therapeutics or "Me-Too" Drugs? Using Desvenlafaxine as an Example. *CNS Spectrums* **2012**, *17*, 103–106.
(d) Sopko, M. A.; Ehret, M. J.; Grgas, M. Desvenlafaxine: Another "Me Too" Drug? *Ann. Pharmacother.* **2008**, *42*, 1439–1446.
10. Dale, E.; Bang-Andersen, B.; Sánchez, C. Emerging mechanisms and treatments for depression beyond SSRIs and SNRIs. *Biochem Pharmacol*. **2015,** *95*, 81–97.

persistent antidepressant effects, such as those produced by ketamine, may lie in their ability to increase the growth of neurites, the number of dendritic spines, and synaptic density in the prefrontal cortex (PFC).[11] Thus, a phenotypic drug discovery approach for antidepressants that measures positive, neutral, and negative outcomes of small molecule treatment (growth, no growth, and retraction, respectively) would increase the likelihood of a therapeutic lead.

Recently, converging data –through human imaging, postmortem studies, and animal models– have pointed to atrophy of neuronal structures in the PFC and hippocampus in chronically depressed patients and rodent models associated to chronic stress.[12] These structural losses, such as the retraction of neurites, loss of dendritic spines, and elimination of synapses are hypothesized to be counteracted by small molecules with the potential to promote structural and functional neural plasticity to rectify the

11. (a) Liu, R.J.; Duman, C.; Kato, T.; Hare, B.; Lopresto, D.; Bang, E.; Burgdorf, J.; Moskal, J.; Taylor, J.; Aghajanian, G.; Duman, R.S. GLYX-13 Produces Rapid Antidepressant Responses with Key Synaptic and Behavioral Effects Distinct from Ketamine. *Neuropsychopharmacology*. **2017**, *42*, 1231–1242.
(b) Castrén, E.; Antila, H. Neuronal plasticity and neurotrophic factors in drug responses. *Mol Psychiatry*, **2017**, *22*, 1085–1095.
(c) Duman, R.S.; Aghajanian, G.K.; Sanacora, G.; Krystal, J.H. Synaptic plasticity and depression: New insights from stress and rapid-acting antidepressants *Nat Med*, **2016**, *22*, 238–249.
(d) Chen, J.L.; Lin, W.C.; Cha, J.W.; So, P.T.; Kubota, Y.; Nedivi, E. Structural basis for the role of inhibition in facilitating adult brain plasticity. *Nat Neurosci* **2011**, *14*, 587–594.
(e) Karpova, N.N.; Pickenhagen, A.; Lindholm, J.; Tiraboschi, E.; Kulesskaya, N.; Agústsdóttir, A.; Antila, H.; Popova, D.; Akamine, Y.; Bahi, A.; Sullivan, R.; Hen, R.; Drew, L.J.; Castrén, E. Fear erasure in mice requires synergy between antidepressant drugs and extinction training. *Science* **2011**, *334*, 1731–1734.
(f) Li, N.; Lee, B.; Liu, R.J.; Banasr, M.; Dwyer, J.M.; Iwata, M.; Li, X.Y.; Aghajanian, G.; Duman, R.S. mTOR-dependent synapse formation underlies the rapid antidepressant effects of NMDA antagonists. *Science* **2010**, *329*, 959–964.
(f) Maya Vetencourt, J.F.; Sale, A.; Viegi, A.; Baroncelli, L.; De Pasquale, R.; O'Leary, O.F.; Castrén, E.; Maffei, L. The antidepressant fluoxetine restores plasticity in the adult visual cortex. *Science* **2008**, *320*, 385–388.
12. (a) Liu R.J.; Aghajanian, G.K. Stress blunts serotonin- and hypocretin evoked EPSCs in prefrontal cortex: Role of corticosterone-mediated apical dendritic atrophy. *Proc. Natl. Acad. Sci. USA.* **2008**, *105*, 359–364.
(b) Rajkowska, G.; Miguel-Hidalgo, J.J.; Wei, J.; Dilley, G.; Pittman, S.D.; Meltzer, H.Y.; Overholser, J.C.; Roth, B.L.; Stockmeier, C.A. Morphometric evidence for neuronal and glial prefrontal cell pathology in major depression. *Biol Psychiatry* **1999**, *45*, 1085–1098.
(c) Liston, C.; Miller, M.M.; Goldwater, D.S.; Radley, J.J.; Rocher, A.B.; Hof, P.R.; Morrison, J.H.; McEwen, B.S. Stress-induced alterations in prefrontal cortical dendritic morphology predict selective impairments in perceptual attentional set-shifting. *J Neurosci.* **2006**, *26*, 7870–7874.
(d) Radley, J.J.; Rocher, A.B.; Janssen, W.G.; Hof, P.R.; McEwen, B.S.; Morrison, J.H. Reversibility of apical dendritic retraction in the rat medial prefrontal cortex following repeated stress. *Exp Neurol.* **2005**, *196*, 199–203.
(e) Goldwater, D.S.; Pavlides, C.; Hunter, R.G.; Bloss, E.B.; Hof, P.R.; McEwen, B.S.; Morrison, J.H. Structural and functional alterations to rat medial prefrontal cortex following chronic restraint stress and recovery. *Neuroscience*. **2009**, *164*, 798–808.
(f) Radley, J.J.; Rocher, A.B.; Miller, M.; Janssen, W.G.; Liston, C.; Hof, P.R.; McEwen, B.S.; Morrison, J.H. Repeated stress induces dendritic spine loss in the rat medial prefrontal cortex. *Cereb Cortex*. **2006**, *16*, 313–320.
(g) Radley, J.J.; Rocher, A.B.; Rodriguez, A.; Ehlenberger, D.B.; Dammann, M.; McEwen, B.S.; Morrison, J.H.; Wearne, S.L.; Hof, P.R. Repeated stress alters dendritic spine morphology in the rat medial prefrontal cortex. *J Comp Neurol.* **2008**, *507*, 1141–1150.
(h) Sheline, Y.I.; Wang, P.W.; Gado, M.H.; Csernansky, J.G.; Vannier, M.W. Hippocampal atrophy in recurrent major depression. *Proc Natl Acad Sci U S A*. **1996**, 93, 3908–3913.
(i) Videbech, P.; Ravnkilde, B. Hippocampal volume and depression: A meta-analysis of MRI studies. *Am. J. Psychiatry* **2004**, *161*, 1957–1966.
(j) Bremner, J.D.; Vythilingam, M.; Vermetten, E.; Nazeer, A.; Adil, J.; Khan, S.; Staib, L.H.; Charney, D.S. Reduced volume of orbitofrontal cortex in major depression. *Biol Psychiatry.* **2002**, *51*, 273–279.
(k) Drevets, W.C.; Price, J.L.; Simpson, J.R. Jr; Todd, R.D.; Reich, T.; Vannier, M.; Raichle, M.E. Subgenual prefrontal cortex abnormalities in mood disorders. *Nature* **1997**, *386*, 824–827.
(l) Rajkowska, G.; Miguel-Hidalgo, J.J.; Wei, J.; Dilley, G.; Pittman, S.D.; Meltzer, H.Y.; Overholser, J.C.; Roth, B.L.; Stockmeier, C.A. Morphometric evidence for neuronal and glial prefrontal cell pathology in major depression. *Biol Psychiatry* **1999**, *45*, 1085–1098.

deficits.[13] As ketamine, and most other antidepressants, promotes the growth of neurites, dendritic spine numbers, and synaptic density, primary assays should evaluate these phenotypes as they are rapidly quantifiable markers for antidepressant potential.[11] This chapter will discuss current models of in vitro primary assays to assess the antidepressant potential of small molecules using neurite outgrowth, dendritic spine numbers, and/or synaptic density in various cell models.

13. (a) Castrén, E.; Antila, H. Neuronal plasticity and neurotrophic factors in drug responses. *Mol. Psychiatry*. **2017**, *22*, 1085–1095.
(b) Cramer, S.C.; Sur, M.; Dobkin, B.H.; O'Brien, C.; Sanger, T.D.; Trojanowski, J.Q.; Rumsey, J.M.; Hicks, R.; Cameron, J.; Chen, D.; Chen, W.G.; Cohen, L.G.; deCharms, C; Duffy, C.J.; Eden, G.F.; Fetz, E.E.; Filart, R.; Freund, M.; Grant, S.J.; Haber, S.; Kalivas, P.W.; Kolb, B.; Kramer, A.F.; Lynch, M.; Mayberg, H.S.; McQuillen, P.S.; Nitkin, R.; Pascual-Leone, A.; Reuter-Lorenz, P.; Schiff, N.; Sharma, A.; Shekim, L.; Stryker, M.; Sullivan, E.V.; Vinogradov, S. Harnessing neuroplasticity for clinical applications. *Brain*. **2011**, *134*, 1591–1609.
(c) Mathew, S.J.; Manji, H.K.; Charney, D.S. Novel drugs and therapeutic targets for severe mood disorders. *Neuropsychopharmacology*., **2008**, *33*, 2080–2092.
(d) Kolb, B.; Muhammad, A. Harnessing the power of neuroplasticity for intervention. *Front. Hum. Neurosci*., **2014**, *8*, 377.
(e) Hayley, S.; Litteljohn, D. Neuroplasticity and the next wave of antidepressant strategies. *Front. Cell Neurosci.*, **2013**, *7*, 218.
(f) Krystal, J.H.; Tolin, D.F.; Sanacora, G.; Castner, S.A.; Williams, G.V.; Aikins, D.E.; Hoffman, R.E.; D'Souza, D.C. Neuroplasticity as a target for the pharmacotherapy of anxiety disorders, mood disorders, and schizophrenia. *Drug Discov Today*. **2009**, 14, 690–697.
(g) Duman, R.S. Synaptic plasticity and mood disorders. *Mol. Psychiatry*, **2002**, *7*, S29–S34.

Chapter 1.2 PC-12 Cells and Structural Plasticity

PC-12 cells are derived from a pheochromocytoma of the rat adrenal medulla.[14] These cells generally are small, irregularly shaped, and cluster as floating cultures. PC-12 cells can be the preferred model to use for drug discovery due to the simplicity of the culturing, regeneration of cells through passages, and robust reproducibility. Once adhered, media containing nerve growth factor (NGF) can be added to induce differentiation to nonmitotic, neuronal-like cells. After 48 hours, neurite outgrowth will be apparent, and media containing NGF is replaced every 48 hours to maintain the cultures. Interestingly, there are two PC-12 lines, the original and the PC-12 Adh. The PC-12 Adh cell line is an adherent cell line. One study by Wiatrak, et al. compared the original PC-12 cell line to the PC-12 Adh cell line and found that PC-12 cells after differentiation had neurite outgrowth whereas the PC-12 Adh did not have as robust neurite growth.[15] Thus, moving forward, we will explore the original PC-12 cell line and its subclonal line associated with neurite outgrowth.

Differentiated PC-12 (dPC-12) cells express tropomyosin receptor kinase A (TrkA, the endogenous receptor of NGF) and neuronal biomarkers, such as hexaribonucleotide binding protein-3 (NeuN, a neuronal biomarker), doublecortin (DCX, a microtubule-associated protein), and synapsin I (a presynaptic marker for synapses).[15c] Neurites can be imaged using light microscopy, staining for βIII-tubulin,[16] or staining with a "Neurite Outgrowth Staining Kit."[17] The quantification of neurites are completed on existing software, such as ZEN software (Zeiss),[18] Cellomics ArrayScan V^{TI} HCS Reader,[16] visually via light microscopy using

14. Greene, L. A.; Tischler, A. S. Establishment of a noradrenergic clonal line of rat adrenal pheochromocytoma cells which respond to nerve growth factor. *Proc Natl Acad Sci U S A*. **1976**, *73*, 2424–2428.
15. (a) ATCC PC-12 Adh (ATCC CRL-1721.1) [(accessed on 4 April 2021)]; Available online: https://www.atcc.org/products/all/CRL-1721.1.aspx.
(b) ATCC PC-12 (ATCC CRL-1721) [(accessed on 4 April 2021)]; Available online: https://www.atcc.org/products/all/CRL-1721.aspx.
(c) Wiatrak, B.; Kubis-Kubiak, A.; Piwowar, A.; Barg, E. PC12 Cell Line: Cell Types, Coating of Culture Vessels, Differentiation and Other Culture Conditions. *Cells*. **2020**, *9*, 958.
16. Harrill, J.A.; Mundy, W.R. Quantitative assessment of neurite outgrowth in PC12 cells. *Methods Mol Biol*. **2011**, 758, 331–348.
17. The neurite outgrowth staining kit is a ThermoFisher Product (A15001). It is specifically for PC-12 related neurite outgrowth staining.
18. (a) Sierra-Fonseca, J.A.; Najera, O.; Martinez-Jurado, J.; Walker, E.M.; Varela-Ramirez, A.; Khan, A.M.; Miranda, M.; Lamango, N.S.; Roychowdhury, S. Nerve growth factor induces neurite outgrowth of PC12 cells by promoting Gβγ-microtubule interaction. *BMC Res Notes*. **2014**, *7*, 840.

ImageJ,[15c,19] BD AttoVision™,[20] and HCS Studio™ Cell Analysis Software.[21] The quantification consists of evaluating length of neurites, density of neurites, and neurite outgrowth overall. Similar to neuronal cultures, PC-12 cells are plated at a low density to prevent crossover of neurites following NGF-induced differentiation to improve the analysis of identifying from which somas the neurites originate. Taken all together, PC-12 cells have many properties of neuronal-like cultures following differentiation.

As a model of antidepressant potential, some FDA approved drugs, such as ketamine, imipramine (a selective serotonin reuptake inhibitor, SSRI), and amitriptyline (a tricyclic antidepressant), have been shown to induce neurite outgrowth in dPC-12 cells.[22] Prior to differentiation, it is unclear whether PC-12 cells express TrkB in small quantities[23] or not at all.[24] Furthermore, it is NGF, and not BDNF, that induces differentiation in PC-12 cells to neuronal-like cells. However, BDNF is secreted following stimulation in dPC-12 cells even though following differentiation there is little TrkB available.[25] To facilitate TrkB related experiments in PC-12 cells, a TrkB/PC-12 stable line was generated, to explore the effects of TrkB-induced neurite outgrowth and are differentiable via NGF and BDNF.[26] Moreover, the morphology of BDNF-induced neurite outgrowth in the TrkB/PC-12 cell line produces longer and thicker neurites with larger and flatter somas as compared to NGF-induced neurite outgrowth. This would suggest that the TrkB/PC-12 stable line would serve as a model to identify small molecules that induce TrkA and TrkB growth. Lastly, a commercially available PC-12 cell line called Neuroscreen-1 is a subclonal line of the PC-12 cell line and

19. Tian, X.; Yue, R.; Zeng, H.; Li, H.; Shan, L.; He, W.; Shen, Y.; Zhang, W. Distinctive effect on nerve growth factor-induced PC12 cell neurite outgrowth by two unique neolignan enantiomers from Illicium merrillianum. *Sci Rep*. **2015**, *5*, 16982.
20. Yeyeodu, S.T.; Witherspoon, S.M.; Gilyazova, N.; Ibeanu, G.C. A rapid, inexpensive high throughput screen method for neurite outgrowth. *Curr Chem Genomics.* **2010**, *4*, 74–83.
21. Pokharel, S.; Lee, C.H.; Gilyazova, N.; Ibeanu, G.C. Analysis of Gene Expression and Neuronal Phenotype in Neuroscreen-1 (NS-1) Cells. *Int J Biomed Investig.* **2018**, *1*, 115.
22. (a) Robson, M.J.; Elliott, M.; Seminerio, M.J.; Matsumoto, R.R. Evaluation of sigma (σ) receptors in the antidepressant-like effects of ketamine in vitro and in vivo. *Eur Neuropsychopharmacol.* **2012**, *22*, 308–317.
(b) Jang, S.W.; Liu, X.; Chan, C.B.; Weinshenker, D.; Hall, R.A.; Xiao, G.; Ye, K. Amitriptyline is a TrkA and TrkB receptor agonist that promotes TrkA/TrkB heterodimerization and has potent neurotrophic activity. *Chem Biol.* **2009**, 16, 644–656.
(c) Matsushima, Y.; Terada, K.; Takata, J.; Karube, Y.; Kamei, C.; Sugimoto, Y. Effects of fluvoxamine on nerve growth factor-induced neurite outgrowth inhibition by dexamethasone in PC12 cells. *Biosci Biotechnol Biochem.* **2019**, *83*, 659–665.
23. Ogura, Y.; Sato, K.; Kawashima, K.; Kobayashi, N.; Imura, S.; Fujino, K.; Kawaguchi, H.; Nedachi, T. Subtoxic levels of hydrogen peroxide induce brain-derived neurotrophic factor expression to protect PC12 cells. BMC research notes, 2014, 7, 840. https://doi.org/10.1186/1756-0500-7-840
24. Shih, C.H.; Chen, C.J.; Chen, L. New function of the adaptor protein SH2B1 in brain-derived neurotrophic factor-induced neurite outgrowth. *PLoS One.* **2013**, *8*, e79619.
25. Wang, H.; Yuan, G.; Prabhakar, N.R.; Boswell, M.; Katz, D.M. Secretion of brain-derived neurotrophic factor from PC12 cells in response to oxidative stress requires autocrine dopamine signaling. *J Neurochem.* **2006**, *96*, 694–705.
26. To my knowledge, this line is not commercially available.
Iwasaki, Y.; Ishikawa, M.; Okada, N.; Koizumi, S. Induction of a distinct morphology and signal transduction in TrkB/PC12 cells by nerve growth factor and brain-derived neurotrophic factor. *J Neurochem.* **1997**, *68*, 927–934.

is advertised specifically for neurite outgrowth quantification.[27,28] While searching for published work using the Neuroscreen-1, there were no examples of Neuroscreen-1 cells used as a primary drug discovery campaign screen. However, there are examples of the potential for Neuroscreen-1 cells as an assay for neurite outgrowth[29] and whether antidepressants promote neurite outgrowth is to be determined.

Following differentiation, dPC-12 cells become dopaminergic and are capable of releasing dopamine following excitation.[30] While these cells have the potential to be a model for neurite outgrowth and mechanistic studies of monoamine release and vesicle-cell membrane fusion, dPC-12 cells cannot form synapses within dPC-12 cells as they do not express postsynaptic proteins. Interestingly, mouse primary hippocampal cultures mixed with dPC-12 cells will form synapses together.[31] Perhaps a mixed culture of dPC-12 and hippocampal cells can be used to reduce the number of animals required to conduct drug discovery screens in neurons. Further studies are required to determine whether dPC-12 cells can be exploited for a rapid, multiplexing assay to screen for neurite outgrowth, the number of dendritic spines, and synaptic density changes. Taken together, while dPC-12 cells have similar phenotypic changes following drug and protein treatments, the cell line has its limitation (no dendritic spines and synapses) and more evidence needs to be provided to determine whether dPC-12 cells are a good model for the screening of antidepressants.

27. Cellomics® Neuroscreen™-1 Cells (ThermoFisher R04-0001-AP) [(accessed on 4 April 2021)]; Available online: https://static.thermoscientific.com/images/D21372~.pdf
28. Pokharel, S.; Lee, C.H.; Gilyazova, N.; Ibeanu, G.C. Analysis of Gene Expression and Neuronal Phenotype in Neuroscreen-1 (NS-1) Cells. *Int J Biomed Investig*. **2018**, *1*, 115.
29. (a) Nichols, A. High content screening as a screening tool in drug discovery. *Methods Mol Biol*. **2007**, 356, 379–387.
(b) Hancock, M.K.; Kopp, L.; Kaur, N.; Hanson, B.J. A facile method for simultaneously measuring neuronal cell viability and neurite outgrowth. *Curr Chem Genom Transl Med*. **2015**, *9*, 6–16.
30. Westerink, R. H. S.; Ewing, A. G. The PC12 cell as model for neurosecretion: PC12 cells as model for neurosecretion. *Acta Physiologica.* **2007**, *192*, 273–285.
31. Bieberich, E.; Anthony, G.E. Neuronal differentiation and synapse formation of PC12 and embryonic stem cells on interdigitated microelectrode arrays: contact structures for neuron-to-electrode signal transmission (NEST). *Biosens Bioelectron.* **2004**, *19*, 923–931.

Chapter 1.3 SH-SY5Y Cells and Structural Plasticity

SH-SY5Y cells are derived from a bone marrow biopsy from a female patient with neuroblastoma.[32] These cells are mixed adherent and floating cells and are a thrice cloned subline originating from the SK-N-SH cell line. Like PC-12 cells, these cells have potential as models for drug discovery due to the simplicity of culturing, regeneration of cells, and robust reproducibility. SH-SY5Y cells can be cultured as an adherent, floating, or mixed cell culture.[33] SH-SY5Y cells that adhere are differentiated using media containing retinoic acid (RA), phorbol esters, or a combination of NGF/BDNF with RA to become neuronal-like cells that grow neurites.[34]

Undifferentiated SH-SY5Y cells resemble immature catecholaminergic neurons.[35] They begin expressing neuronal markers such as microtubule-associated protein-2 (MAP2), synaptophysin, NeuN, synaptic associated protein-97 (SAP-97), and neuron-specific enolase (NSE) following differentiation.[36] Both undifferentiated and differentiated SH-SY5Y cells express dopaminergic neuronal markers, such as tyrosine hydroxylase (TH), dopamine transporter (DAT), dopamine receptor subtypes 2 and 3 (D2R and D3R), and TrkB.[37] Furthermore, undifferentiated SH-SY5Y cells express dopamine-β-hydroxylase, norepinephrine transporter (NET), vesicular monoamine transporter (VMAT), and ligand-gated ion channel

32. ATCC SH-SY5Y (ATCC CRL-2266) [(accessed on 4 April 2021)]; Available online: https://www.atcc.org/products/all/CRL-2266.aspx.
33. In the Olson lab, we currently have SH-SY5Y cells that are primarily adherent cells. When I cultured them, I removed all the floating cells as it was difficult to differentiate between cells that were alive versus cells that were dead. To facilitate healthier cultures, I decided to move with purely adherent cultures.
34. Shipley, M.M.; Mangold, C.A.; Szpara, M.L. Differentiation of the SH-SY5Y Human Neuroblastoma Cell Line. *J Vis Exp.* **2016**, 108, 53193.
35. Kovalevich, J.; Langford, D. Considerations for the use of SH-SY5Y neuroblastoma cells in neurobiology. *Methods Mol Biol*. **2013**, *1078*, 9–21.
36. (a) Lopes, F.M.; Schroder, R.; da Frota, M.L. Jr.; Zanotto-Filho, A.; Muller, C.B.; Pires, A.S.; Meurer, R.T.; Colpo, G.D.; Gelain, D.P.; Kapczinski, F.; Moreira, J.C.; Fernandes Mda, C.; Klamt, F. Comparison between proliferative and neuron-like SH-SY5Y cells as an in vitro model for Parkinson disease studies. *Brain Res*. **2010**, *1337*, 85–94.
(b) Cheung, Y.T.; Lau, W.K.; Yu, M.S.; Lai, C.S.; Yeung, S.C.; So, K.F.; Chang, R.C. Effects of all-trans-retinoic acid on human SH-SY5Y neuroblastoma as in vitro model in neurotoxicity research. *Neurotoxicology*. **2009**, *30*, 127–135.
37. (a) Arun, P.; Madhavarao, C.N.; Moffett, J.R.; Namboodiri, A.M. Antipsychotic drugs increase N-acetylaspartate and N-acetylaspartylglutamate in SH-SY5Y human neuroblastoma cells. *J Neurochem.* **2008**, *106*, 1669–1680.
(b) Presgraves, S.P.; Ahmed, T.; Borwege, S.; Joyce, J.N. Terminally differentiated SH-SY5Y cells provide a model system for studying neuroprotective effects of dopamine agonists. *Neurotox Res*. **2004**, *5*, 579–598.
(c) Edsjö, A.; Lavenius, E.; Nilsson, H.; Hoehner, J.C.; Simonsson, P.; Culp, L.A.; Martinsson, T.; Larsson, C.; Påhlman, S. Expression of trkB in human neuroblastoma in relation to MYCN expression and retinoic acid treatment. *Lab Invest.* **2003**, *83*, 813–823.

nicotinic acetylcholine receptors (nAChR).[38] The expression of these receptors makes SH-SY5Y cells a very attractive cell line to study Parkinson's disease, Alzheimer's disease, and addiction.[39]

Stimulation of differentiated SH-SY5Y (dSH-SY5Y) cells induce neurite outgrowth. Previously, we discussed a hallmark of depression is the atrophy of neurites, and antidepressants have been hypothesized to rectify these deficits. Thus, following differentiation via RA, dSH-SY5Y cells as a phenotypic cell line for the quantification of neurite outgrowth may prove to be a practical model to screen for antidepressant potential in novel molecules.[35] There are a limited number of studies exploring small molecules that induced neurite outgrowth in neuronal cultures that replicate in dSH-SY5Y cells. One known molecule is bucladesine (dibutyryl cyclic AMP, dbcAMP), a cyclic nucleotide derivative that mimics cAMP, facilitate neurite outgrowth in both SH-SY5Y cells[40] and cortical cultures.[41] Unfortunately, dbcAMP, BDNF, and RA are one of the few ligands known to induce neurite outgrowth in dSH-SY5Y cells. Known antidepressants, such as ketamine, have not been tested in dSH-SY5Y cells. Further studies exploring how ketamine may affect neurite outgrowth in dSH-SY5Y cells may enhance our understanding for this cell line as a model of antidepressant potential. Generally, many of these authors quantify neurite outgrowth in dSH-SY5Y cells using brightfield images imaging on widefield brightfield microscopes[42] or whole cell staining with MAP2 or F-actin imaged on a confocal microscope.[43] Analysis following image acquisition relies on Metamorph software[42a] or

38. Gould, J.; Reeve, H.L.; Vaughan, P.F.; Peers, C. Nicotinic acetylcholine receptors in human neuroblastoma (SH-SY5Y) cells. *Neurosci Lett*. **1992**, *145*, 201–204.
39. (a) He, D.Y.; Ron, D. Glial cell line-derived neurotrophic factor reverses ethanol-mediated increases in tyrosine hydroxylase immunoreactivity via altering the activity of heat shock protein 90. *J Biol Chem.* **2008**, *283*, 12811–12818.
(b) Xicoy, H.; Wieringa, B.; Martens, G.J. The SH-SY5Y cell line in Parkinson's disease research: a systematic review. *Mol Neurodegener*. **2017**, *12*, 10.
(c) Greene, A.N.; Parks, L.G.; Solomon, M.B.; Privette Vinnedge, L.M. Loss of DEK Expression Induces Alzheimer's Disease Phenotypes in Differentiated SH-SY5Y Cells. *Front Mol Neurosci.* **2020**, *13*, 594319.
40. Kume, T.; Kawato, Y.; Osakada, F.; Izumi, Y.; Katsuki, H.; Nakagawa, T.; Kaneko, S.; Niidome, T.; Takada-Takatori, Y.; Akaike, A. Dibutyryl cyclic AMP induces differentiation of human neuroblastoma SH-SY5Y cells into a noradrenergic phenotype. *Neurosci Lett.* **2008**, *443*, 199–203.
41. Li, P.; Matsunaga, K.; Yamakuni, T.; Ohizumi, Y. Nardosinone, the first enhancer of neurite outgrowth-promoting activity of staurosporine and dibutyryl cyclic AMP in PC12D cells. *Brain Res Dev Brain Res*. **2003,** *145*, 177–183.
42. Unfortunately, in all the references I listed here, no microscope was specified, and the imaging process was only described as "optical microscopy images" were used for their analysis.
(a) Dwane, S.; Durack, E.; Kiely, P.A. Optimising parameters for the differentiation of SH-SY5Y cells to study cell adhesion and cell migration. *BMC Res Notes.* **2013**, *6*, 366.
(b) Kim, H.B.; Yoo, B.S. Propolis Inhibits Neurite Outgrowth in Differentiating SH-SY5Y Human Neuroblastoma Cells. *Toxicol Res.* **2016**, *32*, 359.
(c) Higgins, S.; Lee, J.S.; Ha, L.; Lim, J.Y. Inducing neurite outgrowth by mechanical cell stretch. *Biores Open Access*. **2013**, *2*, 212–216.
(d) Poudel, I.; Lee, J.S.; Tan, L.; Lim, J.Y. Micropatterning-retinoic acid co-control of neuronal cell morphology and neurite outgrowth. *Acta Biomater*. **2013**, *9*, 4592–4598.
43. (a) Paik, S.; Somvanshi, R.K.; Kumar, U. Somatostatin-Mediated Changes in Microtubule-Associated Proteins and Retinoic Acid-Induced Neurite Outgrowth in SH-SY5Y Cells. *J Mol Neurosci.* **2019**, *68*, 120–134.
(b) Maemoto, Y.; Maruyama, T.; Nemoto, K.; Baba, T.; Motohashi, M.; Ito, A.; Tagaya, M.; Tani, K. DDHD1, but Not DDHD2, Suppresses Neurite Outgrowth in SH-SY5Y and PC12 Cells by Regulating Protein Transport From Recycling Endosomes. *Front Cell Dev Biol.* **2020**, *8*, 670.

ImageJ (Neurite Tracer[42b] or NeuronJ[42c]) plug-ins. While many of these are high-throughput, the lack of postsynaptic proteins makes dSH-SY5Y cells unable to explore formation of synapses following drug treatment. To my knowledge, there is no literature precedence indicating SH-SY5Y or dSH-SY5Y express postsynaptic proteins nor dendritic spines. This is a major limitation of the cells as antidepressants are hypothesized to rectify the atrophy of dendrites, reduction in the number of dendritic spines, and loss of synaptic density and the change in all three phenotypes may be required to be an indication of antidepressant potential.[11] Further studies and experiments are needed to assess whether small molecules known to be antidepressants in the clinic, have antidepressant potential in rodent models of depression, or induce neurite outgrowth in primary cortical cultures would induce neurite outgrowth in dSH-SY5Y cells.

Chapter 1.4 Primary Rodent Embryonic Cortical Cultures and Structural Plasticity

Primary cortical cultures are disassociated cells generated through tissues collected and triturated to be plated as a single layer of cells in a dish. These models tend to be mixed cultures, containing neurons, glial cells, and astrocytes, which help to recapitulate the interactions of the environment in the brain. Generally, primary embryonic cultures are harvested between embryonic days 16 and 20 (E16 and E20), usually yielding 6 to 20 pups (or on average 18 million cells, **Fig. 1.2**). An advantage of using embryonic cultures is that the culturing conditions are 5% CO_2, similar to that of cancer cell lines and thus available in most tissue culture rooms. Furthermore, no differentiation is required as these cells are already postmitotic and contain the basic components for many signaling pathways found in vivo. This model is rapid, and cultures can be robust, usually surviving up to 30 days in vitro (DIV30).

As a model of antidepressant potential, primary rodent cortical cultures can assess the growth of neurites, the dynamics of dendritic spines, and changes in synaptic density, which we could not with PC-12 and SH-SY5Y cells. Immunocytochemistry using anti-MAP2,[44] anti-β-III-tubulin,[45] or a "Neurite Outgrowth Assay Staining Kit"[17,46] are stained to quantify neurite outgrowth. Furthermore, quantifying neurite outgrowth ranges from automated high-content image analysis using MATLAB[47] to semi-manual to manual analysis using ImageJ.[48] The major advantage to using primary cortical cultures is that quantification of dendritic spines and synaptic density are possible. In terms of small molecules that have been hypothesized to increase neurite outgrowth, dendritic spines, and synaptic density includes traditional antidepressants and fast-acting antidepressants.[11] Therefore, examining the effects of potential therapeutics in this model would most likely identify a small molecule with antidepressant-like effects.

44. Chamak, B.; Fellous, A.; Glowinski, J.; Prochiantz, A. MAP2 expression and neuritic outgrowth and branching are coregulated through region-specific neuro-astroglial interactions. *J Neurosci*. **1987**, *7*, 3163–3170.
45. Sanders, T.R.; Kim, D.W.; Glendining, K.A.; Jasoni, C.L. Maternal obesity and IL-6 lead to aberrant developmental gene expression and deregulated neurite growth in the fetal arcuate nucleus. *Endocrinology*. **2014**, *155*, 2566–2577.
46. Su, Y.; Cui, L.; Piao, C.; Li, B.; Zhao, L.R. The effects of hematopoietic growth factors on neurite outgrowth. *PLoS One*. **2013**, 8, e75562.
47. Schmuck, M.R.; Keil, K.P.; Sethi, S.; Morgan, R.K.; Lein, P.J. Automated high content image analysis of dendritic arborization in primary mouse hippocampal and rat cortical neurons in culture. *J Neurosci Methods*. **2020** *341*, 108793.
48. (a) Pemberton, K.; Mersman, B.; Xu, F. Using ImageJ to Assess Neurite Outgrowth in Mammalian Cell Cultures: Research Data Quantification Exercises in Undergraduate Neuroscience Lab. *J Undergrad Neurosci Educ*. **2018**, *16*, A186-A194.
(b) Longair, M.H.; Baker, D.A.; Armstrong, J.D. Simple Neurite Tracer: open source software for reconstruction, visualization and analysis of neuronal processes. *Bioinformatics.* **2011**, *27*, 2453–2454.

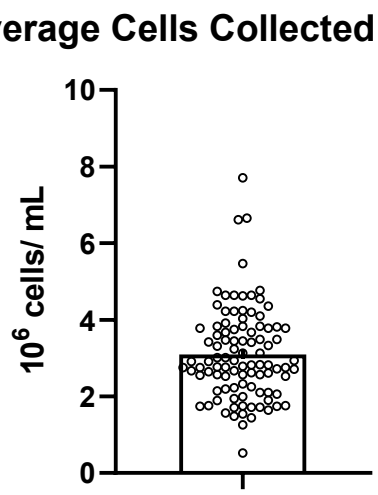

Figure 1.2. Number of cells collected from rat embryonic cortices. The average number of cells harvested was 3.103 ± 0.122 cells per mL with a total volume of 6 mL (total of 18.618 ± .732 cells in total), n = 97. The cells were harvested between January 11, 2018 to January 30, 2020. The average viability was 82.57%.[49]

For imaging of dendritic spines, neurons stained with fluorescent dyes (such as 1,1'-dioctadecyl-3,3,3',3'-tetramethylindocarbocyanine perchlorate or DiI),[50] phalloidin,[51] or transiently expressing green or red fluorescent proteins (GFP or RFP) are fixed and stained.[52] Quantification can be done through high-magnification (60x or 100x) confocal or structure illuminating microscopy (SIM) imaging requiring manual or automated quantification.[50–52]

For synaptic density, neurons are fixed and stained for pre- and postsynaptic densities. Presynaptic markers include vesicular glutamate transporter 1 (VGLUT1), synapsin I, and synaptophysin and postsynaptic markers include gephyrin and postsynaptic density-95 (PSD-95).[53] The quantification of

49. The viability of the cells was lower than expected. This is due in part to using expired trypan blue which caused false positive trypan blue cells. These false positive trypan blue cells were counted as “dead” cells rather than live. After changing to a new trypan blue stock, I was able to get back to an average of 91.2% viability.
50. Cheng, C.; Trzcinski, O.; Doering, L.C. Fluorescent labeling of dendritic spines in cell cultures with the carbocyanine dye “DiI”. *Front Neuroanat* **2014**, *8*, 30.
51. Bär, J.; Kobler, O.; van Bommel, B.; Mikhaylova, M. Periodic F-actin structures shape the neck of dendritic spines. *Sci Rep.* **2016**, *6*, 37136.
52. Kashiwagi, Y.; Higashi, T.; Obashi, K.; Sato, Y.; Komiyama, N.H.; Grant, S.G.N.; Okabe, S. Computational geometry analysis of dendritic spines by structured illumination microscopy. *Nat Commun*. **2019**, *10*, 1285.
53. (a) Harrill, J.A.; Chen, H.; Streifel, K.M.; Yang, D.; Mundy, W.R.; Lein, P.J. Ontogeny of biochemical, morphological and functional parameters of synaptogenesis in primary cultures of rat hippocampal and cortical neurons. *Mol Brain*. **2015**, *8*, 10.

synaptic density is conducted through colocalization of pre- and postsynaptic markers. Traditionally, synaptic density imaging is done on confocal or electron microscopy, but with better technology, the field is moving towards lower magnification and wide-field image and data acquisition.[53b]

While rat embryonic cortical cultures are a more biologically relevant model when compared to PC-12 and SH-SY5Y cells, there are some drawbacks. The cells need to be replenished continuously as pregnant dams are euthanized to obtain each batch of non-mitotic cortical cultures. To alleviate this, freezing protocols for primary embryonic cortical cultures have been established consisting of upwards of 20% dimethyl sulfoxide (DMSO) concentration to safely freeze the cells.[54] Both Ishizuka, et al. and Parker, et al. demonstrated that after freezing and thawing in an inhouse DMSO solution or commercially available freezing media (CryoStor10, ThermoFisher) cell viability and functionality was retained (up to 1 year by Parker, et al.). Lastly, while the cortical cells can be robust, they are extremely prone to contamination and sensitive to changes in the environment, such as slight temperature, CO_2 concentration, or pH changes.

Table 1.1 summarizes the topics discussed in this chapter.

	PC-12	SH-SY5Y	Embryonic Cortical Cultures
Cell type	Adherent cultures/ Dopaminergic	Adherent and floating cultures/ Dopaminergic	Adherent cultures/ Cortex
Cell ancestry	Rat adrenal medulla (pheochromocytoma)	Human bone marrow (neuroblastoma)	Embryonic rodent cortex
Regeneration of cells?	Yes	Yes	No
Neurite outgrowth	Yes	Yes	Yes
Dendritic spines	No	No	Yes
Synaptic Density	Presynaptic only	Presynaptic only	Pre- and postsynaptic
Differentiation?	Yes NGF or BDNF	Yes NGF, BDNF, RA, Phorbol esters	No
Neuronal protein expression	Missing postsynaptic markers	Missing postsynaptic markers	All biologically relevant markers
Imaging	Light and fluorescent microscopy	Light and fluorescent microscopy	Fluorescent microscopy

Table 1.1. Comparison of characteristics of PC-12, SH-SY5Y, and embryonic cortical cultures.

(b) Nieland, T.J.; Logan, D.J.; Saulnier, J.; Lam, D.; Johnson, C.; Root, D.E.; Carpenter, A.E.; Sabatini, B.L. High content image analysis identifies novel regulators of synaptogenesis in a high-throughput RNAi screen of primary neurons. *PLoS One*. **2014**, *9*, e91744.

54. (a) Ishizuka, Y.; Bramham, C.R. A simple DMSO-based method for cryopreservation of primary hippocampal and cortical neurons. *J Neurosci Methods*. **2020**, *333*, 108578.

(b) Parker, S.S.; Moutal, A.; Cai, S.; Chandrasekaran, S.; Roman, M.R.; Koshy, A.A.; Khanna, R.; Zinsmaier, K.E.; Mouneimne, G. High Fidelity Cryopreservation and Recovery of Primary Rodent Cortical Neurons. *eNeuro*. **2018**, 5, ENEURO.0135–18.

Chapter 1.5 Conclusion

In closing, dPC-12, dSH-SY5Y, and primary rodent embryonic cultures each have their pros and cons with respect to their potential as models for screening next-generation antidepressants. However, primary rodent embryonic cultures may be superior as we can quantify dendritic spines and synapses. Both these structural phenotypes, in addition to neurite outgrowth, are critical for the antidepressant therapeutic potential as seen with ketamine.[55] Furthermore, the lack of critical postsynaptic biomarkers from dPC-12 and dSH-SY5Y cells further diminishes their value as biologically relevant models for drug discovery for antidepressants. Moving forward, I will be describing structural plasticity in primary rat embryonic cortical cultures as a model for screening next-generation antidepressants.

A hallmark of depression is the retraction of neurites, reduction of the number of dendritic spines, and loss of synapses. Small molecules that can rapidly rectify these deficits have the potential to be potent antidepressants and categorized as psychoplastogens. To identify these molecules, I have developed the primary assays discussed earlier. First, we selected structural plasticity as an output for antidepressant potential as ketamine—the current state-of-the-art fast-acting antidepressant—promotes increases in neurite outgrowth, the number of dendritic spines, and synaptic density in cortical cultures. Therefore, using ketamine as a benchmark, we sought to find small molecules with similar therapeutic potential and identified the scaffolds of the classic psychedelics as a target of interest. When I compared the classic psychedelics to ketamine, I found that the classic psychedelics were equally efficacious as ketamine. Furthermore, I discovered that short stimulation with the classic psychedelics and ketamine were substantial to sustain long-lasting structural changes. Next, I discovered psychoplastogens required activation of the α-amino-3-hydroxy-5-methyl-4-isoxazolepropionic acid (AMPA) receptor, tropomyosin receptor kinase B (TrkB), and mechanistic target of rapamycin (mTOR) pathways for the increase in structural plasticity.

After identifying the potential mechanism of action of the psychoplastogens, I became more interested in developing assays to facilitate the development, prioritization, and optimization of next-generation non-hallucinogenic analogs of the classic psychedelics. Traditionally, small molecules are

55. Duman, C.H.; Duman, R.S. Spine synapse remodeling in the pathophysiology and treatment of depression. *Neurosci Lett*. **2015**, *601,* 20–29.

screened in behavioral assays such as sucrose preference and forced swim test (FST) for antidepressant potential. Furthermore, to determine hallucinogenic potential, head-twitch response (HTR) or drug discrimination (DD) is used. While behavioral assays identify small molecules with therapeutic potential and off-target effects, they are not amendable for the rapid screening of thousands of analogs. To facilitate the prioritization of small molecules developed in the Olson lab, I established and optimized two orthogonal in cellular assays: an antidepressant potential assay in cortical cultures and an assay to identify hallucinogens in human embryonic kidney 293T (HEK293T) cells. The antidepressant potential assay focuses on identifying molecules that promote structural plasticity and cell survival. The hallucinogenic potential assay used a genetically encoded serotonin 2A (5-HT2A) receptor conjugated to a circular permutated GFP (cpGFP) that increases in fluorescence when hallucinogenic molecules bind to the receptor. The molecules that the assay identified as hallucinogenic were validated in vivo using the HTR. Together, these two assays identified AAZ-A-154, a novel, a non-hallucinogenic small molecule with antidepressant potential in FST and sucrose preference. In closing, these two assays are the starting point as drug discovery platforms for facilitating the identification of next-generation fast-acting antidepressants.

Chapter 2 Psychedelics Promote Neural Plasticity[1]

Chapter 2.1 Introduction

A hallmark of depression is the loss of neural structures in the prefrontal cortex (PFC), such as the atrophy of neurites, reduction in the number of dendritic spines, and loss of synaptic density.[2] These deficits have been hypothesized to be counteracted by small molecules capable of promoting structural and functional plasticity in the PFC.[3] We have named these molecules, psychoplastogens, for their ability to rapidly promote structural growth regardless of their mechanism of action.[4]

The psychoplastogen ketamine has been approved by the Food and Drug Administration (FDA) for use in treatment-resistant depression (TRD). Like ketamine, the serotonergic psychedelics have

1. The work presented in this chapter has been published in the following publications:
(a) Ly, C.; Greb, A. C.; Cameron, L. P.; Wong, J. M.; Barragan, E. V.; Wilson, P. C.; Burbach, K. F.; Soltanzadeh Zarandi, S.; Sood, A.; Paddy, M. R.; Duim, W. C.; Dennis, M. Y.; McAllister, A. K.; Ori-McKenney, K. M.; Gray, J. A.; Olson, D. E. Psychedelics Promote Structural and Functional Neural Plasticity. *Cell Rep*. **2018**, *23*, 3170–3182.
(b) Ly, C.; Greb, C. A.; Vargas, M. V.; Duim, W. C.; Grodzki, A. C. G.; Lein, P. J.; Olson, D. E. Transient Stimulation with Psychoplastogens is Sufficient to Initiate Neuronal Growth. *ACS Pharmacol. Transl. Sci*., **2021**, *4*, 452–460.
2. (a) Autry, A.E.; Monteggia, L.M. Brain-derived neurotrophic factor and neuropsychiatric disorders. *Pharmacol. Rev*. **2012**, *64*, 238–258.
(b) Russo, S.J.; Nestler, E.J. The brain reward circuitry in mood disorders. *Nat. Rev. Neurosci.* **2013**, *14*, 609–625.
Qiao, H; Li, M.X.; Xu, C.; Chen, H.B.; An, S.C.; Ma, X.M. Dendritic Spines in Depression: What We Learned from Animal Models. *Neural Plast.* **2016**, *2016*, 8056370.
(c) Izquierdo A, Wellman CL, Holmes A. Brief uncontrollable stress causes dendritic retraction in infralimbic cortex and resistance to fear extinction in mice. *J Neurosci.* **2006**, *26*,5733–5738.
Pittenger, C.; Duman, R.S. Stress, depression, and neuroplasticity: a convergence of mechanisms. *Neuropsychopharmacology*. **2008**, *33*, 88–109.
(d) Duman, R.S.; Aghajanian, G.K.; Sanacora, G.; Krystal, J.H. Synaptic plasticity and depression: new insights from stress and rapid-acting antidepressants. *Nat. Med.* **2016**, *22*, 238–249.
(d) Duman, R.S.; Aghajanian, G.K. Synaptic dysfunction in depression: potential therapeutic targets. *Science*. **2012**, 338, 68–72.
Christoffel, D.J.; Golden, S.A.; Russo, S.J. Structural and synaptic plasticity in stress-related disorders. *Rev. Neurosci*. **2011,** *22,* 535–549.
(e) Christoffel, D. J.; Golden, S. A.; Russo, R. J. *Rev. Neurosci*. **2011**, 22, 535–549.
3. (a) Castrén, E.; Antila, H. Neuronal plasticity and neurotrophic factors in drug responses. *Mol. Psychiatry*. **2017**, *22*, 1085–1095.
Cramer, S.C.; Sur, M.; Dobkin, B.H.; O'Brien, C.; Sanger, T.D.; Trojanowski, J.Q.; Rumsey, J.M.; Hicks, R.; Cameron, J.; Chen, D.; Chen, W.G.; Cohen, L.G.; deCharms, C.; Duffy, C.J.; Eden, G.F.; Fetz, E.E.; Filart, R.; Freund, M.; Grant, S.J.; Haber, S.; Kalivas, P.W.; Kolb, B.; Kramer, A.F.; Lynch, M.; Mayberg, H.S.; McQuillen, P.S.; Nitkin, R.; Pascual-Leone, A.; Reuter-Lorenz, P.; Schiff, N.; Sharma, A.; Shekim, L.; Stryker, M.; Sullivan, E.V.; Vinogradov, S. Harnessing neuroplasticity for clinical applications. *Brain*. **2011**, *134*, 1591–609.
(b) Duman, R.S. Synaptic plasticity and mood disorders. *Mol. Psychiatry*. **2002**, *7*, S29–S34.
(c) Hayley, S.; Litteljohn, D. Neuroplasticity and the next wave of antidepressant strategies. *Front. Cell. Neurosci*. **2013**, *7*, 218.
(d) Kolb, B.; Muhammad, A. Harnessing the power of neuroplasticity for intervention. *Front. Hum. Neurosci*. **2014**, *8*, 377.
(e) Krystal, J.H.; Tolin, D.F.; Sanacora, G.; Castner, S.A.; Williams, G.V.; Aikins, D.E.; Hoffman, R.E.; D'Souza, D.C. Neuroplasticity as a target for the pharmacotherapy of anxiety disorders, mood disorders, and schizophrenia. *Drug Discov. Today*. **2009**, *14*, 690–697.
(e) Mathew, S.J.; Manji, H.K.; Charney, D.S. Novel drugs and therapeutic targets for severe mood disorders. *Neuropsychopharmacology*. **2008**, *33*, 2080–2092.
4. (a) Olson, D.E. Psychoplastogens: A Promising Class of Plasticity-Promoting Neurotherapeutics. *J. Exp. Neurosci.* **2018**, *12*, 1179069518800508.
(b) Olson, D. E. The Promise of Psychedelic Science. *ACS Pharmacol. Transl. Sci.*, **2021**, *4*, 413–415.
(c) Benko, J.; Vranková, S. Natural Psychoplastogens As Antidepressant Agents. *Molecules*. **2020**, *25*, 1172.

demonstrated rapid and long-lasting antidepressant effects in both rodent models and the clinic following a single dose.[5] Despite their clinical success, the mechanism of action is not well understood and there have been many safety concerns that have limited their use in a clinical setting, (i.e. hallucinations).[6] Because of the similarity in preclinical and clinical data between ketamine and the classic psychedelics, we hypothesized that the classic psychedelics may share the ability to promote neural plasticity.[7,8] In this chapter, I will show data that indicates the classic psychedelics promote neural plasticity equipotent to that of ketamine in neuritogenesis, spinogenesis, and synaptogenesis. Furthermore, I present evidence that the classic psychedelics promote structural plasticity through the serotonin 2 receptor (5-HT2R), tropomyosin receptor kinase B (TrkB), mechanistic target of rapamycin (mTOR), and α-amino-3-hydroxy-5-methyl-4-isoxazolepropionic acid receptors (AMPARs) in chronic and short transient treatments with the psychoplastogens.

5. (a) Berman, R.M.; Cappiello, A.; Anand, A.; Oren, D.A.; Heninger, G.R.; Charney, D.S.; Krystal, J.H. Antidepressant effects of ketamine in depressed patients. *Biol. Psychiatry*. **2000**, *47*, 351–354.
(b) Ionescu, D.F.; Swee, M.B.; Pavone, K.J.; Taylor, N.; Akeju, O.; Baer, L.; Nyer, M.; Cassano, P.; Mischoulon, D.; Alpert, J.E.; Brown, E.N.; Nock, M.K.; Fava, M.; Cusin, C. Rapid and Sustained Reductions in Current Suicidal Ideation Following Repeated Doses of Intravenous Ketamine: Secondary Analysis of an Open-Label Study. *J. Clin. Psychiatry*. **2016**, *77*, e719–e725.
(c) Zarate, C.A. Jr.; Brutsche, N.E.; Ibrahim, L.; Franco-Chaves, J.; Diazgranados, N.; Cravchik, A.; Selter, J.; Marquardt, C.A.; Liberty, V.; Luckenbaugh, D.A. Replication of ketamine's antidepressant efficacy in bipolar depression: a randomized controlled add-on trial. *Biol. Psychiatry.* **2012**, *71*, 939–946.
(d) DiazGranados, N.; Ibrahim, L.A.; Brutsche, N.E.; Ameli, R.; Henter, I.D.; Luckenbaugh, D.A.; Machado-Vieira, R.; Zarate, C.A. Jr. Rapid resolution of suicidal ideation after a single infusion of an N-methyl-D-aspartate antagonist in patients with treatment-resistant major depressive disorder. *J. Clin. Psychiatry*. **2010**, *71*, 1605–1611.
(e) Murrough, J.W.; Perez, A.M.; Pillemer, S.; Stern, J.; Parides, M.K.; aan het Rot, M.; Collins, K.A.; Mathew, S.J.; Charney, D.S.; Iosifescu, D.V. Rapid and longer-term antidepressant effects of repeated ketamine infusions in treatment-resistant major depression. *Biol. Psychiatry.* **2013**, *74*, 250–256.
(f) Zarate, C.A. Jr.; Singh, J.B.; Carlson, P.J.; Brutsche, N.E.; Ameli, R.; Luckenbaugh, D.A.; Charney, D.S.; Manji. H.K. A randomized trial of an N-methyl-D-aspartate antagonist in treatment-resistant major depression. *Arch. Gen. Psychiatry*. **2006**, *63*, 856–864.
6. (a) Carhart-Harris, R.L.; Kaelen, M.; Whalley, M.G.; Bolstridge, M.; Feilding, A.; Nutt, D.J. LSD enhances suggestibility in healthy volunteers. *Psychopharmacology (Berl).* **2015**, *232*, 785–794.
(b) Freedman, D.X. On the Use and Abuse of LSD. *Arch. Gen. Psychiatry*. **1968**, *18*, 330–347.
7. **Psychedelics:** (a) Cameron, L. P.; Benson, C. J.; Dunlap, L. E.; Olson, D. E. Effects of N,N-dimethyltryptamine (DMT) on rat behaviors relevant to anxiety and depression *ACS Chem. Neurosci.* **2018**, *9*, 1582–1590.
(b) Catlow, B.J.; Song, S.; Paredes, D.A.; Kirstein, C.L.; Sanchez-Ramos, J. Effects of psilocybin on hippocampal neurogenesis and extinction of trace fear conditioning. *Exp. Brain Res*. **2013,** *228*, 481–491.
(c) Young, M.B.; Andero, R.; Ressler, K.J.; Howell, L.L. 3,4-Methylenedioxymethamphetamine facilitates fear extinction learning. *Transl. Psychiatry*. **2015**, *5*, e634.
8. **Ketamine**: (a) Autry, A.E.; Adachi, M.; Nosyreva, E.; Na, E.S.; Los, M.F.; Cheng, P.F.; Kavalali, E.T.; Monteggia, L.M. NMDA receptor blockade at rest triggers rapid behavioural antidepressant responses. *Nature*. **2011**, *475*, 91–95.
(b) Girgenti, M.J.; Ghosal, S.; LoPresto, D.; Taylor, J.R.; Duman, R.S. Ketamine accelerates fear extinction via mTORC1 signaling. *Neurobiol. Dis*. **2017**, *100*, 1–8.
(c) Li, N.; Lee, B.; Liu, R.J.; Banasr, M.; Dwyer, J.M.; Iwata, M.; Li, X.Y.; Aghajanian, G.; Duman, R.S. mTOR-dependent synapse formation underlies the rapid antidepressant effects of NMDA antagonists. *Science*. **2010**, *329*, 959–964.

Chapter 2.2 Psychedelics Promote Neurite Outgrowth

We treated rat embryonic cortical cultures with the classic psychedelics **(Fig. 2.1A)** from a variety of structural classes and quantified dendritic arbors using Sholl analysis.[9] Sholl analysis takes the tracing of the neurites and overlays concentric circles radiating out from the center of the soma. Each time a circle intersects with a neurite that has been traced, a "crossing" is counted. These "crossings" are averaged together to generate a Sholl plot **(Fig. 2.1B)**. Using the Sholl plots, we were able to quantify multiple phenotypic outputs such as the maximum number of crossings (Nmax) and the area under the curve (AUC) as determined by the Sholl plot. Further, we were able to quantify the number of primary branches, the number of secondary and higher-order branches, the total length of the dendritic arbor, and the length of the longest neurite that was traced. We found that lysergic acid diethylamide (LSD), 2,5-dimethoxy-4-iodoamphetamine (DOI), and *N*,*N*-dimethyltryptamine (DMT) increased Nmax **(Fig. 2.1C)**, the area under the curve **(Fig. 2.1D)**, and the number of branches **(Fig. 2.1F)**. LSD and DMT were able to increase the number of primary dendrites **(Fig. 2.1E)** and total neurite length **(Fig. 2.1G)**, but DOI was not. Furthermore, the longest neurite **(Fig. 2.1H)** for all compounds did not change.

We then compared these changes to ketamine (KET) and other psychedelics (psilocin [PSI] and 3,4-methyl enedioxymethamphetamine [MDMA]) **(Fig. 2.1A–B, 2.1I–N)**, and found that KET increased Nmax **(Fig. 2.1I)**, AUC **(Fig. 2.1J)**, and total neurite length **(Fig. 2.1M)**. PSI increased Nmax **(Fig. 21I)** and the number of branches **(Fig.2.1L)**. Lastly, MDMA trended upwards in the Nmax, the number of primary branches and the number of secondary branches. This suggests too low of the number of cells tested (n = 10). Other Olson lab members and I have tested and found that MDMA does increase the Nmax significantly with enough cells (N > 30).[10]

9. Ristanović, D.; Milosević, N.T.; Stulić, V. Application of modified Sholl analysis to neuronal dendritic arborization of the cat spinal cord. *J. Neurosci. Methods.* **2006**, *158*, 212–218.
10. See **Fig. 2.4**.

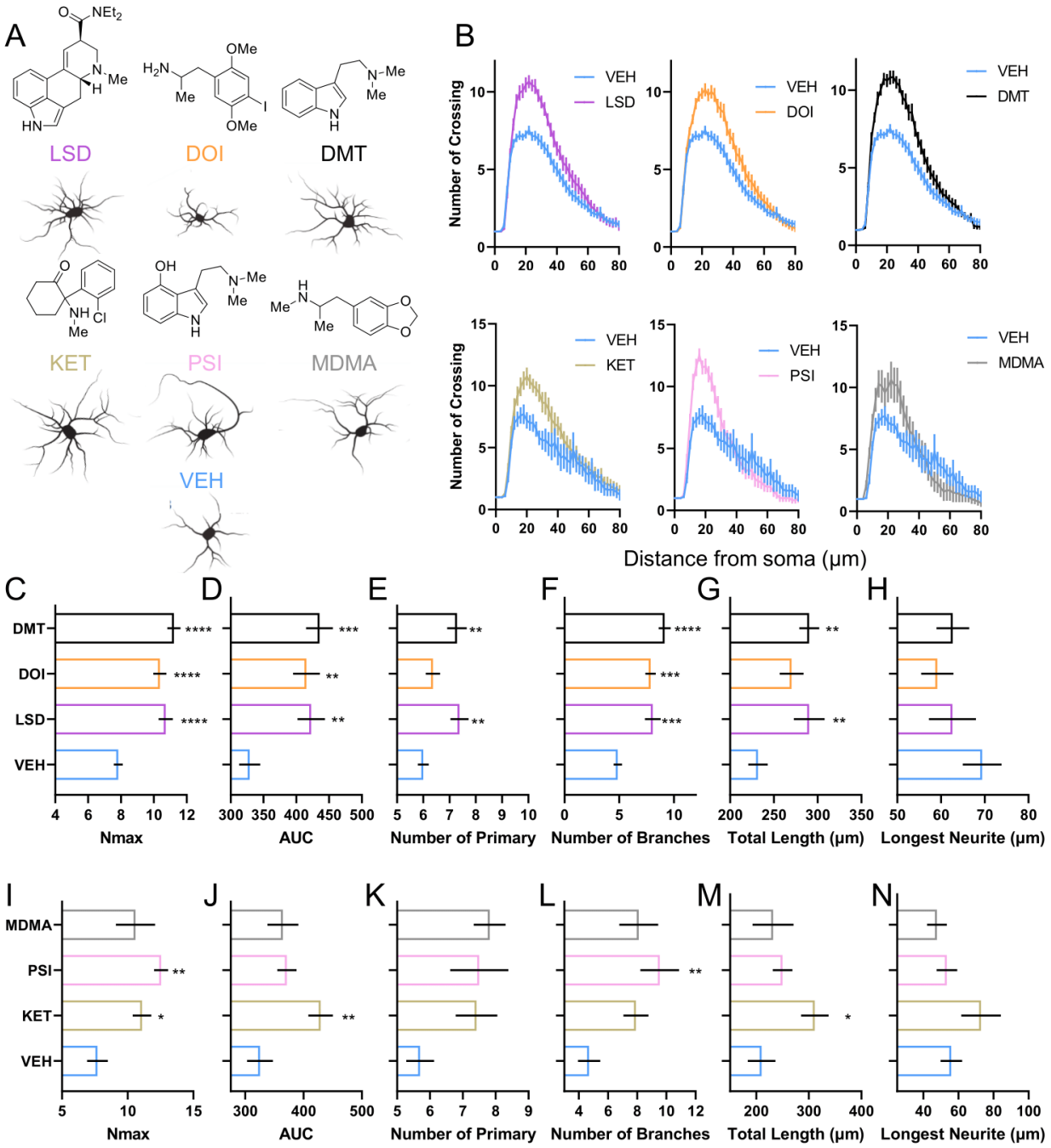

Figure 2.1. Psychedelics and ketamine promote structural plasticity. **(A)** Structures of classic psychedelics and ketamine tested and neuronal traces following treatment. **(B)** Sholl plot from Sholl analysis. **(C, I)** The Nmax, **(D, J)** the AUC, **(E, K)** the number of primary dendrites, **(F, L)** the number of branches, **(G, M)** the total neurite length, and **(H, N)** the longest neurite were all measured using Simple Neurite Tracer and Sholl analysis plug-ins on ImageJ Fiji. LSD, DOI, DMT N = 39–41 neurons. KET, PSI, MDMA N = 10–12 neurons.

Data on **(B–N)** are represented as mean ± SEM. *p < 0.05, **p < 0.01, ***p < 0.001, ****p < 0.0001, as compared to VEH control. For **(C–N)**, a one-way analysis of variance with a Dunnett's post hoc test was utilized. VEH = vehicle; LSD = lysergic acid diethylamide; DOI = ± 2,5-Dimethoxy-4-iodoamphetamine; DMT = *N*,*N*-dimethyltryptamine; KET = ketamine; PSI = psilocin; MDMA = (±)-3,4-Methylenedioxy methamphetamine.

Next, we tested 7,8-dihydroxyflavone (7,8-DHF), D-amphetamine (D-AMP), and serotonin (5-HT) **(Fig. 2.2A)** to determine if this phenotypic change was selective to psychoplastogens or if other classes of compounds would exhibit a similar response. We chose these compounds because 7,8-DHF is a potent and selective small molecule agonist of TrkB[11] and has demonstrated some therapeutic efficacy as an antidepressant in the forced swim test (FST).[12] D-AMP is a psychostimulant, which is believed to improve cognitive function.[13] Lastly, 5-HT is the endogenous ligand for the serotonin receptors to which the psychedelics bind. We observed increases in Nmax and AUC for neurons treated with 7,8-DHF, but not D-AMP **(Fig. 2.2B–D)**. While 5-HT increased Nmax and AUC **(Fig. 2.2B–D)**, the Sholl curve was different than that of the classic psychedelics and 7,8-DHF.[14] 5-HT and D-AMP's effects on the number of primary dendrites **(Fig. 2.2E)**, the number of branches **(Fig. 2.2F)**, and the total neurite length **(Fig. 2.2G)** were not significant and were different from observed results with the treatment of LSD, DOI, and DMT **(Fig. 2.1)**. The results with 7,8-DHF closely resembled those of the LSD, DOI, and DMT, i.e. able to increase 4 out of the 6 phenotypes, **(Fig. 2.2)** which is not surprising as 7,8-DHF is known as a brain-derived neurotrophic factor (BDNF) mimetic that was thought to facilitate antidepressant-like response in rodents albeit not as persistent as ketamine.[15]

11. Jang, S.W.; Liu, X.; Yepes, M.; Shepherd, K. R.; Miller, G. W.; Liu, Y.; Wilson, W. D.; Xiao, G.; Blanchi, B.; Sun, Y. E.; Ye, K. A selective TrkB agonist with potent neurotrophic activities by 7,8-dihydroxyflavone. *Proc Natl Acad Sci U S A*. **2010**, *107*, 2687–2692.
12. Liu, X.; Chan, C. B.; Jang, S. W.; Pradoldej, S.; Huang, J.; He, K.; Phun, L. H.; France, S.; Xiao, G.; Jia, Y.; Luo, H. R.; Ye, K. A synthetic 7,8-dihydroxyflavone derivative promotes neurogenesis and exhibits potent antidepressant effect. *J Med Chem*. **2010**, *53*, 8274–8286.
13. Wood, S.; Sage, J.R.; Shuman, T.; Anagnostaras, S.G. Psychostimulants and cognition: a continuum of behavioral and cognitive activation. *Pharmacol Rev*. **2013**, *66*, 193–221.
14. The Olson lab has revisited these results and we have shown that long stimulation with 5-HT will increase neurite outgrowth and short stimulation does not. We postulate this to be true because 5-HT is not cell permeable and the receptor of interest that promotes neurite outgrowth is predominately inside the cell. Max Vargas has observed cortical cultures stimulated for 1 hour with 5-HT does not promote neurite outgrowth. However, when he transiently expressed the serotonin transporter (SERT) and treated with 5-HT, neurite outgrowth was promoted. The mechanism of action is still being explored. We hypothesize the serotonin 2 receptors are responsible for the neurite outgrowth phenotype observed following classic psychedelic and 5-HT treatments.
15. (a) Liu, X.; Chan, C.B.; Jang, S.W.; Pradoldej, S.; Huang, J.; He, K.; Phun, L.H.; France, S.; Xiao, G.; Jia, Y.; Luo, H.R.; Ye, K. A synthetic 7,8-dihydroxyflavone derivative promotes neurogenesis and exhibits potent antidepressant effect. *J. Med. Chem.* **2010**, *53*, 8274–8286.

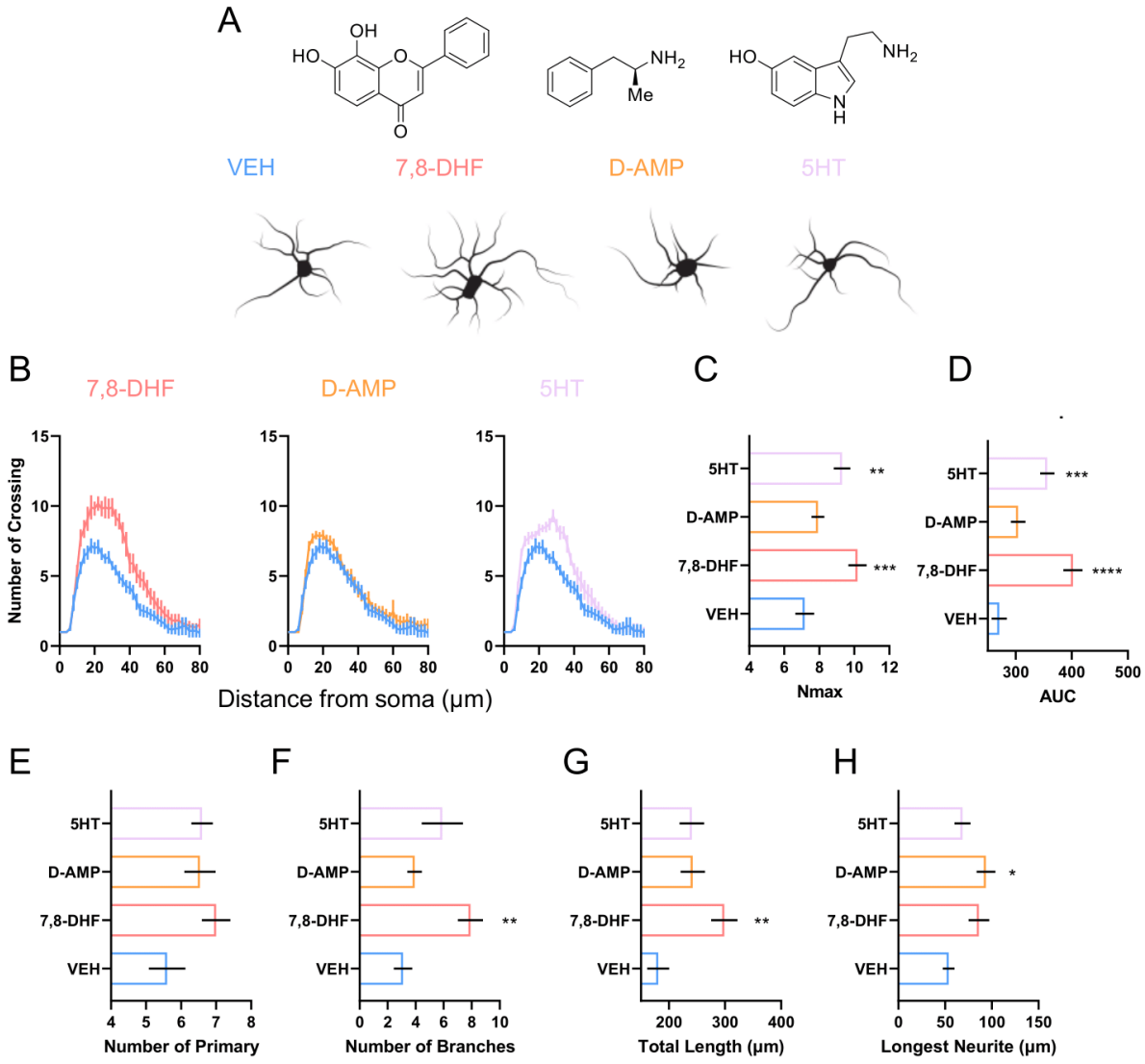

Figure 2.2. Quantification of neurite outgrowth in Sholl analysis following treatment with a TrkB agonist, stimulant, and monoamine. **(A)** Structures of 7,8-DHF (TrkB agonist), D-AMP (stimulant), and 5-HT (monoamine) tested and neuronal traces following treatment. **(B)** Sholl plot from Sholl analysis. **(C)** The Nmax, **(D)** the AUC, **(E)** the number of primary dendrites, **(F)** the number of branches, **(G)** the total neurite

(b) Zhang, J.C.; Wu, J.; Fujita, Y.; Yao, W.; Ren, Q.; Yang, C.; Li, S.X.; Shirayama, Y.; Hashimoto, K. Antidepressant effects of TrkB ligands on depression-like behavior and dendritic changes in mice after inflammation. *Int. J. Neuropsychopharmacol.* **2014**, *18*, pyu077.
(c) Zhang, J.C.; Yao, W.; Dong, C.; Yang, C.; Ren, Q.; Ma, M.; Han, M.; Hashimoto, K. Comparison of ketamine, 7,8-dihydroxyflavone, and ANA-12 antidepressant effects in the social defeat stress model of depression. *Psychopharmacology (Berl).* **2015**, *232*, 4325–4335.
(d) Chang, H.A.; Wang, Y.H.; Tung, C.S.; Yeh, C.B.; Liu, Y.P. 7,8-Dihydroxyflavone, a Tropomyosin-Kinase Related Receptor B Agonist, Produces Fast-Onset Antidepressant-Like Effects in Rats Exposed to Chronic Mild Stress. *Psychiatry Investig.* **2016**, *13*, 531–540.

length, and **(H)** the longest neurite were all measured using Simple Neurite Tracer and the Sholl analysis plug-ins on ImageJ Fiji. Data in **(B–H)** (n = 9–13) are represented as mean ± SEM. *p < 0.05, **p < 0.01, ***p < 0.001, ****p < 0.0001, as compared to VEH control. For **(C–H)**, a one-way analysis of variance with a Dunnett's post hoc test was utilized. VEH = vehicle; 7,8-DHF = 7,8-dihydroxyflavone; D-AMP = D-amphetamine; 5-HT = 5-hydroxytryptamine or serotonin.

As we saw increases in neurite outgrowth, we wanted to compare the classic psychedelics' response to the endogenous ligand that induces neural plasticity, BDNF.[16] Furthermore, ketamine's behavioral effects have been shown to be BDNF-dependent.[17] I treated neurons with BDNF (50 ng/mL, 5 ng/mL, and 500 pg/mL) and found a significant increase in the same morphological phenotypes observed after treatment with the classic psychedelics **(Fig. 2.3 A–F)**. We then attempted to co-treat DOI with BDNF to see if there was a synergistic effect but observed no synergy **(Fig. 2.3G)**. We hypothesize that we did not observe a synergistic effect because of one of two reasons. The first reason was that we had already maxed out the possible response from the neurons and hit a ceiling effect. The second reason was that the psychedelics like DOI and BDNF work through a similar mechanism, perhaps through upregulation of BDNF mRNA or BDNF protein levels as BDNF is known to autoregulate itself.[18] Thus, I measured *BDNF* mRNA expression through droplet digital PCR (ddPCR) **(Fig. 2.3H)** and BDNF total protein with enzyme-linked immunosorbent assay (ELISA) **(Fig. 2.3I)**.[19] I found that *BDNF* transcript levels did not change whereas total BDNF protein levels increased, albeit only DOI significantly increased protein levels. These data

16. Lu, B.; Nagappan, G.; Lu, Y. BDNF and synaptic plasticity, cognitive function, and dysfunction. *Handb. Exp. Pharmacol.* **2014**, *220*, 223–250.
17. Lepack, A.E.; Bang, E.; Lee, B.; Dwyer, J.M.; Duman, R.S. Fast-acting antidepressants rapidly stimulate ERK signaling and BDNF release in primary neuronal cultures. *Neuropharmacology*. **2016**, *111*, 242–252.
18. (a) Jiang, C.; Lin, W. J.; Salton, S. R. Role of a VGF/BDNF/TrkB Autoregulatory Feedback Loop in Rapid-Acting Antidepressant Efficacy. *J. Mol. Neurosci.* **2019**, *68*, 504–509.
(b) Esvald, E. E.; Tuvikene, J.; Sirp, A.; Patil, S.; Bramham, C. R.; Timmusk, T. CREB Family Transcription Factors Are Major Mediators of BDNF Transcriptional Autoregulation in Cortical Neurons. *J. Neurosci.* **2020**, *40*, 1405–1426.
(c) Tuvikene, J., Pruunsild, P., Orav, E., Esvald, E. E., and Timmusk, T. AP-1 Transcription Factors Mediate BDNF-Positive Feedback Loop in Cortical Neurons. *J. Neurosci.* **2016**, *36*, 1290–1305.
(d) Bambah-Mukku, D.; Travaglia, A.; Chen, D. Y.; Pollonini, G.; Alberini, C. M. A Positive Autoregulatory BDNF Feedback Loop via C/EBPβ Mediates Hippocampal Memory Consolidation. *J. Neurosci.* **2014**, *34*, 12547–12559.
19. To note, optimizing the ELISA protocol was difficult as the major limitation to the assay was that the antibodies used to capture BDNF in the ELISA were not very sensitive to BDNF. Our cultures also did not seem to secrete a large amount of BDNF (less than 10 pg/mL) when I tried quantifying BDNF in the cell culture media. To measure BDNF protein levels, I lysed the entire cell to quantify total BDNF protein levels to get significantly above the noise of the assay. Furthermore, I tried two different kits: ThermoFisher (ERBDNF) and Promega (G7611). Both kits did not give good resolution when I tried to quantify secreted BDNF in the culture media following stimulation.
Lepack, A.E.; et al.17 quantified BDNF release in cortical culture, which I also attempted to follow using their protocols for immunoprecipitation but was never successful in pulling down secreted (media) or total protein (lysed cells).Unfortunately, the antibodies used in the Lepack, A.E.; et al. publication were discontinued when I began my experiments following their procedure.

suggests that the classic psychedelics may increase the production and/or release of BDNF protein to facilitate their increased neurite outgrowth.

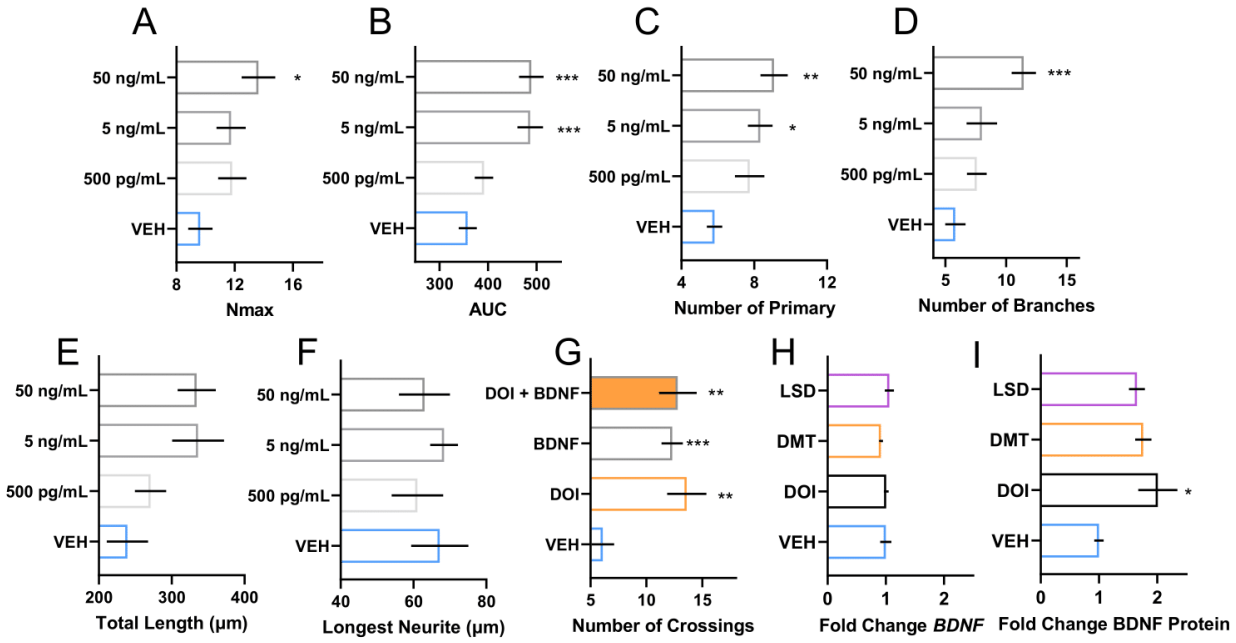

Figure 2.3. BDNF promotes neurite outgrowth in a dose dependent manner. **(A–F)** Quantification of neurite outgrowth via Simple Neurite Tracer and Sholl analysis plug-ins using ImageJ Fiji for **(A)** the Nmax, **(B)** the AUC, **(C)** the number of primary dendrites, **(D)** the number of branches, **(E)** the total neurite length, and **(F)** the longest neurite (n = 11–12). **(G)** DOI (10 µM) and BDNF (50 ng/mL) cotreatments did not synergize their effects at promoting neurite outgrowth in Nmax (n = 5–10). **(H)** *BDNF* mRNA quantified via ddPCR (n = 3) and **(I)** BDNF total protein quantified by ELISA (n = 3–4). Data on **(A–I)** are represented as mean ± SEM. *p < 0.05, **p < 0.01, ***p < 0.001, ****p < 0.0001, as compared to VEH control. For **(A–I)**, a one-way analysis of variance with a Dunnett's post hoc test was utilized. VEH = vehicle; BDNF = brain-derived neurotrophic factor; DOI = ± 2,5-Dimethoxy-4-iodoamphetamine. LSD = lysergic acid diethylamide; DMT = *N*,*N*-dimethyltryptamine.

Following our results with BDNF, we wanted to explore the potencies of our psychoplastogens. A dose-response of these six psychoplastogens in Sholl analysis and Nmax values were collected **(Fig 2.4A)**. Unfortunately, due to large variation between batches of cortical cultures, we could not achieve a traditional

dose-response curve.[20] While the raw Nmax varied, the overall fold change between VEH and compound remained the same. The data was normalized by setting 10 μM ketamine to 100% efficacy and vehicle control (0.1% dimethyl sulfoxide, DMSO, VEH) as 0% efficacy. While this process allowed us to fit the data to a dose-response curve, the EC_{50}, hill slope, and percent efficacy for these molecules vary drastically **(Fig. 2.4B)**. Furthermore, the hill slopes calculated suggested a polypharmacological mechanism of action for these molecules. This may have been exacerbated due to the long stimulation with psychedelics in this experiment (72 hours). Taken together, the data indicate that further optimization and assay development is required to properly measure and quantify potencies for psychoplastogens using the Sholl analysis and Nmax. To do so, we tried to optimize the assay by exploring whether short periods of transient stimulation could induce increases in structural plasticity to reduce off-target effects from prolonged periods of treatment.

20. I hypothesize the variability between batches of cultures is due to one of the following: differences in the time of tissue collection, plating density, and treatment times. I noticed that tissue harvested at different times of the day had variable viability and response. I normalized this by conducting my tissue collections in the early morning. Next, plating density varied between experimenters based on their calculations and tissue culture experience. I reduced the variability as I gained more experience. This dataset was one of my first experiments thus had large variability, but the overall results and conclusions have not changed. Lastly, treatment times for these experiments were chronic for 72 hours. While these initial studies looked at 72-hour treatments, I believe that shortened times (see **Fig. 2.5** for more details) allow for less variability between all the treatment groups.

A

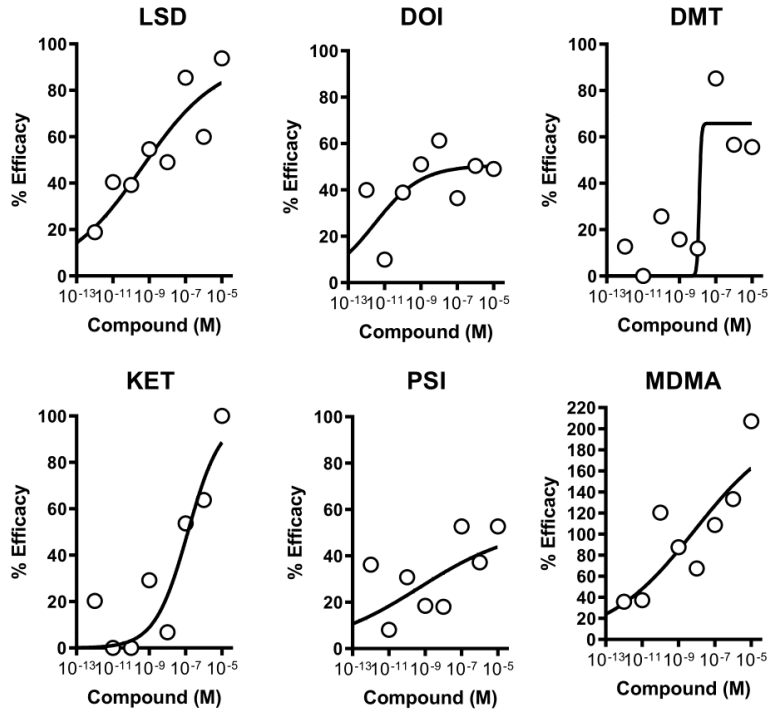

B

Compound	EC_{50}	Hill slope
LSD	0.409 nM	0.206
DOI	2.76 pM	0.003
DMT	109.8 nM	7.59
KET	132 nM	0.476
PSI	0.359 nM	0.165
MDMA	7.405 nM	0.181

Figure 2.4. Percent efficacy of a dose response in Sholl analysis. **(A)** Dose response of percent efficacy normalized to 10 μM ketamine as 100% efficacy and VEH as 0% efficacy. The Sholl analysis plug-in on ImageJ Fiji was used to quantify the images. **(B)** EC_{50} and Hill slope associated with the dose-responses in **(A)**.[21]

21. See **Chapter 2.8.2** for calculation and restraints used.

To explore the rate of induced neural plasticity in our cortical cultures, we reduced the stimulation time of the psychoplastogens to mitigate off-target effects. I began stimulating cells using different durations: 15 minutes, 1 hour, and 24 hours **(Fig. 2.5A)**. Ideally, the shorter stimulation times would better mimic the short period of transient stimulation of psychoplastogens in vivo given their short half-lives.[22] Then cells were allowed to grow in ligand-free media until a total of 72 hours had elapsed since the start of the stimulation. These short durations of stimulation were then compared to the 72-hour treatments and observed that 1 hour of ligand followed by 71 hours of ligand-free media gave the most robust increase in Nmax **(Fig. 2.5B–C)**. I thought this reduction in Nmax in the 72 hours of stimulation could be due to overstimulation causing the cells to retract slightly. Furthermore, we found that LSD and ketamine both responded equally efficaciously and comparable to BDNF in Nmax **(Fig. 2.5C)**. We then wanted to determine whether the remaining 71 hours of growth were critical for the increases in Nmax. We treated our cultures with ligand for 1 hour and immediately quantified neurite outgrowth. We found no change after 1 hour of ligand stimulation, indicating the remaining 71 hours after the first hour of treatment were critical for the long-lasting effects to persist **(Fig. 2.5D)**. Furthermore, these data suggested that short transient stimulations with psychoplastogens were enough to induce persistent changes to neurite outgrowth.

22. (a) Dolder, P.C.; Schmid, Y.; Steuer, A.E.; Kraemer, T.; Rentsch, K.M.; Hammann, F.; Liechti, M.E.; Pharmacokinetics and Pharmacodynamics of Lysergic Acid Diethylamide in Healthy Subjects. *Clin. Pharmacokinet*. **2017**, *56*, 1219–1230.
(b) Wieber, J.; Gugler, R.; Hengstmann, J.H.; Dengler, H.J. Pharmacokinetics of ketamine in man. *Anaesthesist*. **1975**, *24*, 260–263.

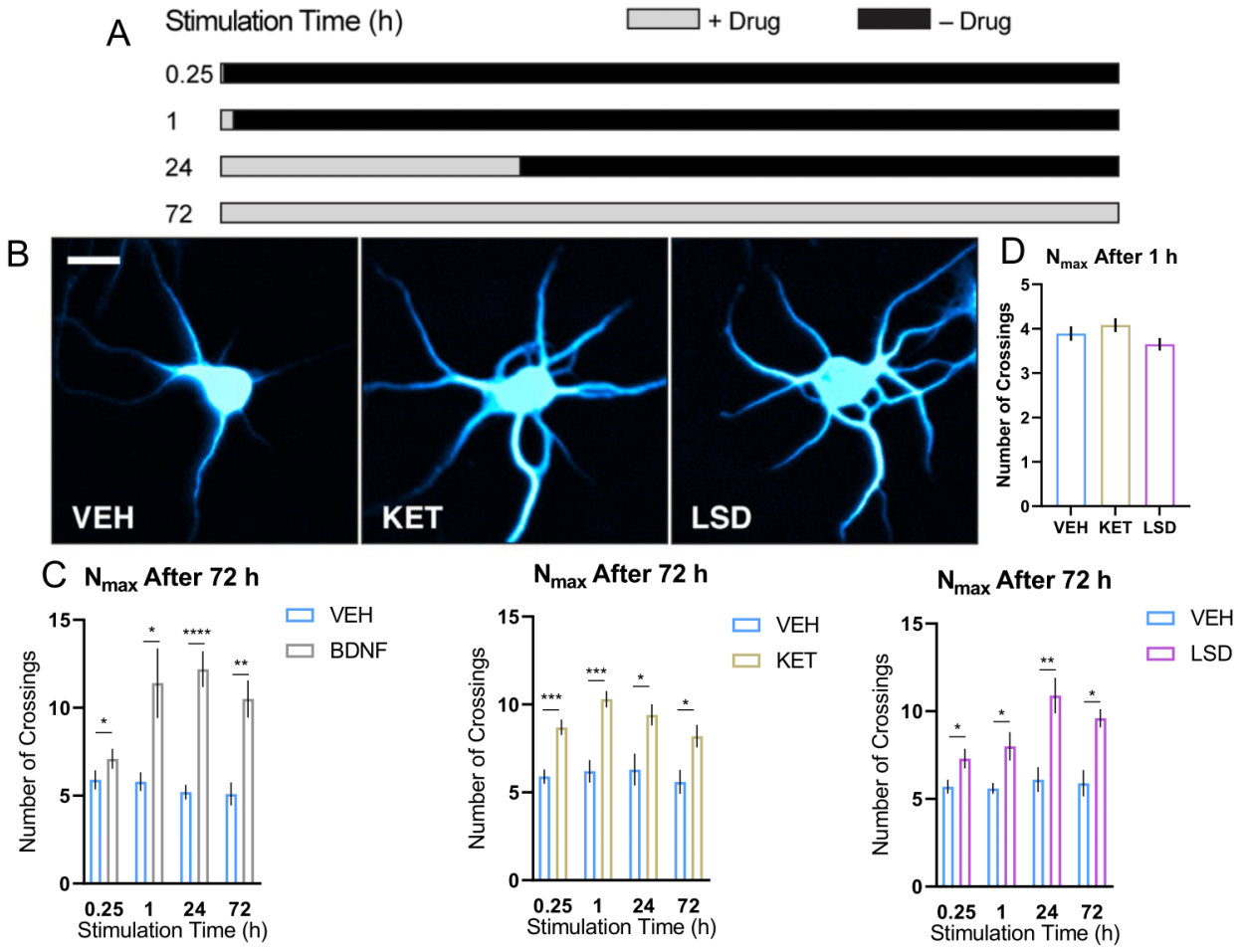

Figure 2.5. Short transient stimulation with the psychoplastogens induce neurite outgrowth. **(A)** Timeline of stimulation time with (gray) and without (black) drug. **(B)** Representative images of neurons that received drug for 1 hour followed by 71 hours of growth in drug free medium. Scale bar = 10 μm. **(C)** Nmax of BDNF, Ketamine (KET) and LSD for 15 mins, 1 hour, 24 hours, and 72 hours (total growth period for all treatments is 72 hours; n = 10 neurons). **(D)** KET and LSD following only 1 hour of stimulation and immediately quantified (total growth period is 1 hour; n = 37 neurons). Data are represented as mean ± SEM. *p < 0.05, **p < 0.01, ***p < 0.001, ****p < 0.0001, as compared to VEH control. For **(C)**, multiple t-tests were performed and p values were corrected for multiple comparisons using the Holm-Sidak method. For **(D)**, a one-way analysis of variance with a Dunnett's post hoc test was utilized. VEH = vehicle; KET = ketamine; LSD = lysergic acid diethylamide; BDNF = brain-derived neurotrophic factor.

Chapter 2.3 Psychedelics Increase Dendritic Spines and Synaptic Density

Next, we sought to determine whether classic psychedelics could increase the number of dendritic spines. Using 18 days in vitro (DIV18) neurons, I treated the maximal dose, 10 μM LSD, DOI, and DMT for 24 hours and found an increase in the total number of dendritic spines **(Fig. 2.6A–B)**. Furthermore, when we quantified the types of dendritic spines, we found that following psychedelic treatment, we observed a lower percentage of mushroom spines **(Fig. 2.6C)** compared to neural plasticity-related spines (thin, filopodia, and stubby spines).[23]

After observing the increase in dendritic spines, we hypothesized that there would be an increase in synaptic density. Following the treatment of cortical cultures with psychedelics, we observed an overall increase in synaptic density **(Fig. 2.6D–E)**. Furthermore, there was no change in synaptic size **(Fig. 2.6F)** and postsynaptic density-95 (PSD-95) density **(Fig. 2.6H)**. We were surprised to see an increase in vesicular glutamate transporter 1 (VGLUT1), albeit trending for most psychedelics **(Fig. 2.6G)**. This result was different than what is known for ketamine and its mechanism of action in increasing both pre-and postsynaptic densities.[24]

23. Pchitskaya, E; Bezprozvanny, I. Dendritic Spines Shape Analysis-Classification or Clusterization? Perspective. *Front. Synaptic Neurosci.* **2020**, *12*, 31.
24. Li, N.; Lee, B.; Liu, R.J.; Banasr, M.; Dwyer, J.M.; Iwata, M.; Li, X.Y.; Aghajanian, G.; Duman, R.S. mTOR-dependent synapse formation underlies the rapid antidepressant effects of NMDA antagonists. *Science*. **2010**, *329*, 959–964.

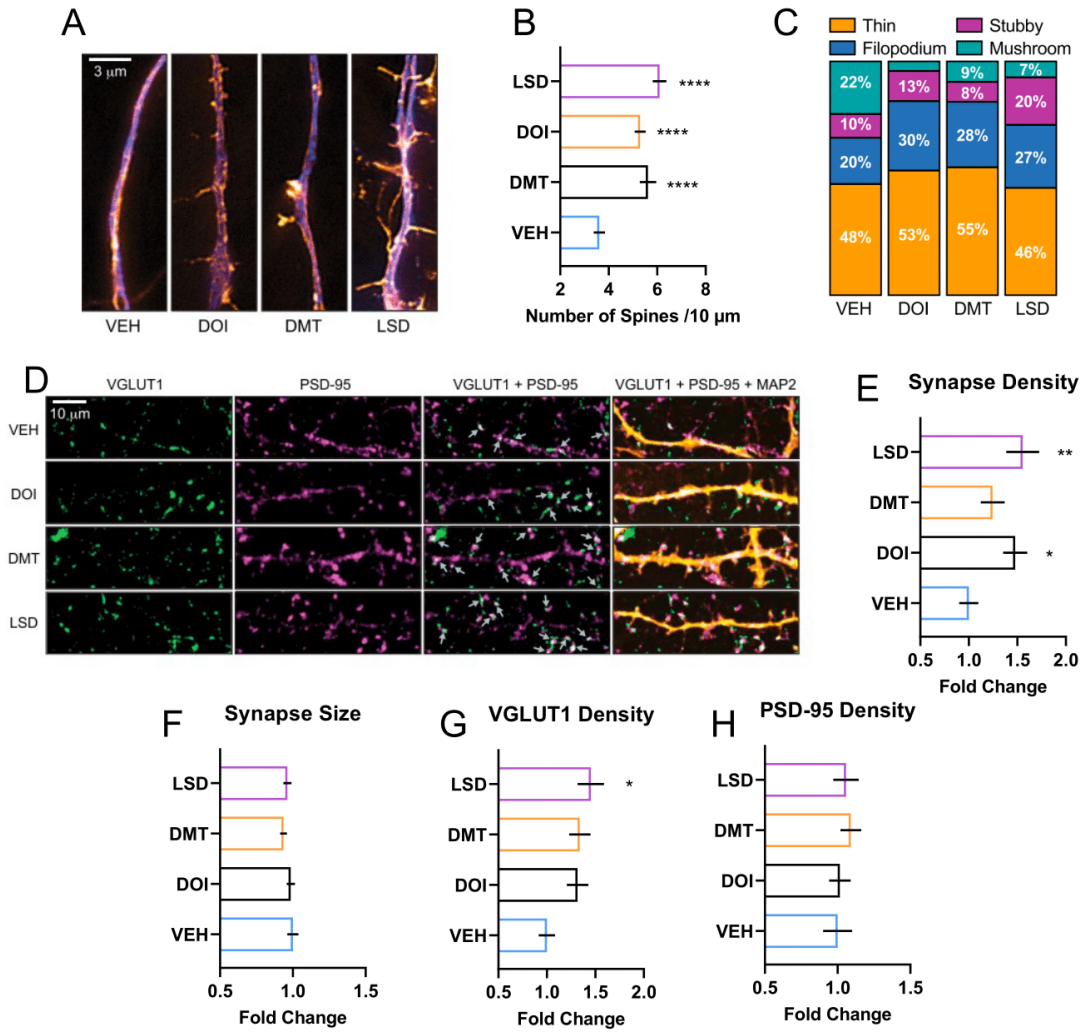

Figure 2.6. Classic psychedelics increase the number of dendritic spines and synaptic density. **(A)** Representative images of DIV18 neurons treated with DOI, DMT, and LSD. Blue represents MAP2 and orange represents F-actin. Scale bar = 3 µm. **(B)** Quantification of number of dendritic spines per 10 µm (n = 39–47) **(C)** Quantification of spine type by percentages (n = 16–21). **(D)** Representative images of DIV18 neurons treated with DOI, DMT, and LSD. Green represents VGLUT1, magenta represents PSD-95, and orange represents MAP2. Scale bar = 10 µm. **(E)** Quantification of synaptic density (n = 39–40), **(F)** synapse size (n = 40–41), **(G)** VGLUT1 density (n = 38–41), and **(H)** PSD-95 density (n = 39–43) from **(D)**. Data plotted for **(B)** and **(E–H)** are represented as mean ± SEM. *p < 0.05, **p < 0.01, ***p < 0.001, ****p < 0.0001, as compared to VEH control. A one-way analysis of variance with a Dunnett's post hoc test was utilized. VEH = vehicle; VGLUT1 = vesicular glutamate transporter 1; PSD-95 = postsynaptic density protein

95; MAP2 = microtubule-associated protein 2; LSD = lysergic acid diethylamide; DOI = ± 2,5-Dimethoxy-4-iodoamphetamine; DMT = N,N-dimethyltryptamine.

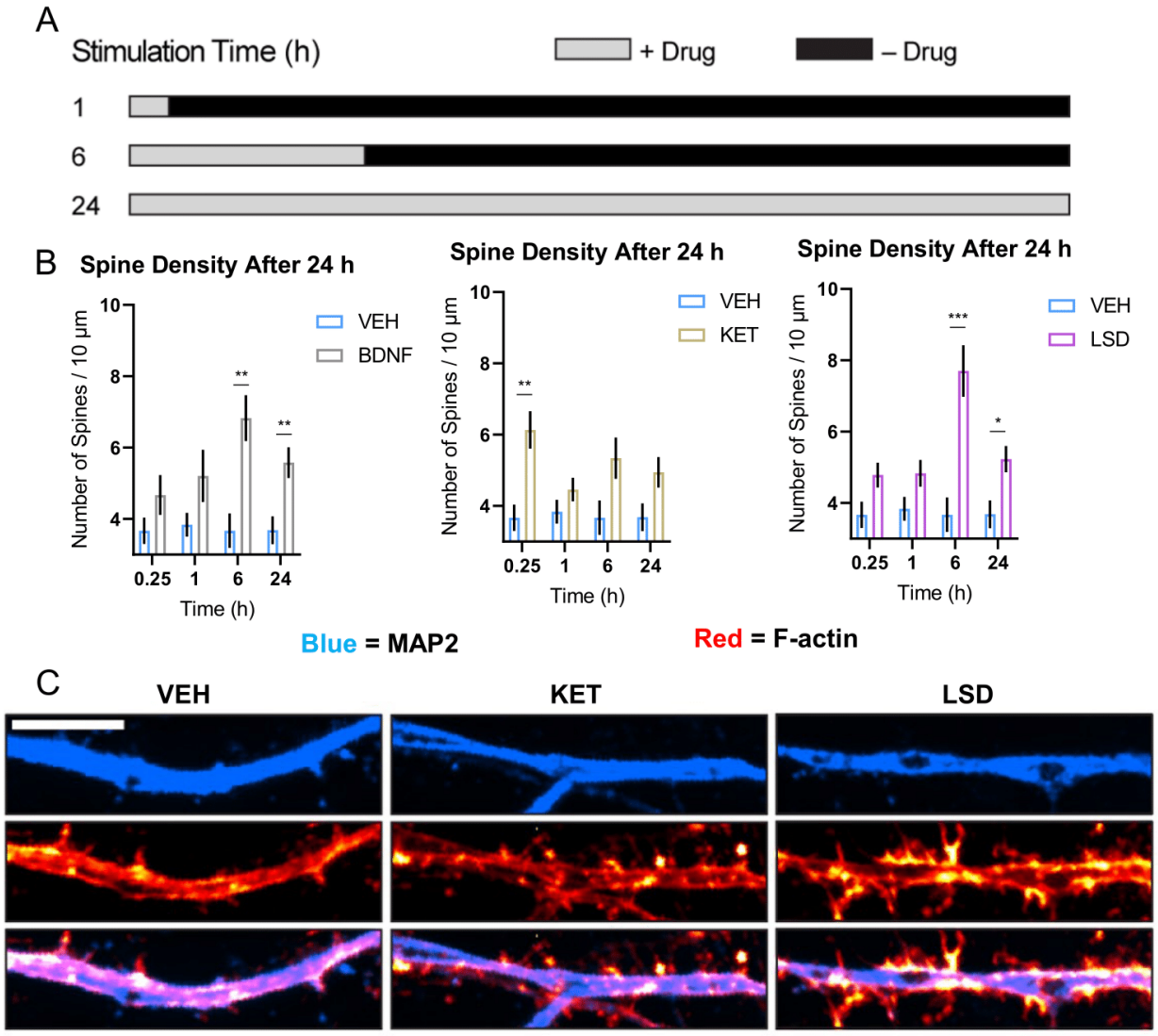

Figure 2.7. Short, transient stimulation with psychoplastogens increases the number of dendritic spines. **(A)** Timeline of stimulation time with (gray) and without (black) drug. **(B)** Spine density quantified following treatment with BDNF, ketamine (KET), and LSD for 15 minutes, 1 hour, 6 hours, and 24 hours (total growth period for all treatments is 24 hours). **(C)** Representative images of neurons that received drug for 6 hours followed by 18 hours of growth period in drug free medium. Blue represents MAP2 and red represents F-actin. Scale bar = 5 µm. Data are represented as mean ± SEM (n = 11–30 neurons). *p < 0.05, **p < 0.01,

***p < 0.001, ****p < 0.0001, as compared to VEH control following multiple t-tests and correction of p values for multiple comparisons using the Holm-Sidak method. VEH = vehicle; KET = ketamine; LSD = lysergic acid diethylamide; BDNF = brain-derived neurotrophic factor; MAP2 = Microtubule-associated protein 2.

We then wondered whether 24 hours of drug stimulation was too long. Ketamine is known to increase pre-and postsynaptic densities within 2 hours and reach a maximum response by 6 hours.[24] We postulated that like the neurite outgrowth, a shorter stimulation for dendritic spines and synaptic densities would still induce similar results. We designed a time course consisting of 15-minute, 1-hour, and 6-hour treatments followed by a change of medium into ligand-free media until a total of 24 hours had elapsed since the addition of ligand **(Fig 2.7A)**. When compared to the 24-hour time point in dendritic spines, we found that 6 hours of stimulation with ligand maximized the response of LSD and BDNF, whereas ketamine was slightly lower than both, indicating that LSD is more efficacious than ketamine and BDNF **(Fig 2.7B–C)**. Furthermore, at 6 hours of stimulation, the increase in synaptic density mirrored the timepoint of the dendritic spines **(Fig. 2.8B–C)**. We also found that at 6 hours, we see an increase in synaptic density for both LSD and BDNF. Ketamine, however, seems to require the remaining 18 hours to observe increases in synaptic density **(Fig. 2.8D)**. This result was further evidence that LSD may produce more rapid changes in neural plasticity than ketamine. The additional experiment to conduct in the future is to determine whether dendritic spines after 6 hours of stimulation is sufficient to induce maximal efficacy. I hypothesize that the 6 hours for ketamine will not induce a significant increase in the number of dendritic spines because synaptic density, in principle, also represents dendritic spine dynamics.

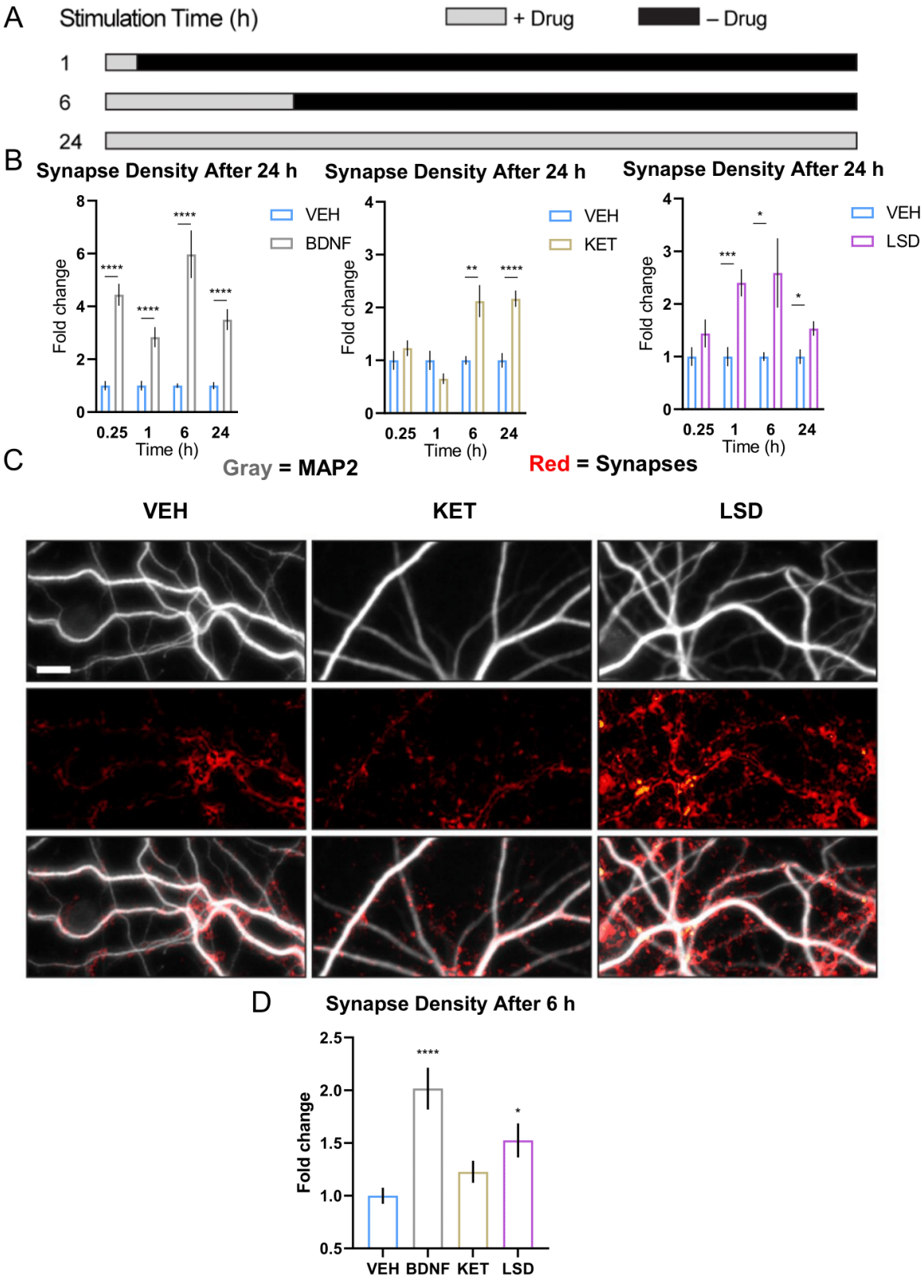
A
Stimulation Time (h)
+ Drug
– Drug
1
6
24
B
Synapse Density After 24 h
Fold change
VEH
BDNF
KET
LSD
Time (h)
0.25
1
6
24
C
Gray = MAP2
Red = Synapses
VEH
KET
LSD
D
Synapse Density After 6 h
VEH BDNF KET LSD

Figure 2.8. Short transient stimulation with the psychoplastogens increases synaptic density. **(A)** Timeline of stimulation time with (gray) and without (black) drug. **(B)** Synaptic density quantified following treatment with BDNF, ketamine (KET), and LSD for 15 mins, 1 hour, 6 hour, and 24 hours (total growth period for all treatments is 24 hours; n = 25–27 neurons). **(C)** Representative images of neurons that received drug for 6 hours followed by 18 hours of growth period in drug free medium. Gray represents MAP2 and red represents colocalization of VGLUT1 and PSD-95 densities. Scale bar = 10 μm. **(D)** Synaptic density measured after 6 hours of treatment (total growth period is 6 hours; n = 50–54 neurons). Data are represented as mean ± SEM. *p < 0.05, **p < 0.01, ***p < 0.001, ****p < 0.0001, as compared to VEH control. For **(B)**, multiple t-tests were performed and p values were corrected for multiple comparisons using the Holm-Sidak method. For **(D)**, a one-way analysis of variance with a Dunnett's post hoc test was utilized. VEH = vehicle; KET = ketamine; LSD = lysergic acid diethylamide; BDNF = brain-derived neurotrophic factor; MAP2 = Microtubule-associated protein 2.

Chapter 2.4 Inhibition of TrkB and mTOR Block Psychedelic-induced Growth

After we saw an increase in all three structural plasticity phenotypes, we sought to examine the potential mechanisms of actions responsible for the changes from the stimulation with classic psychedelics. As we observed changes in total BDNF protein levels, we first targeted the TrkB receptor, the endogenous receptor for BDNF. We first blocked 50 ng/mL BDNF with 10 μM ANA-12 **(Fig. 2.9A)**—a selective TrkB inhibitor— to confirm that we could abolish neurite outgrowth induced by the endogenous ligand **(Fig 2.9B)**.[25,26] We chose the 10 μM dose for ANA-12 because the Kd of the high- and low-affinity binding pockets of TrkB are 10 nM and 12 μM, respectively. [27] ANA-12 inhibited the psychedelic-induced increases in neurite outgrowth **(Fig 2.9C–G)**. Furthermore, we conducted ANA-12 blocking experiments in dendritic spines and found that inhibition of TrkB also resulted in blocking psychedelic-induced increases **(Fig. 2.9H)**. These results suggested that TrkB may be playing a role in the effects of classic psychedelics. BDNF protein may be upregulated by the classic psychedelics through activation of TrkB and leading to the phosphorylation of mTOR to facilitate the changes in structural plasticity.[28] To examine the role of mTOR in psychedelic-induced structural plasticity, we attempted to inhibit the neurite outgrowth phenotype with rapamycin (100 nM, **Fig. 2.10A**). As expected, blocking mTOR abolished all increases of neurites induced by classic psychedelics **(Fig. 2.10B–F)**. Furthermore, rapamycin did not reduce basal level neurite outgrowth, thus indicating rapamycin blocked psychedelic-induced growth.

25. Cazorla, M.; Prémont, J.; Mann, A.; Girard, N.; Kellendonk, C.; Rognan, D. Identification of a low-molecular weight TrkB antagonist with anxiolytic and antidepressant activity in mice. *J Clin Invest*. **2011**, *121*, 1846–1857.
26. ANA-12 is not soluble in water. To facilitate solubility, ANA-12 was dissolved in Dimethyl sulfoxide (DMSO) and when dilutions were made, media containing 1x B-27 serum free supplement was used to assist in the solubility.
27. Cazorla, M.; Prémont, J.; Mann, A.; Girard, N.; Kellendonk, C.; Rognan, D. Identification of a low-molecular weight TrkB antagonist with anxiolytic and antidepressant activity in mice. *J Clin Invest.* **2011**, *121*, 1846–1857.
28. Takei, N.; Inamura, N.; Kawamura, M.; Namba, H.; Hara, K.; Yonezawa, K.; Nawa, H. Brain-derived neurotrophic factor induces mammalian target of rapamycin-dependent local activation of translation machinery and protein synthesis in neuronal dendrites. *J. Neurosci.* **2004**, *24*, 9760–9769.

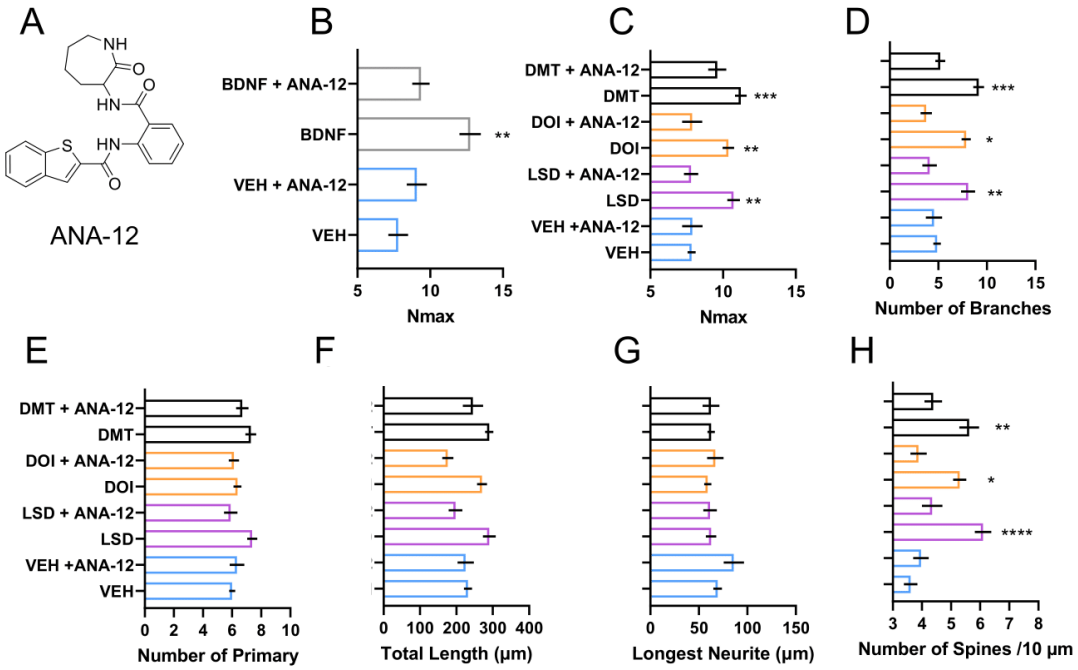

Figure 2.9. ANA-12, a selective inhibitor of TrkB, blocks the increase in neurite outgrowth and number of dendritic spines. **(A)** Structure of ANA-12. **(B)** 50 ng/mL BDNF is blocked by 10 µM ANA-12 (n = 11–15). **(C–G)** Quantification of neurite outgrowth via the Simple Neurite Tracer and Sholl analysis plug-ins using ImageJ Fiji shows that ANA-12 blocks **(C)** Nmax, and the **(D)** number of branches. However, no significant changes were observed with **(E)** number of primary dendrites, **(F)** the total neurite length, and **(G)** the longest neurite (n = 8–10 neurons). **(H)** ANA-12 cotreatment was able to abolish the increase in number of dendritic spines (n = 19–21 neurons). Data on **(B–H)** are represented as mean ± SEM. *p < 0.05, **p < 0.01, ***p < 0.001, ****p < 0.0001, as compared to VEH + ANA-12 control. For **(B–H)**, a one-way analysis of variance with a Dunnett's post hoc test was utilized. VEH = vehicle; BDNF = brain-derived neurotrophic factor, LSD = lysergic acid diethylamide; DOI = ± 2,5-Dimethoxy-4-iodoamphetamine; DMT = N,N-dimethyltryptamine.

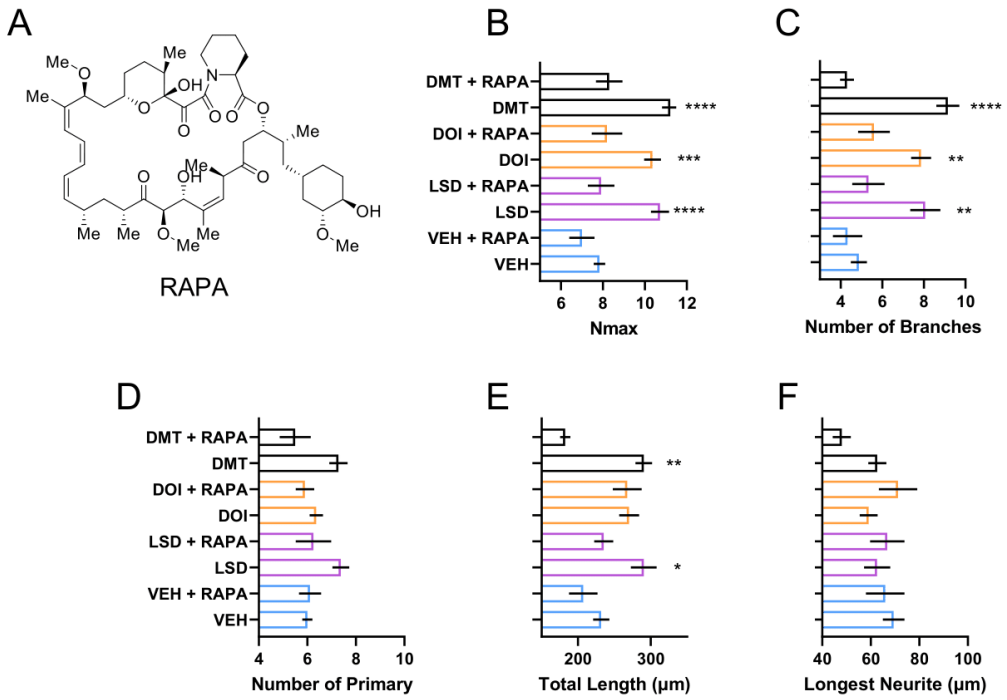

Figure 2.10. Rapamycin, an inhibitor of mTOR, blocks the increase in neurite outgrowth and number of dendritic spines. **(A)** Structure of RAPA. **(B–F)** Quantification of neurite outgrowth via the Simple Neurite Tracer and Sholl analysis plug-ins using ImageJ Fiji shows that 100 nM RAPA[29] blocks **(B)** Nmax, **(C)** number of branches and some blocking in **(E)** the total neurite length. However, no significant changes were observed with **(D)** number of primary dendrites and **(F)** the longest neurite. Data on **(B–F)** are represented as mean ± SEM (n = 9–12 neurons). *p < 0.05, **p < 0.01, ***p < 0.001, ****p < 0.0001, as compared to VEH + RAPA control. For **(B–F)**, a one-way analysis of variance with a Dunnett's post hoc test was utilized. VEH = vehicle; RAPA = rapamycin, LSD = lysergic acid diethylamide; DOI = ± 2,5-Dimethoxy-4-iodoamphetamine; DMT = N,N-dimethyltryptamine.

29. Rapamycin is dosed at 100 nM to inhibit both mTOR and s6k1. This concentration was chosen as a range (20 nM–200 nM) of rapamycin doses reported in vitro. See the following:
(a) Smith, E.D.; Prieto, G.A.; Tong, L.; Sears-Kraxberger, I.; Rice, J.D.; Steward, O.; Cotman, C.W. Rapamycin and interleukin-1β impair brain-derived neurotrophic factor-dependent neuron survival by modulating autophagy. *J Biol Chem*. **2014**, *289*, 20615–20629.
(b) Fletcher, L.; Evans, T.M.; Watts, L.T.; Jimenez, D.F.; Digicaylioglu, M. Rapamycin treatment improves neuron viability in an in vitro model of stroke. *PLoS One.* **2013**, *8*, e68281.
Future studies for neurite outgrowth, the number of dendritic spines, synaptic density should use a lower dosage of rapamycin (20 nM) to test whether these phenotypes can be abolished.

Chapter 2.5 Ketanserin Blocks Psychedelic- and BDNF-induced Growth

The classic psychedelics are known as potent serotonergic agonists. Therefore we wanted to explore whether the serotonin receptors played a role in the structural plasticity phenotypes we observed. Gonzalez-Maeso et al.[30] has demonstrated that the 5-HT2ARs are necessarily for the head-twitch response (HTR), a behavioral phenotype in mice that correlates well with 5-HT2AR activation.[31] Furthermore, 5-HT2AR activation and downstream signaling are known to be relevant for antidepressants and antipsychotic drug actions.[32] Thus, we used ketanserin (KTSN), a 5-HT2R antagonist **(Fig. 2.11A)**, to attempt to block the neurite outgrowth phenotypes. We observed an inhibition of cell growth for all psychedelics tested, indicating a role of 5-HT2R in the neurite outgrowth phenotype **(Fig. 2.11B–F)**. Furthermore, we co-treated ketanserin with our psychedelics in our dendritic spine assay and found ketanserin inhibited the increase in dendritic spines **(Fig. 2.11G)**. This result suggested that 5-HT2R was playing a role in neural plasticity. We hypothesized that 5-HT2R and TrkB might be interacting with each other. An example of such interaction is a dimerization event that might cause the two receptors to signal through mTOR. I tested this hypothesis by co-treating BDNF with ketanserin and found that ketanserin could inhibit the neurite outgrowth induced by BDNF **(Fig. 2.11H)**. These data further suggests that the 5-HT2R and TrkB are interconnected and may interact at the receptor level that signals positive changes in neural plasticity. A caveat in these studies is the ketanserin concentration. During this study, 100 μM ketanserin was co-treated to obtain a 10-fold greater ligand concentration than what the psychedelics were treated (10 μM). We chose such a high dose because the upper limit of ketamine in the brain following an antidepressant dose in rats via intraperitoneal injection was ~10 μM.[33,34]

30. González-Maeso, J.; Yuen, T.; Ebersole, B.J.; Wurmbach, E.; Lira, A.; Zhou, M.; Weisstaub, N.; Hen, R.; Gingrich, J.A.; Sealfon, S.C. Transcriptome fingerprints distinguish hallucinogenic and nonhallucinogenic 5-hydroxytryptamine 2A receptor agonist effects in mouse somatosensory cortex. *J Neurosci.* **2003**, *23*, 8836–8843.
31. (a) Willins, D.L.; Meltzer, H.Y. Direct injection of 5-HT2A receptor agonists into the medial prefrontal cortex produces a head-twitch response in rats. *J Pharmacol Exp Ther* 1997, *282*, 699–706.
(b) Gewirtz, J.C.; Marek, G.J. Behavioral evidence for interactions between a hallucinogenic drug and group II metabotropic glutamate receptors. *Neuropsychopharmacology* **2000**, *23*, 569–576.
32. Roth, B.L.; Berry, S.A.; Kroeze, W.K.; Willins, D.L.; Kristiansen, K. Serotonin 5-HT2A receptors: molecular biology and mechanisms of regulation. *Crit Rev Neurobiol.* **1998**, *12*, 319–338.
33. Yang, Y.; Cui, Y.; Sang, K.; Dong, Y.; Ni, Z.; Ma, S.; Hu, H. Ketamine blocks bursting in the lateral habenula to rapidly relieve depression. *Nature*. **2018**, *554*, 317–322.
34. One of the major limitations of this study is the heroic levels of ketanserin used here. At the time, we had not established the working range of doses that would induce neural plasticity yet. We now know that as low as 100 nM psychoplastogen will induced neural plasticity. Furthermore, because of such a high dose, polypharmacology and off-target effects may be contributing to the response seen here. Lastly, at 100 μM doses of ketanserin, I experienced some level of precipitation due to the low solubility of the

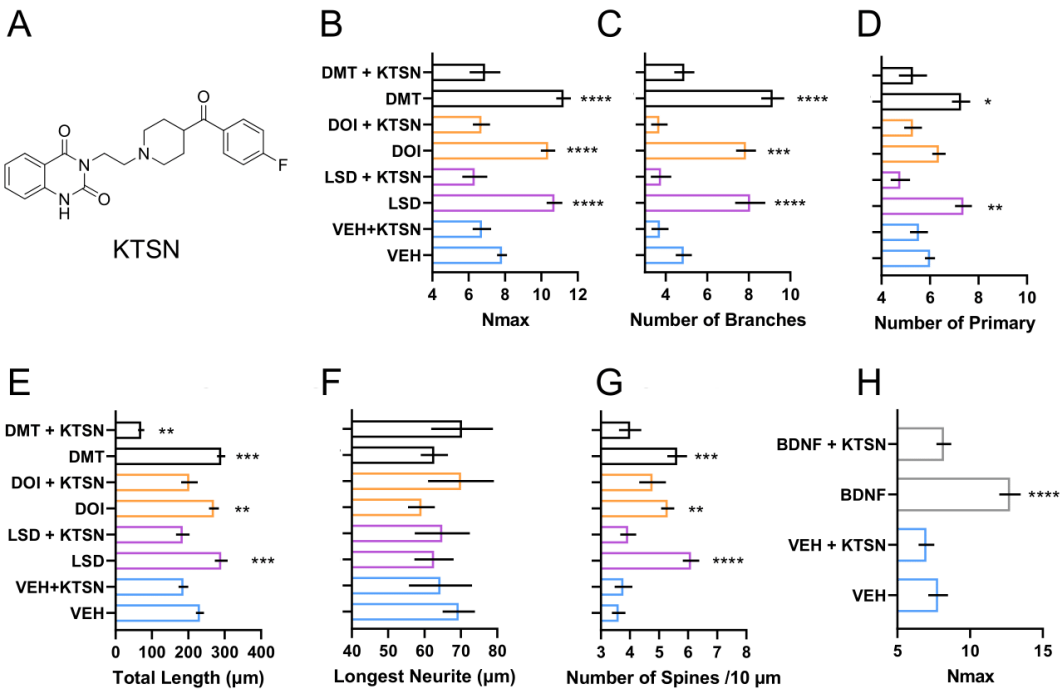

Figure 2.11. Ketanserin, an antagonist of the serotonin 2 receptor, blocks the increase in neurite outgrowth and number of dendritic spines. **(A)** Structure of ketanserin (KTSN). **(B–F)** Quantification of neurite outgrowth via the Simple Neurite Tracer and Sholl analysis plug-ins using ImageJ Fiji shows that 100 µM KTSN blocks **(B)** Nmax, **(C)** number of branches, **(E)** the total neurite length, and some blocking in **(D)** the number of primary dendrites. However, no significant changes were observed with **(F)** the longest neurite. **(H)** KTSN also blocks BDNF and its ability to increase Nmax. For **(B–G)**, n = 19–46 neurons. For **(H)**, n = 11-16 neurons. For **(B–H)**, a one-way analysis of variance with a Dunnett's post hoc test was utilized. VEH = vehicle; KTSN = ketanserin; LSD = lysergic acid diethylamide; DOI = ± 2,5-Dimethoxy-4-iodoamphetamine; DMT = N,N-dimethyltryptamine BDNF = brain-derived neurotrophic factor.

free base ketanserin. Thus, to increase solubility, I used media containing 1x B-27 serum free supplement to assist in preventing ketanserin from precipitating out of solution.

Chapter 2.6 Prolonged Activation of mTOR and AMPARs, But Not TrkB, is Required for Neurite Outgrowth

---

To further probe the mechanism of action of the psychoplastogens, I separated ligand and inhibition into two epics: co-treatment (stimulation) and post-treatment (growth period) antagonizing studies. In the stimulation epoch, ligand and antagonist are co-treated for 1 hour. Next, I replaced the media with drug-free feeding media after 1 hour. The cells were allowed to grow for 71 hours **(Fig. 2.12A)**. In the post-treatment antagonizing studies, the ligand is treated first for an hour. Then I removed the media and replaced it with the proper concentration of antagonist in the feeding media. The cells were allowed to grow for 71 hours. We chose the 1-hour stimulation because we previously showed that 1 hour was sufficient stimulation to induce long-lasting structural plasticity changes in neurite outgrowth **(Fig. 2.5)**.

Previously, we observed that chronically antagonizing TrkB abolished psychoplastogen-induced neurite outgrowth. We hypothesized that psychoplastogen-induced neuritogenesis required TrkB activation during the first hour and not the remaining 71 hours of growth. TrkB signaling is known to upregulate BDNF transcripts and thus the translation of BDNF protein. BDNF protein then induces the upregulation of neural plasticity through the activation of TrkB and continues this positive feedback loop to potentiate the signaling pathways, primarily through the activation of MAPK pathways.[35] Thus, once initiated, we anticipated continuous cell signaling downstream leading to long-lasting changes in neurite outgrowth. As expected, ANA-12 co-treatment with ligand prevented the long-lasting changes in neurite outgrowth. TrkB inhibition in the growth period (latter 71 hours) did not block the neurite outgrowth **(Fig. 2.12B–C)**. These data suggested TrkB activation with psychoplastogens is critical for the initiation of neurite outgrowth but not the maintenance. Earlier, we showed that inhibition of mTOR abolished the neurite outgrowth induced by psychedelics. Thus, we wanted to explore the effects of blocking mTOR in both epics. Rapamycin (RAPA) blocked all cell growth regardless of when cortical cultures were treated **(Fig. 2.12D–E)**. Once again, it did not affect the basal level of neurite outgrowth as RAPA-treated neurons had similar structural plasticity changes to VEH-treated neurons. To further probe the system, preclinical data shows the mechanism of

35. Tuvikene, J.; Pruunsild, P.; Orav, E.; Esvald, E.E.; Timmusk, T. AP-1 Transcription Factors Mediate BDNF-Positive Feedback Loop in Cortical Neurons. *J Neurosci.* **2016**, *36*, 1290–1305.

action of ketamine to be associated with an increase in glutamate in the synapse facilitating AMPAR activation and the release of BDNF.[24,36] Thus, we attempted to block AMPAR, using 6,7-dinitroquinoxaline-2,3-dione (DNQX, 20 μM). To our surprise, DNQX inhibited growth in both the co-treatment and post-treatment experiments **(Fig. 2.12F–G)**. This result indicated the critical role that AMPAR signaling played in neurite outgrowth. Next, we were curious as to whether the neuronal activity would synergize with psychoplastogens. Thus, we treated cortical cultures with KCl (40 mM), which is known to induce depolarization and glutamate release in neurons.[37] In the co-treatment, we saw no significant changes in neurite outgrowth **(Fig. 2.12H)**. Thus, we were able to determine that TrkB activation is required only during the initial stimulation. mTOR and AMPAR activation is required from initiation to growth to see significant increases in neurite outgrowth. Finally, a recent study showed the importance of the serotonin 1A receptor (5-HT1AR) in ketamine's antidepressant behaviors.[38] As LSD is a potent 5-HT1AR agonist, we wanted to rule out the 5-HT1A receptor by using the selective agonist 7-(dipropylamino)-5,6,7,8-tetrahydronaphthalen-1-ol (8-OH-DPAT), which has previously been demonstrated to have antidepressant like effects and are blocked by NBQX (an analogous inhibitor of AMPARs to DNQX) and anti-BDNF neutralizing antibody.[39] We found that ketamine and LSD dose dependently increased neurite outgrowth, however, the 5-HT1A agonist 8-OH-DPAT did not elicit any changes in neuritogenesis **(Fig. 2.12I)**. At the concentration of 10 μM 8-OH-DPAT, we start seeing a trend of increasing neurite outgrowth, however, at that concentration, 8-OH-DPAT begins to interact with 5-HT2AR, which might explain why it demonstrates some antidepressant potential.[39,40]

36. Koike, H.; Iijima, M.; Chaki, S. Involvement of AMPA receptor in both the rapid and sustained antidepressant-like effects of ketamine in animal models of depression. *Behav. Brain Res.* **2011**, *224*, 107–111.
37. Tavares, R.G.; Tasca, C.I.; Santos, C.E.; Alves, L.B.; Porciúncula, L.O.; Emanuelli, T.; Souza, D.O. Quinolinic acid stimulates synaptosomal glutamate release and inhibits glutamate uptake into astrocytes. *Neurochem Int.* **2002**, *40*, 621–627.
38. Fukumoto K, Iijima M, Funakoshi T, Chaki S. Role of 5-HT1A Receptor Stimulation in the Medial Prefrontal Cortex in the Sustained Antidepressant Effects of Ketamine. Int J Neuropsychopharmacol. 2018 Apr 1;21(4):371-381.
39. Fukumoto, K.; Fogaça, M.V.; Liu, R.J.; Duman, C.H.; Li, X.Y.; Chaki, S.; Duman, R.S. Medial PFC AMPA receptor and BDNF signaling are required for the rapid and sustained antidepressant-like effects of 5-HT1A receptor stimulation. *Neuropsychopharmacology.* **2020**, *45*, 1725–1734.
40. McKenna, D.J.; Peroutka, S.J. Differentiation of 5-hydroxytryptamine2 receptor subtypes using 125I-R-(-)2,5-dimethoxy-4-iodo-phenylisopropylamine and 3H-ketanserin. *J. Neurosci.* **1989**, *9*, 3482–3490.

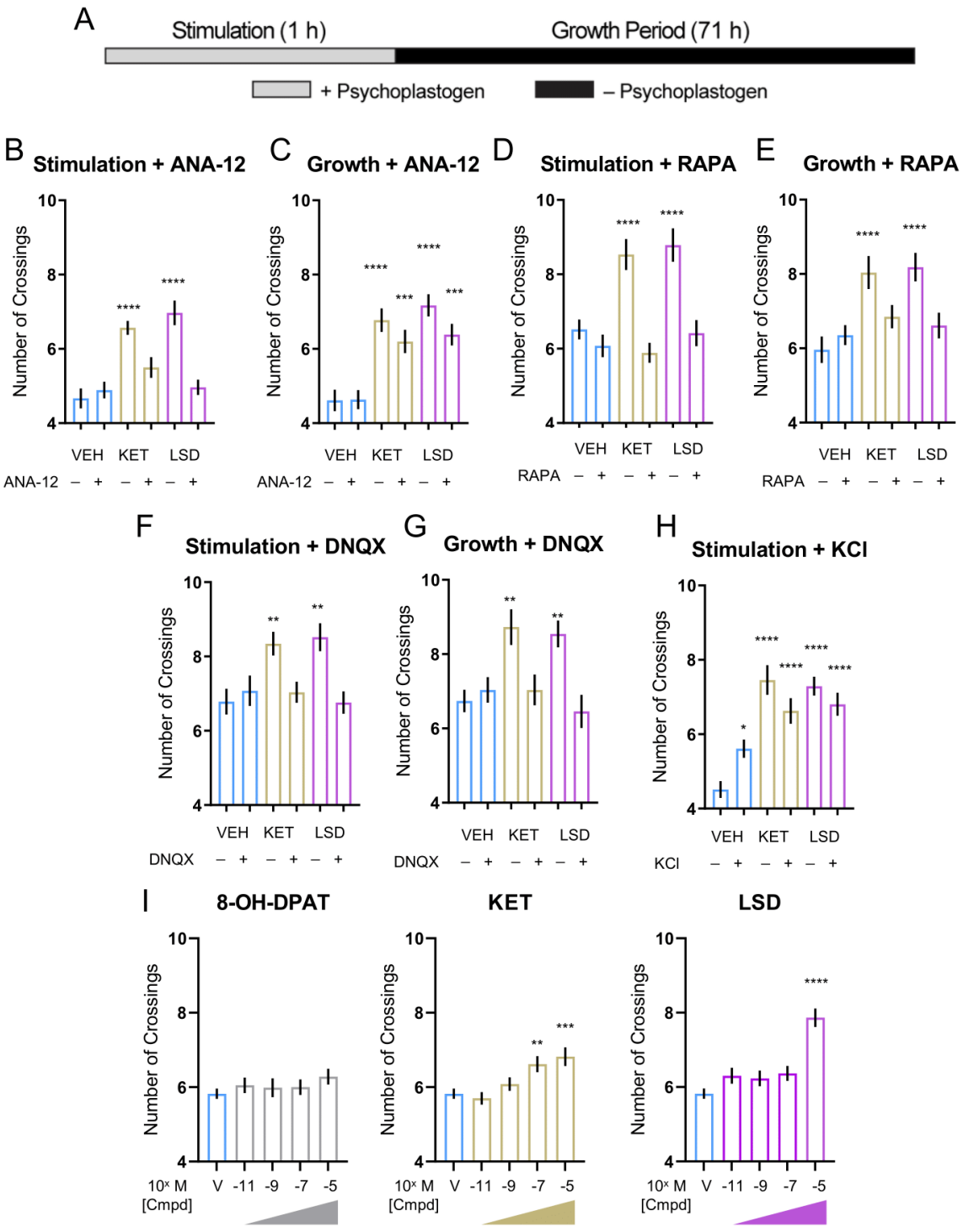

Figure 2.12. TrkB, mTOR, and AMPAR play a role in the neurite outgrowth of short-, transient-stimulation with the psychoplastogens. **(A)** Timeline of stimulation time with (gray) and without (black) drug. **(B–C)** ANA-12 cotreated with compound blocked the effects of LSD and ketamine **(B)** but not when treated during

the growth period **(C)**. **(D–E)** RAPA treatments blocked Nmax during both **(D)** cotreatment and **(E)** growth period. **(F–G)** DNQX blocked Nmax during both **(F)** cotreatment and **(G)** growth period. **(H)** KCl (40 mM) applied during the stimulation phase. **(I)** A 5-HT1A agonist 8-OH-DPAT does not induce neurite outgrowth whereas KET (NDMA antagonist) and LSD (5-HT receptors agonist) do dose dependently. Data are represented as mean ± SEM (n = 22–41 neurons). *p < 0.05, **p < 0.01, ***p < 0.001, ****p < 0.0001, as compared to VEH control without inhibitor following a one-way analysis of variance with a Dunnett's post hoc test. VEH = vehicle; KET = ketamine; LSD = lysergic acid diethylamide; DNQX = 6,7-dinitroquinoxaline-2,3-dione; RAPA = rapamycin; KCl = potassium chloride; 8-OH-DPAT = 7-(dipropylamino)-5,6,7,8-tetrahydronaphthalen-1-ol.

Chapter 2.7 Conclusion

Psychedelics, like ketamine, have garnered much attention for their antidepressant-like properties and rapid onset of therapeutic action. We have demonstrated here that, like ketamine, the classic psychedelics can robustly promote increases in structural plasticity. Furthermore, these changes in neuritogenesis, spinogenesis, and synaptogenesis may be responsible for the therapeutic actions of these molecules. We further evaluated the mechanism of psychedelics and discovered that TrkB, mTOR, and 5-HT2R signaling mediates their ability to promote structural plasticity. Next, we examined ketamine and LSD and observed that TrkB, AMPAR, and mTOR signaling mediates their ability to promote structural plasticity. We hypothesize that 5-HT2Rs are responsible for psychedelic-induced plasticity. TrkB, AMPAR, and mTOR signaling may be activated downstream of 5-HT2R. These data suggest that psychedelics are mechanistically like ketamine with the exception that 5-HT2R is involved.[41] However, both scaffolds have the same phenotypic output following treatment. Thus, a phenotypic drug discovery platform such as neuroplasticity would likely lead to improved therapeutic leads. Classic psychedelics promote structural plasticity in cortical cultures and serve as potential scaffolds to develop next-generation therapeutics.

While the chronic and short-stimulated neural plasticity assays allow us to explore what and when receptors/pathways need to be active for neurite outgrowth, we still need to further investigate these chronic and short-stimulation studies in dendritic spines and synaptic density. Moreover, using this 1-hour stimulation followed by 71 hours of growth allowed me to obtain a reasonable dose-response. This result indicates that short stimulation of ligand is a better model for measuring structural plasticity. Furthermore, this model is more relevant as most psychoplastogens have shorter half-lives in vivo than the 72 hours of stimulation in our earlier studies. A model with shorter incubation times better mimics drug administration in patients. Therefore, a standardized primary assay to facilitate, optimize, and prioritize lead therapeutics for the treatment of depression would accelerate the efforts for next-generation antidepressants. The following chapters will discuss the development of two separate orthogonal assays: an antidepressant

41. I have blocked ketamine-induced neurite outgrowth with ketanserin (data not shown). This likely indicates ketamine also may have an effect at the 5-HT2 receptors. This dose of ketanserin was at 100 μM and so many off-target receptors may have mired this result. Further studies with lower doses of ketanserin and ketamine may help to elucidate the role of 5-HT2R in ketamine-induced neural plasticity.

potential assay and a counter screen assay for off-target effects relating to the hallucinogenic potential of hallucinogenic congeners.

Chapter 2.8.1 General Methods for Chapter 2

Drugs

The NIH Drug Supply Program provided (+)-Lysergic acid diethylamide (+)-tartrate (2:1) (LSD), (±)-3,4-methylenedioxymethamphetamine hydrochloride (MDMA), psilocin (PSI), D-amphetamine hydrochloride (D-AMP). Other chemicals/proteins were purchased from commercial sources such as ketamine hydrochloride (KET, Fagron), serotonin hydrochloride (5-HT, Alfa Aesar) 7,8-dihydroxyflavone (7,8-DHF, TCI), ANA-12 (MedChem Express), rapamycin (RAPA, Alfa Aesar), ketanserin (KETSN, ApexBio), (±)-2,5-dimethoxy-4-iodoamphetamine (DOI, Cayman), (±)-8-hydroxy-2-(dipropylamino)tetralin hydrobromide (8-OH-DPAT, Sigma), potassium chloride (KCl, Fisher Scientific), 6,7-dinitroquinoxaline-2,3-dione (DNQX, Sigma), brain-derived neurotrophic factor (BDNF, Sigma). The fumarate salts of *N*,*N*-dimethyltryptamine (DMT) was synthesized in-house as described previously. All stock solutions were 10 mM except for the following: DMT (90 mM), DNQX (20 mM), KTSN (100 mM), RAPA (100 µM), and BDNF (100µg/mL, dissolved in Nuclease-free water, VWR). All drugs were dissolved in DMSO unless otherwise statedThe final concentration of ligand was 10 µM and 0.1% DMSO except for DMT (90 µM), BDNF (50 ng/mL) and KCl (40 mM). For inhibition studies, the inhibitor final concentration varied depending on the inhibitor: RAPA (100 nM), KTSN (100 µM), DNQX (20 µM), and ANA-12 (10 µM). All antagonist studies were conducted with final concentration of DMSO of 0.2%.

Animals

All experimental procedures involving animals were approved by the University of California, Davis Institutional Animal Care and Use Committee (IACUC) and adhered to principles described in the National Institutes of Health Guide for the Care and Use of Laboratory Animals. The University of California, Davis is accredited by the Association for Assessment and Accreditation of Laboratory Animal Care International (AAALAC).

Rat embryonic cortical cultures

Coating media was generated using 2.48g boric acid (BDH) and 3.80g borax (MP) dissolved in 900 mL of water. The mixture was stirred overnight at room temperature to dissolve the solid. The next day, the pH of the solution was adjusted to 8.5 with 1N HCl or 1N NaOH. Next, two bottles of poly-D-lysine hydrobromide (10 mg/ bottle×2) were added. Autoclaved water was used to filled to 1L for a final PDL concentration of 20 µg/mL PDL hydrobromide. The media was stirred overnight. The next day it was then filtered and stored in the dark at 4°C.

Plating media was generated by combining 500 mL Neurobasal Medium (Fisher Scientific), 50 mL Heat Inactivated (HI) FBS (Fisher Scientific), 1.25 mL 200mM glutamine (Fisher Scientific), and 5 mL penicillin-streptomycin (Fisher Scientific). The media was then filtered and stored in the dark at 4°C.

HBSS 1X was generated by combining 100 mL 10X HBSS (Fisher Scientific), 20 mL 1M HEPES (Fisher Scientific) 10 mL penicillin-streptomycin (Fisher Scientific) and filling to 1 L with autoclaved water. The HBSS was filtered and stored in the dark at 4°C.

Replacement media (50 mL) was generated by combining 48.5 mL Neurobasal Medium (Fisher Scientific), 1 mL B-27(Fisher Scientific), 125 µL 200mM glutamine (Fisher Scientific), 62.5 µL 10 mM glutamic acid (Fisher Scientific), and 0.5 mL penicillin-streptomycin (Fisher Scientific). The replacement media was prewarmed to 37°C before use and made fresh.[42]

Feeding media (50 mL) was generated by combining 48.5 mL Neurobasal Medium (Fisher Scientific), 1 mL B-27(Fisher Scientific), 125 µL 200mM glutamine (Fisher Scientific), 0.5 mL penicillin-streptomycin (Fisher Scientific). The feeding media was prewarmed to 37°C before use and made fresh.[42]

General neurite outgrowth cell culturing in 24-well plates

42. When mixing, either invert or allow it to mix in the bead bath over time. Any bubbles generated is due to proteins in B-27 being denatured.

For **Figures 2.1B–N, 2.2B–H, 2.3A–G, 2.5B–C, 2.9B–G, 2.10B–F,** and **2.11B–F**, neurite outgrowth was conducted in a low-throughput manner assay 24-well plastic bottom plates (VWR) using the center 8 wells. This was conducted using methods previously described.[1a] In brief, 24-well plates were coated with 250 µL of coating media overnight at room temperature in the tissue culture hood. The next day, plates were washed 3× with 500 µL autoclaved water. After the last wash, 500 µL of plating media was added to each of the center 8 wells and autoclaved water was added to the remaining outer wells to reduce evaporation. The plates were placed into a 37°C and 5% CO_2 water-jacketed incubator prior to dissection. After dissection (see **Tissue Collection** below), 50,000 cells per well were added to each well and returned to the incubator. After 16–24 hours, plating media was aspirated and 500 µL of prewarmed replacement media was added to each well. Cells were ready to be treated at 3 days in vitro (DIV3).

General neurite outgrowth cell culturing in 96-well plates

For **Figures 2.4A–B, 2.5D,** and **2.12B–I**, neurite outgrowth assay was conducted in a medium-throughput assay using black 96-well plastic bottom plates (Corning) using the center 60 wells. 96-well plates were coated with 100 µL of coating media overnight at room temperature. The next day, plates were washed 3× with 200 µL autoclaved water. After the last wash, 200 µL of Neurobasal was added to each of the center 60 wells and autoclaved water was added to the remaining outer wells to reduce evaporation. The plates were placed into a 37°C and 5% CO_2 water-jacketed incubator prior to dissection. After dissection (see **Tissue Collection** below), the Neurobasal was aspirated and 200 µL of a 75,000 cell per mL diluted in plating media (final cell density of 15,000 cells per well) and returned to the incubator. [43] After 16–24 hours, plating media was aspirated and 200 µL of prewarmed replacement media was added to each well. Cells were ready to treat at DIV3.

General dendritic spine and synaptic density cell culturing in 24-well plates

For **Figures 2.6A–H, 2.7B–C, 2.9H,** and **2.11H**, dendritic spine and synapse experiments were conducted in a low-throughput assay using 24-well plastic bottom plates (VWR). First, 12 mm circular 1.5

43. While plating, I will continuously move the reservoir and pipette up and down with the multi-channel pipette every 5 columns. This is to prevent cells from settling on the bottom of the reservoir. Additionally, if I am plating greater than 3 plates at a time (greater than 45 mL volume of plating media and cells as we use 50 mL reservoirs), I use a new reservoir for every additional set of 3 plates.

mm thick coverslips (Fisher Scientific) were briefly dipped in 70% ethanol and flame sterilized using an ethanol flame.[44] After, coverslips and a pair of tweezers were covered with foil and were autoclaved on the dry cycle for 30 minutes. Once coverslips were sterilized, autoclaved, and cooled, they were sprayed with 70% ethanol and placed into the tissue culture (TC) hood. The tweezers were sprayed with 70% ethanol and wiped down for any residue that might have accumulated during the flame sterilization. Next, a single coverslip was added into each of the center 8 wells on a 24-well plate. These wells and coverslips were coated with coating media overnight at room temperature in the TC hood with 500 µL. The coverslips were gently pressed down to ensure it was completely submerged in the coating media. The next day, coating media was aspirated and washed 3× with 500 µL autoclaved water.[45] After the last wash was aspirated, 500 µL plating media was added to each of the 8 center wells. Autoclaved water was added to the remaining 16 wells to protect against evaporation. Plates were then put into a water-jacketed incubator at 37°C at 5% CO_2 before beginning dissection. 24-well plates are plated at 35,000 cells per well. Plates were then put back into a water-jacketed incubator at 37°C at 5% CO_2. After 16–24 hours, plating media was aspirated and 500 µL replacement media per well was added. On DIV6 and DIV13, 250 µL of the culture media in the well was removed and 350 µL of prewarmed feeding media was added. Cells were treated on DIV18–20.

Fixing procedure for 24- and 96-well plates

After treatments are complete, cells were fixed and stained. To fix cells, the plates were removed from the incubator and checked under a light microscope and returned to the incubator. Following this, in a chemical fume hood, 16% stock paraformaldehyde (PFA, Fisher Scientific) was diluted to 4% PFA in dPBS (1:3 dilution, 10 mL PFA into 30 mL dPBS, total volume 40 mL, 4% final concentration of PFA).[46] The solution was warmed to 37°C. The plates were then removed from incubator and into the chemical fume

44. I recommend using 70% ethanol here because 100% ethanol burns off quick, thus heating up the coverslips too quickly and causing them to crack and break. The extra water content prevents it from cracking.
45. To make sure the coverslips do not float up after this step, I will aspirate off any air that may be underneath the coverslips. This helps to make sure the coverslip is completely flat on the bottom of the well.
46. From experience, this 4% PFA solution can be freeze-thawed to up to 5 times. To avoid this, make 5 mL aliquots to freeze to prevent multiple freeze thaws. Next, I do not recommend leaving the 4% PFA in the bead bath at 37°C as PFA can polymerize and not fix your cells. Furthermore, when making the 4% PFA dilutions from 16%, use dPBS and not Neurobasal. Neurobasal contains amino acids that will crosslink with the PFA and render it inactive. Lastly, when fixing, do not exceed 25 minutes incubation and do not fix at 4°C. Fixing beyond 25 minutes will cause additional crosslinking that may occlude the epitope for your antibody. Fixing cells at 4°C causes your cells to contract and will affect the morphology of your cells. Neurites will retract as well during this. Lastly, I do recommend fixing using prewarmed 4% PFA at 37°C to avoid any retraction or contractions that may occur.

hood where 80% of the working volume per well (400 µL in 24-well plates and 160 µL in 96-well plates) was removed. Next, a 50% working volume of 4% PFA (250 µL in 24-well plates and 100 µL in 96-well plates) was added per well.[47] The plates were incubated at room temperature without shaking for 20 minutes. After 20 minutes, the plates were washed with 3× dPBS (500µL in 24-well plates and 200 µL in 96-well plates) and filled with dPBS (500 µL in 24-well plates and 200 µL in 96-well plates). The cells were then either immediately stained or stored at 4°C until ready to begin staining procedure (viable up to 2 weeks).

Staining for neurite outgrowth assays

To stain, the dPBS was removed and the cells were permeabilized with a 0.2% Triton X-100 (Fisher Scientific) in dPBS (250 µL in 24-well plates and 100 µL in 96-well plates) solution for 20 minutes at room temperature without shaking. This 0.2% Triton X-100 solution was generated by combining 9.8 mL of dPBS and 200 µL of 10% Triton X-100. Next, a 2% bovine serum albumin (BSA, VWR) solution in dPBS was generated by dissolving 0.2g of BSA in 10 mL of dPBS.[48] Each well was blocked with 2% BSA for 1 hour at room temperature without shaking (250 µL in 24-well plates and 100 µL in 96-well plates). During the blocking, microtubule-associated protein 2 (MAP2, EnCor) chicken IgY antibody 1:10,000 was diluted into fresh 2% BSA. After 1 hour has elapsed, the blocking 2% BSA was aspirated and the 2% BSA solution containing MAP2 antibody was added (250 µL in 24-well plates and 100 µL in 96-well plates) and the plates were incubated overnight at 4°C. The next day (16–24 hours), plates were washed 3× with dPBS (500 µL in 24-well plates and 200 µL in 96-well plates) and 1× with fresh 2% BSA. A 1:500 dilution of goat anti-chicken IgY secondary antibody Alexa Fluor 488 conjugate (Life Technologies) in 2% BSA was generated. This 2% BSA solution containing the Alexa Fluor 488 was added into each well (250 µL in 24-well plates and 100 µL in 96-well plates). The plate was covered with foil and incubated at room temperature for 1 hour with gentle shaking. After 1 hour, the plates were washed 3× with dPBS (500 µL in 24-well plates and 200 µL in 96-well plates) and filled with dPBS after the last wash (500 µL in 24-well plates and 100 µL in 96-well plates). The plates were covered with foil and kept in the dark at 4°C until I was ready to image.

47. Neurons are extremely sensitive to changes in environment. Therefore, we retain 20% of the media to prevents the neurons from contracting and changing the morphology.
48. Do not vortex this solution, use a gentle rocking motion to mix the solution together. The vortex will denature the BSA.

Staining for dendritic spines assays

To stain, the dPBS was removed and the cells were permeabilized with a 0.2% Triton X-100 (Fisher Scientific) in dPBS (250 µL) solution for 20 minutes at room temperature without shaking. This 0.2% Triton X-100 solution was generated by combining 9.8 mL of dPBS and 200 µL of 10% Triton X-100. Next, a 2% bovine serum albumin (BSA, VWR) solution in dPBS was generated by dissolving 0.2g of BSA in 10 mL of dPBS.[48] Each well was blocked with 2% BSA for 1 hour at room temperature without shaking (250 µL). During the blocking, microtubule-associated protein 2 (MAP2, EnCor) chicken IgY antibody 1:10,000 was diluted into fresh 2% BSA. After 1 hour has elapsed, the blocking 2% BSA was aspirated and the 2% BSA solution containing MAP2 antibody was added (250 µL) and the plates were incubated overnight at 4°C. The next day (16–24 hours), plates were washed 3× with dPBS (500 µL) and 1× with fresh 2% BSA. A 1:500 dilution of goat anti-chicken IgY secondary antibody Alexa Fluor 568 conjugate (Life Technologies) in 2% BSA was generated. This 2% BSA solution containing the phalloidin conjugated to Alexa Fluor 488 (Life Technologies) and anti-chicken Alexa Fluor 568 was added into each well (250 µL). The plate was covered with foil and incubated at room temperature for 1 hour with gentle shaking. After 1 hour, the plates were washed 3× with dPBS (500 µL) and filled with dPBS after the last wash (500 µL). The plates were covered with foil and kept in the dark at 4°C until I was ready to mount.

Staining for synaptic density assays

To stain, the dPBS was removed and the cells were permeabilized with a 0.2% Triton X-100 (Fisher Scientific) in dPBS (250 µL in 24-well plates and 100 µL in 96-well plates) solution for 20 minutes at room temperature without shaking. This 0.2% Triton X-100 solution was generated by combining 9.8 mL of dPBS and 200 µL of 10% Triton X-100. Next, a 2% bovine serum albumin (BSA, VWR) solution in dPBS was generated by dissolving 0.2g of BSA in 10 mL of dPBS.[48] Each well was blocked with 2% BSA for 1 hour at room temperature without shaking (250 µL in 24-well plates and 100 µL in 96-well plates). During the blocking, microtubule-associated protein 2 (MAP2) chicken IgY (EnCor, 1:10,000), guinea pig anti-VGLUT1 (Millipore, 1:1000), and mouse anti-PSD-95 (Millipore, 1:500) antibodies was diluted into fresh 2% BSA. After 1 hour has elapsed, the blocking 2% BSA was aspirated and the 2% BSA solution containing MAP2

antibody was added (250 µL in 24-well plates and 100 µL in 96-well plates) and the plates were incubated overnight at 4°C. The next day (16–24 hours), plates were washed 3× with dPBS (500 µL in 24-well plates and 200 µL in 96-well plates) and 1× with fresh 2% BSA. A 1:500 dilution of goat anti-chicken IgY secondary antibody Alexa Fluor 488 (Life Technologies, 1:500), Cy3 AffiniPure donkey anti-guinea pig IgG (H+L) (Jackson ImmunoResearch Inc, 1:500), and Alexa Fluor 647 AffiniPure donkey anti-Mouse IgG (H+L) (Jackson ImmunoResearch Inc, 1:500) in 2% BSA was generated. This 2% BSA solution containing the phalloidin conjugated to Alexa Fluor 488 (Life Technologies) and anti-chicken Alexa Fluor 568 was added into each well (250 µL in 24-well plates and 100 µL in 96-well plates). The plate was covered with foil and incubated at room temperature for 1 hour with gentle shaking. After 1 hour, the plates were washed 3× with dPBS (500 µL in 24-well plates and 200 µL in 96-well plates) and filled with dPBS after the last wash (500 µL in 24-well plates and 100 µL in 96-well plates). The plates were covered with foil and kept in the dark at 4°C until I was ready to mount.

Mounting procedures

To mount, I used ProLong Gold Antifade Mountant (Thermofisher) and added a single drop onto a microscope slide (Fisher Scientific) using a P200 micropipette. Once the ProLong Gold was dropped onto the microscope slide, the dPBS in the well was aspirated and the coverslip was removed using a pair of tweezers. The coverslip was inverted onto the coverslip. The slides were then stored at room temperature for 24 hours to allow the ProLong Gold to cure. After 24 hours, the coverslip was sealed using clear nail polish. The slides were stored in a microscope slide box and kept in the dark at 4°C until I was ready to image.

Imaging and analysis for neurite outgrowth on 24-well plates.

24-well plate image acquisition was done on the Leica inverted epifluorescence microscope at 40x magnification. Images were then analyzed using the Simple Neurite Tracer and Sholl analysis plug-ins from ImageJ Fiji **(version 1.51N)**. In brief, neurons captured on epifluorescence microscopy were traced using the Simple Neurite Tracer plug-in. The initial neurite was set to the start at the center of the soma to establish an epicenter for the Sholl analysis plug-in to build concentric circles from. Next, neurites were

traced by hand and the "paths" of each trace were saved. Once fully traced, the traces were analyzed through the Sholl analysis plug-in and the data was output to Excel for further averaging between treatments. Sholl analysis circle radii = 2 μm increments. All images were taken and analyzed by an experimenter blinded to treatment conditions.

Imaging and analysis for neurite outgrowth on 96-well plates.

96-well plate image acquisition was done on the Molecular Devices ImageXpress Micro XLS Widefield High-Content Analysis System at 9 sites per well using 20x magnification. Images were analyzed using the Sholl analysis plug-in ImageJ Fiji **(version 1.51N)**. First, 0–2 representative neurons were selected per site using the "rectangle" function.[49] Once neurons were selected, a copy of the selected neuron would be generated using the "duplicate" function. After selecting all the neurons for that treatment group, duplicated copies were saved. Once all groups were completed, I was unblinded to VEH and KET plate controls[50] on the plate and adjusted "brightness and contrast" that was used for the rest of the plate.[51] Next, these "brightness and contrast" "maximum" and "minimum" values were recorded and applied to the images within the same plate. The images then were converted to a binary image using the "threshold" function. From there, the "minimum" and "maximum" values of the threshold were adjusted obtain the best binary image that represented the respective fluorescent image. These values were recorded. All "brightness and contrast" and "threshold" were kept the same between all images from the same plate. Finally, images were cleaned using the "paint brush" tool for artifacts in the image, and the center of the

49. This part is very subjective and can take a couple of attempts to get used to what is a representative neuron. We select neurons that are not overlapping with other neurons in the field of view (FOV). We search for pyramidal-like neurons and avoid bipolar neurons (neurons that only have two neurites growing on opposite sides of one another). Furthermore, I look at the FOV as a whole to determine the average neurite per soma and select the best representative(s) in that FOV. If the FOV has a very sparse number of neurons (generally less than 10 per FOV), I will opt to skip that FOV as the small sample size can skewer the results. Neurons that are alone have longer neurites and branch less. Neurons that are clustered together will have more branching and shorter neurites. Finding a neuron that is far enough away from each other while still having neighbors nearby for neurotrophic support will offer the best representative neuron. This publication for examples:
Dunlap, L. E.; Azinfar, A.; Ly, C.; Cameron, L. P.; Viswanathan, J.; Tombari, R. J.; Myers-Turnbull, D.; Taylor, J. C.; Grodzki, A. C.; Lein, P. J.; Kokel, D.; Olson, D. E. Identification of Psychoplastogenic N,N-Dimethylaminoisotryptamine (isoDMT) Analogs Through Structure-Activity Relationship Studies. *J. Med. Chem.*, **2020**, *63*, 1142–1155.
50. The ketamine (positive control) and vehicle (negative control) here are plate controls not used for publication. I use these as quality controls for my plates to ensure that the experiment worked and confirm the data recorded is robust. The edge wells (columns 2 and 11, 6 wells total per condition) are used as controls because these wells have the most potential for variability due to plate effects. I rotate ketamine and vehicle between the columns to prevent any bias during the selection of neurons.
51. This is critical as ketamine and other psychoplastogens will cause very thin, dim, minute neurites to grow that can be overlooked if the image brightness and contrast are not adjusted.

neuron was then dotted using the “point” function. Images were saved and ran through the “batch process macro” on ImageJ Fiji using the following script:

run("Sholl Analysis...", "starting=0 ending=NaN radius_step=2 #_samples=1 integration=Mean enclosing=1 #_primary=4 infer fit linear polynomial=[Best fitting degree] most semi-log normalizer=Area create background=228 save do");

Sholl analysis circle radii = 2-pixel increments. All analysis was done by blinded to treatment conditions except for VEH and KET plate controls.

Tissue Collection

Pregnant Sprague-Dawley dams were euthanized at embryonic day 18 (E18) via CO_2 and cortices of pups were extracted and placed into ice-cold 1X Hanks Buffered Saline Solution (HBSS, ThermoFisher) in a 14 mL culture tube. Afterward, cortices were washed 3× with sterile 1X HBSS in the tissue culture hood and removed HBSS until 2 mL of volume remained. 200 µL of 2.5% trypsin (10x, Fisher Scientific) was added and the culture tube was placed in a 37°C bead bath for 10 minutes. After 10 minutes, using a 10 mL serological pipette, only cortices were collected and moved into a new, sterile 14 mL culture tube. Cortices were washed 3× gently with cold 1X HBSS. Following the last wash, the tube was filled to a total volume of 6 mL with 1X HBSS. The cells were triturated using a 5 mL serological pipette to pipette up and down against the bottom of the tube. Following trituration, 10 µL of cell suspension was mixed with 10 µL of trypan blue stain 0.4% (ThermoFisher). Cell counting and viability was quantified on a slide for the TC20 automated Cell Counter (BioRad). Cell viability was recorded,[52] and cells are plated.[53] For specific sections of cell culture, please see the related figures.

52. Cell viability following dissection should be greater than 90% (with 90% being the lowest). Generally, the dissection will take a total of 2–3 hours, depending on the number of pups and plates being plated. Furthermore, I have noticed briefly that cell viability went down to 60–70% during dissection but immediately realized that trypan blue was expired and precipitating out of solution. Thus, make sure when doing the trypan blue staining that the trypan blue has no precipitants. See **Figure 1.1.**

53. Cells were diluted directly into the wells containing plating media. Then gently, keeping the plate flat on the TC hood, move the plate away and towards the experimenter, pause at the center, move the plate to the left and to the right, pause at the center, and repeat a total of three times. This is to help spread the cells out and equally distribute them. I pause to prevent a circular motion which would force your cells to the edge of the plate instead. Furthermore, make sure the plating media is warm (30°C–37°C). This is critical because cooled plating media will rewarm in the incubator. The rewarming process will cause a convection current that will push cells that have not settled to the edge of the plate.

Chapter 2.8.2 Methods for Chapter 2.2

Treatment for neurite outgrowth in 24-well plates

At 3 days in vitro (DIV3), cells were ready for treatment.[54] For **Figures 2.1B–N, 2.2B–H, 2.3A–F, and 2.5B–C**, first, plates had 5 µL of media removed. Next, DMSO stock solutions of ligands were diluted 1:10 in Neurobasal (1 mM, 10% DMSO). Then, 5 µL of this solution was added to the well for a 1:100 dilution (LSD = 10 µM; DOI = 10 µM; DMT = 90 µM; BDNF = 50 ng/mL;[55] DMSO = 0.1%).[56] For **Figure 2.3G**, 10 µL of media was removed and 5 µL of a 1:10 diluted DMSO or DOI was added to each well. Then 5 µL of a BDNF[55] was added to each well (final concentration DOI = 10 µM; BDNF = 50 ng/mL; DMSO = 0.2%). Finally, plates were gently shaken in the TC hood and placed back into the incubator to incubate for 72 hours. After 72 hours, cells were fixed and stained. See **Chapter 2.8.1** Staining for neurite outgrowth assays for staining and Imaging and analysis for neurite outgrowth on 24-well plates for the imaging and analysis.

Treatment for neurite outgrowth in 96-well plates

At DIV3, cells were ready for treatment. For **Figures 2.4A–B**, first, plates had 20 µL of media removed. Next, DMSO stock solutions of ligands were diluted 1:100 in replacement media (100 µM, 1% DMSO). Then, 20 µL of this solution was added to the well for a 1:10 dilution (LSD = 10 µM; KET = 10 µM; BDNF = 50 ng/mL; DMSO = 0.1%). Finally, plates were gently shaken in the TC hood and placed back into the incubator to incubate for 72 hours. After 72 hours, cells were fixed and stained following **Chapter 2.8.1 Staining for neurite outgrowth assays**. See **Chapter 2.8.1 Imaging and analysis for neurite outgrowth on 96-well plates** for imaging and data analysis.

For **Figure 2.5D**, at DIV3, 20 µL of media was removed and 20 µL of a 1:100 diluted ligand was added to each well (LSD = 10 µM; KET = 10 µM; DMSO = 0.1%). Finally, plates were gently shaken in the

54. Before doing treatments, always check the health of the cells under the microscope before starting any experiment. Once the experiment is over, before moving to the fixing and staining protocol, check the health once more and note any changes that treatments may have caused. This will help troubleshoot if anything happens when fixing, staining, and imaging.
55. BDNF dilution is done with a starting concentration of 100 µg/mL. Then I conduct a 1:20 dilution in Neurobasal and supplement with DMSO (1 µL of 100 µg/mL BDNF, 17 µL Neurobasal, and 2 µL DMSO). Then a final 1:10 dilution into each well for treatment.
56. When adding drugs into the 24-well plates, make sure that the plate is tilted towards you to briefly create a larger volume of media at the bottom of the tilted well. This helps to dilute DMSO quicker and prevents cell death from exposure to high concentrations of DMSO.

TC hood and placed back into the incubator to incubate for 1 hour. After 1 hour, the experiment was stopped, and cells were fixed and stained following **Chapter 2.8.1 Staining for neurite outgrowth assays**. Imaging and data analysis was done as described in **Chapter 2.8.1 Imaging and analysis for neurite outgrowth on 96-well plates**.

Calculating the percent efficacy:

$$\%\ \text{Efficacy} = \left(\frac{\text{Nmax drug} - \text{Nmax VEH}}{\text{Nmax 10μM KET} - \text{Nmax VEH}}\right) 100\%$$

VEH was set to 0% and 10 μM KET was set to 100%. When calculating the graphs, we used GraphPad Version 7 and used the following constraints: Top = % Efficacy of Nmax 10 μM drug and bottom = % Efficacy of VEH (0%). Furthermore, any value that was recorded as less than 0% (i.e. % efficacy = negative %), the value was normalized to 0%.[57]

Imaging and quantification of dendritic spines

Coverslips were imaged on a Nikon N-SIM Structured Illumination Super-resolution Microscope with a 100x/NA 1.49 objective, 100 EX V-R diffraction grating, and an Andor iXon3 DU-897E EMCCD. Specifically, secondary dendrites were taken and images were recollected and reconstructed using "2D-SIM" mode (no out-of-focus light removal; the reconstruction used three diffraction grating angles each with three translations). Dendritic spines were counted manually by an experimenter blinded to the treatment conditions. Mushroom spines were classified as a dendritic spine with a large f-actin head and a short spine neck. Filopodia spines were classified as a long f-actin structure that protruded off the dendritic shaft. Thin spines were classified as an f-actin structure that was shorter than a filopodia spine and longer than a mushroom spine. Thin spines also had a spine head larger than a filopodia spine and smaller than a mushroom. Lastly, stubby spines were classified as an f-actin structure on the dendritic shaft without a spine neck.[58]

57. This is a major limitation of the method as the assay was not sensitive enough to determine the Nmax changes well. This comparison in percent efficacy did make MDMA seem like it was more potent than KET. However, if looking at the fold change compared to VEH, MDMA was 1.40 versus KET at 1.31, which is not significant from each other. The short-transient stimulation studies are better models for determining EC50s as the amount of time ligand is on board is reduced.
58. Dendritic spines were classified based on these qualifications listed in this publication:
Hering, H.; Sheng, M. Dendritic spines: structure, dynamics and regulation. *Nat. Rev. Neurosci.* **2001**, *2,* 880–888.

Synaptic Density assays in 24-well plates

For **Figures 2.6 D–H**, images of secondary dendrites were collected using a confocal microscope (Olympus FV1000) with a 60x oil objective and a 1.42 numerical aperture.

Synaptic density and size as well as PSD-95 and VGLUT1 densities were determined using custom software that works in three stages.[59] The first stage is a foreground/background separation that outputs a mask of pixels within the image that corresponds to the neuron. Next, puncta of synaptic proteins are identified using only pixels belonging to the foreground mask from the first stage. Finally, synapses are identified as colocalizations of puncta of pre-and post-synaptic proteins. The foreground mask is determined using a fluorescence intensity threshold chosen to maximize the connectedness of both the foreground and the background. Specifically, for a given threshold, connected pixels that pass the threshold are clustered together, and connected pixels that fall below the threshold are clustered together. The average cluster size is computed for each type of cluster, and the threshold that maximizes the product of these averages is chosen. The resulting foreground mask is cleaned by removing clusters smaller than 0.06 μm2 and smoothed by eliminating pixels connected to fewer than three other pixels that passed the threshold and adding pixels connected to more than four pixels that passed the threshold. Within the foreground mask, every pixel that has a greater intensity than its neighbors is treated as a seed point for a potential punctum. The median and standard deviation of pixel intensities are computed for foreground pixels in the neighborhood of each seed point. The size of the local neighborhood is made dynamic in order to maintain sufficient statistics, with a minimum size of 5 μm^2. Seed points with intensities less than 3 standard deviations above the local median are rejected. For seed points that pass this threshold, adjacent pixels that pass a less stringent threshold (the minimum of 2 standard deviations above the median and the average of the median and seed point intensities) are clustered. In order to prevent neighboring puncta from being clustered together, intensities for newly added pixels are required to decrease if adjacent

59. Dr. Alexander Sood (alexandersood@gmail.com) of UC Davis in the lab of Dr. Kim Mcallister wrote the original program. This program is specific for confocal-type images. Microscopes with higher resolution (super-resolution) or widefield microscope images do not work with this program as they have too high or low pixel resolution, respectively. For widefield microscope images, we currently use MetaXpress's software to calculate the colocalization of synapses.
For MetaXpress analysis parameters, see 1b, **Chapter 2.8.3**, and Ly, C.; Shimizu, A. J.; Vargas, M. V.; Duim, W. C.; Wender, P. A.; Olson, D. E. Bryostatin 1 Promotes Synaptogenesis and Reduces Dendritic Spine Density in Cortical Cultures Through a PKC-Dependent Mechanism. *ACS Chem. Neurosci.*, **2020**, *11*, 1545–1554.

established pixels are already close to the lower threshold. Once the clustering is complete, puncta are smoothed in the same manner as the foreground and rejected if they are smaller than 0.03 μm^2. Pixels that are part of a punctum passing all of the above criteria are removed from the foreground mask so as not to be included in the threshold calculation for future puncta. After every seed point has been tested, those that failed are iterated over again until no new puncta are added. At the beginning of each iteration, puncta smaller the 3 times the minimum size threshold are removed to be reclustered. Synapses are defined as colocalization of PSD-95 and VGLUT1 puncta. Two puncta are considered colocalized if they have at least 1 pixel of overlap. Synapse densities, as well as the densities of presynaptic and postsynaptic markers, are calculated using dendrite areas computed by counting pixels within a region of interest belonging to the foreground mask in the MAP2 channel. Synapse size was calculated using the number of pixels representing each colocalization event. Outliers were removed using the ROUT method in GraphPad Prism (version 7.0a) with a Q value equal to 5%.

BDNF ELISA

Cortical cultures were grown in 6-well plates (600,000 cells per well). At DIV17–18, all media was removed and replaced with fresh Neurobasal. After 4 hours, each well was treated with a compound dissolved in DMSO (1:1000) for 24 hours. After the treatment period, the media was removed and the cells washed once with ice-cold DPBS. Cell Extraction Buffer (Life Technologies, 200 µL) supplemented with cOmplete (Sigma) and PhoSTOP (Sigma) inhibitors was added to each well and incubated on ice for 5–10 min. Plates were scrapped and the contents were collected. The samples were centrifuged at 10,000 x g for 10 min at 4 ºC and subjected to a BDNF ELISA assay (ThermoFisher) as per the manufacturer's protocol except the colorimetric signal was only allowed to develop for 8 minutes.

***BDNF* ddPCR**

Cortical cultures were grown in 6-well plates (600,000 cells per well) until DIV17–18. The cells were treated with compounds (1:1000 dilution from DMSO stock solutions) for 24h. Cells were then lysed using QIAzol Lysis Reagent (QIAGEN) and RNA extracted using the RNeasy isolation kit (QIAGEN) following instructions of the manufacturer. The resulting RNA was converted to cDNA using the iScript cDNA

Synthesis Kit (BioRad). Droplets containing PCR master mix and Taqman probes for BDNF (ThermoFisher, RN02531967_s1) and ESD (ThermoFisher, RN01468295_g1) were generated using the QX200 Droplet Digital PCR System (BioRad). Following PCR amplification, the BDNF signal was quantified and normalized to the housekeeping gene ESD.

Chapter 2.8.3 Methods for Chapter 2.3

Short stimulation synaptic density assay in 96-well plate

For **Figure 2.8B–D**, synaptic density assay was conducted in a medium-throughput assay using black 96-well plastic bottom plates (Corning) using the center 60 wells. 96-well plates were coated with 100 µL of coating media overnight at room temperature. The next day, plates were washed 3× with 200 µL autoclaved water. After the last wash, 200 µL of Neurobasal was added to each of the center 60 wells and autoclaved water was added to the remaining outer wells to reduce evaporation. The plates were placed into a 37°C and 5% CO_2 water-jacketed incubator prior to dissection. After dissection (see **Chapter 2.3.1 Tissue collection**), the Neurobasal was aspirated and 200 µL of a 75,000 cell per mL diluted in plating media (final cell density of 15,000 cells per well) and returned to the incubator.[43] After 16–24 hours, plating media was aspirated and 200 µL of prewarmed replacement media was added to each well. On DIV6 and DIV13, 100 µL of the culture media in the well was removed and 140 µL of prewarmed feeding media was added. Cells were treated on DIV18–20.

At DIV18–20, cells were ready for treatment.[54] First, plates had 20 µL of media removed. Next, DMSO stock solutions of ligands were diluted 1:100 in feeding media (100 µM, 1% DMSO). Then, 20 µL of this solution was added to the well for a 1:10 dilution (LSD = 10 µM; KET = 10 µM; BDNF = 50 ng/mL;[55] DMSO = 0.1%). Finally, plates were gently shaken in the TC hood and placed back into the incubator to incubate for 15 minutes, 1 hour, or 6 hours. At the end of those time points, media was removed and replaced with fresh feeding media free of ligand. After a total of 24 hours has passed since the beginning of the experiment, cells were fixed and stained. For fixing and staining, see **Chapter 2.8.1 Fixing procedure for 24- and 96-well plates** and **Staining for synaptic density assays.**

All images were obtained using a Molecular Devices ImageXpress Micro XLS Widefield High-Content Analysis System at nine sites per well using 40× magnification. Image analysis was performed using MetaXpress software. Analysis was completed by first using the MAP2 channel to establish a mask of the neuron using thresholds between 0 and 30 µm. Then, the mask of the neuron was expanded by 1 µm. The size of the objects for the presynaptic and postsynaptic fluorescent images was established, and only signals of 0–1.5 µm punctate were used to generate a mask. To measure synaptic density, the

presynaptic and postsynaptic masks were overlaid using the logical operation “and” to retain the only signal that colocalized to form the synapse mask. The number of events occurring in this synapse mask was quantified and normalized to the MAP2 channel mask area (number of counts per µm2). Normalized data were then tested for outliers using the ROUT method in Graphpad Prism (version 8) at Q = 1%. The outlier test was completed to remove artifacts in an unbiased manner.

Dendritic spine imaging in 24-well plates

At DIV18–20, cells were ready for treatment.[54] First, plates had 5 µL of media removed. Next, DMSO stock solutions of ligands were diluted 1:10 in Neurobasal (1 mM, 10% DMSO). Then, 5 µL of this solution was added to the well for a 1:100 dilution (LSD = 10 µM; KET = 10 µM; BDNF = 50 ng/mL;[55] DMSO = 0.1%). Finally, plates were gently shaken in the TC hood and placed back into the incubator to incubate for 15 minutes, 1 hour, or 6 hours. At the end of those time points, media was removed and replaced with fresh feeding media free of ligand. After a total of 24 hours has passed since the beginning of the experiment, cells were fixed and stained. For fixing and staining, see **Chapter 2.8.1 Fixing procedure for 24- and 96-well plates** and **Staining for dendritic spine assays.**

After microscope slides with coverslips mounted as described in **Chapter 2.8.1 Mounting procedures** have been allowed to cure and sealed using nail polish, slides were imaged on a Nikon HCA Confocal microscope with a 100×/NA 1.45 oil objective. Dendritic spines were counted manually by an experimenter blinded to the treatment conditions. See **Chapter 2.8.2 Imaging and quantification of dendritic spines.**

Chapter 2.8.4 Methods for Chapter 2.4 and 2.5

Treatment for neurite outgrowth in 24-well plates

For **Figures 2.9B–G, 2.10 B–F, and 2.11 B–G**, first, plates had 10 µL of media removed. Next, DMSO stock solutions of ligands were diluted 1:10 in Neurobasal (1 mM, 10% DMSO). Then, DMSO stock solutions of the antagonist (ANA-12, RAPA, or KTSN) were diluted 1:100 in Neurobasal. Then, 5 µL of the antagonist was added to the respective well for a 1:100 dilution.[60] For wells without an antagonist, a 5 µL addition of a 1:10 DMSO to a Neurobasal solution was added to maintain the 0.1% DMSO concentration. Plates were incubated for 5 minutes in the incubator. After 5 minutes, 5 µL of the ligand dilution was added to each well (LSD = 10 µM; DOI = 10 µM; DMT = 90 µM; ANA-12 = 10 µM; RAPA = 100 nM; KTSN = 100 µM; BDNF = 50 ng/mL; DMSO = 0.2%). Finally, plates were gently shaken in the TC hood and placed back into the incubator to incubate for 72 hours. After 72 hours, cells were fixed and stained. **Chapter 2.8.1 Fixing procedure for 24- and 96-well plates** for fixing, **Staining for neurite outgrowth assays** for staining, and **Imaging and analysis for neurite outgrowth on 24-well plates** for imaging and analysis**.**

60. When adding drugs into the wells for 24-well plates, make sure that the plate is tilted towards you to briefly create a larger volume of media at the bottom of the tilted well. This helps to dilute DMSO quicker and prevents cell death from exposure to high concentrations of DMSO.

Chapter 2.8.5 Methods for Chapter 2.6

For **Figures 2.12B–G**, DMSO stock solutions of ligands were diluted 1:100 in replacement media (100 µM, 1% DMSO). Then, DMSO stock solutions of the antagonist (ANA-12, RAPA, or DNQX) were diluted 1:100 in replacement media.

Figures 2.12B, D, F, H had ligand cotreated with drugs. In brief, plates had 40 µL of media removed. Next, 20 µL of the antagonist from above (1:100) was added to the respective well for a 1:10 dilution (final dilution = 1:1000). For wells without an antagonist, a 20 µL addition of a 1:100 DMSO to replacement media solution was added to maintain the 0.1% DMSO concentration. Plates were incubated for 5 minutes in the incubator. After 5 minutes, 20 µL of the ligand dilution from above (1:100) was added to each well (LSD = 10 µM; KET = 10 µM; ANA-12 = 10 µM; RAPA = 100 nM; DNQX = 10 µM; KCl = 40 mM; DMSO = 0.2%). Finally, plates were gently shaken in the TC hood and placed back into the incubator to incubate for 1 hour. After 1 hour elapsed, the medium was aspirated and fresh ligand-free replacement media was added to each cell (200 µL). Cells were incubated for another 71 hours. Cells were fixed and stained.

For **Figures 2.12C, E,** and **G**, cortical cultures were treated first for 1 hour followed by antagonists for 71 hours. In brief, plates had 20 µL of media removed. Next, 20 µL of the ligand from above (1:100 dilution) to the respective well for a 1:10 dilution (final dilution = 1:1000; LSD = 10 µM; KET = 10 µM; DMSO = 0.1%). Finally, plates were gently shaken in the TC hood and placed back into the incubator to incubate for 1 hour. After 1 hour elapsed, the medium was aspirated and fresh replacement media containing antagonist was added (ANA-12 = 10 µM; RAPA = 100 nM; DNQX = 20 µM was added to each cell (200 µL). Cells were incubated for another 71 hours. Cells were fixed and stained.

For **Figure 2.12I**, cortical cultures were stimulated with ligand for 1 hour followed by 71 hours of growth in ligand-free media. DIV3 cortical cultures had 20 µL of media removed. Next, 10 mM DMSO stock solutions of ligands (8-OH-DPAT, LSD, and KET) were serial diluted 1:100 in DMSO (10 mM, 100 µM, 1 µM, and 10 nM). Each of the serial dilution concentrations was diluted 1:100 in replacement media (100 µM, 1 µM, 10 nM, and 100 pM). Then, 20 µL of the 1:100 solution in replacement media was added to the plate for a 1:10 dilution (final dilution = 1:1000; final ligand concentration = 10 µM, 100 nM, 1 nM, 10 pM).

After 1 hour, media was removed and fresh ligand-free replacement media was added. The cells were then allowed to grow for an additional 71 hours. At the end of the 71 hours, cells were fixed and stained.
For fixing, staining, and imaging, please see **Chapter 2.8.1 Fixing procedure for 24- and 96-well plates** for fixing, **Chapter 2.8.1 Staining for neurite outgrowth assays**, and Imaging and data analysis was done as described in **Chapter 2.8.1 Imaging and analysis for neurite outgrowth on 96-well plates.**

Chapter 3 Medium-Throughput Assay for Prioritizing and Optimizing Psychoplastogen Drug Discovery[1]

Chapter 3.1 Introduction

The mechanism of action of antidepressants is hypothesized to be mediated through structural plasticity (iPlasticity).[2] These structural changes are critical for the clinical effects of antidepressants.[3] Furthermore, as the mechanisms of MDD are not well understood, developing next-generation therapeutics to treat depression via a target-directed drug discovery program may lead to false positives or other me-too drugs.[4] A hallmark of depression is the atrophy of neurites, the reduction of dendritic spine numbers, and loss of synaptic density in the prefrontal cortex (PFC). Therefore, a phenotypic drug discovery platform examining these changes would best assist in the endeavor to design better-tolerated therapeutics. These phenotypes include the promotion of neuritogenesis, spinogenesis, and synaptogenesis like ketamine and classic psychedelics.

Previously, I demonstrated that classic psychedelics promoted neuritogenesis, spinogenesis, and synaptogenesis equally efficacious to and as potent as ketamine. Many classic psychedelics and ketamine have therapeutic potential in the clinic. Therefore, we want to develop, optimize, and scale a primary assay using embryonic cortical cultures as a drug discovery model for psychoplastogens.

I established an assay by comparing the phenotypic changes induced by psychoplastogens, current traditional antidepressant medications, and small molecules unlikely to produce antidepressant effects. We selected ketamine (KET, FDA approved), N,N-dimethyltryptamine (DMT), scopolamine,

---

1. Data in this chapter is unpublished.
2. Umemori, J.; Winkel, F.; Didio, G.; Llach Pou, M.; Castrén, E. iPlasticity: Induced juvenile-like plasticity in the adult brain as a mechanism of antidepressants. *Psychiatry Clin. Neurosci.* **2018**, *72*, 633–653.
3. (a) Castrén, E.; Antila, H. Neuronal plasticity and neurotrophic factors in drug responses. *Mol. Psychiatry***. 2017**, *22*, 1085–1095.
(b) Cramer, S.C.; Sur, M.; Dobkin, B.H.; O'Brien, C.; Sanger, T.D.; Trojanowski, J.Q.; Rumsey, J.M.; Hicks, R.; Cameron, J.; Chen, D.; Chen, W.G.; Cohen, L.G.; deCharms, C.; Duffy, C.J.; Eden, G.F.; Fetz, E.E.; Filart, R.; Freund, M.; Grant, S.J.; Haber, S.; Kalivas, P.W.; Kolb, B.; Kramer, A.F.; Lynch, M.; Mayberg, H.S.; McQuillen, P.S.; Nitkin, R.; Pascual-Leone, A.; Reuter-Lorenz, P.; Schiff, N.; Sharma, A.; Shekim, L.; Stryker, M.; Sullivan, E.V.; Vinogradov, S. Harnessing neuroplasticity for clinical applications. *Brain*. **2011**, *134*, 1591–1609.
(c) Duman, R.S. Synaptic plasticity and mood disorders. *Mol. Psychiatry*. **2002**, *7*, S29–S34.
(d) Hayley, S.; Litteljohn, D. Neuroplasticity and the next wave of antidepressant strategies. *Front. Cell Neurosci.* **2013**, *7*, 218.
4. (a) Gagny, J. J.; Choudhry, N. K. How Many “Me-Too” Drugs Is Too Many? *JAMA* **2011**, *305*, 711–712.
(b) Schwartz, T. L. Metabolites: Novel Therapeutics or “Me-Too” Drugs? Using Desvenlafaxine as an Example. *CNS Spectrums* **2012**, *17*, 103–106.
(c) Sopko, M. A.; Ehret, M. J.; Grgas, M. Desvenlafaxine: Another “Me Too” Drug? *Ann. Pharmacother.* **2008**, *42*, 1439–1446.

allopregnanolone (Brexanolone, FDA approved), and Glyx-13 (Rapastinel) as psychoplastogens that exert rapid-acting therapeutic action within hours to days in rodents or humans..[5] Next, we selected duloxetine (Cymbalta), fluoxetine (Prozac), sertraline (Zoloft), amitriptyline (Elavil), and bupropion (Wellbutrin) as currently prescribed medications for the treatment of depression. Finally, we selected morphine, D-amphetamine, caffeine, nicotine, and modafinil as molecules that were unlikely to produce antidepressant effects but were known to be psychoactive **(Fig. 3.1)**.[6] Using these 15 molecules, I set out to build a series of phenotypic components that could assess the antidepressant potential of each molecule.

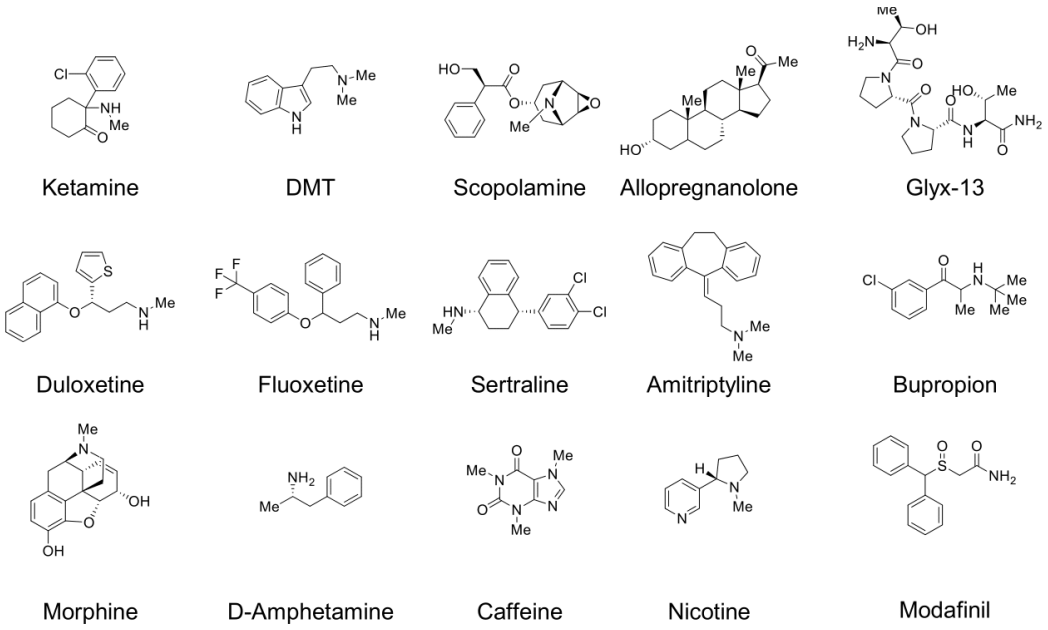

Figure 3.1. Structures of various psychoplastogens, traditional antidepressants, and non-antidepressant small molecules.

5. (a) Liu, R. J.; Duman, C.; Kato, T.; Hare, B.; Lopresto, D.; Bang, E.; Burgdorf, J.; Moskal, J.; Taylor, J.; Aghajanian, G.; Duman, R. S. GLYX-13 Produces Rapid Antidepressant Responses with Key Synaptic and Behavioral Effects Distinct from Ketamine. *Neuropsychopharmacology*, **2017**, *42*, 1231–1242.
(b) Sanches, R.F.; de Lima Osório, F.; Dos Santos, R.G.; Macedo, L.R.; Maia-de-Oliveira, J.P.; Wichert-Ana, L.; de Araujo, D.B.; Riba, J.; Crippa, J.A.; Hallak, J.E. Antidepressant Effects of a Single Dose of Ayahuasca in Patients With Recurrent Depression: A SPECT Study. *J. Clin. Psychopharmacol.* **2016**, *36*, 77–81.
(c) Navarria, A.; Wohleb, E.S.; Voleti, B.; Ota, K.T.; Dutheil, S.; Lepack, A.E.; Dwyer, J.M.; Fuchikami, M.; Becker, A.; Drago, F.; Duman, R.S. Rapid antidepressant actions of scopolamine: Role of medial prefrontal cortex and M1-subtype muscarinic acetylcholine receptors. *Neurobiol. Dis.* **2015**, *82*, 254–261.
6. (a) Broom, D.C.; Jutkiewicz, E.M.; Folk, J.E.; Traynor, J.R.; Rice, K.C.; Woods, J.H. Nonpeptidic delta-opioid receptor agonists reduce immobility in the forced swim assay in rats. *Neuropsychopharmacology*. **2002**, *26*, 744–755.
(b) Porsolt, R.D.; Anton, G.; Blavet, N.; Jalfre, M.; Behavioural despair in rats: a new model sensitive to antidepressant treatments. *Eur. J. Pharmacol.* **1978**, *47*, 379–391.
(c) Andreasen, J.T.; Olsen, G.M.; Wiborg, O.; Redrobe, J.P. Antidepressant-like effects of nicotinic acetylcholine receptor antagonists, but not agonists, in the mouse forced swim and mouse tail suspension tests. *J. Psychopharmacol.* **2009**, *23*, 797–804.

Chapter 3.2 Neurite Outgrowth in Cortical Neurons as a Phenotype of Antidepressants

To explore the neurite outgrowth potential of the test ligands **(Fig. 3.1)**, I began by incubating DIV3 embryonic cortical cultures at 10 μM for 72 hours. I hypothesized that an extended treatment time would maximize the response in vitro due to the continuous treatment with traditional antidepressants in the clinic. To our surprise, many of the slow-acting antidepressants were cytotoxic and caused cell death **(Fig. 3.2A)**. Bupropion was the only traditional antidepressant that did not exhibit cell death. Amitriptyline caused limited cell death as there was still a sparse number of cells. Sertraline, duloxetine, and fluoxetine killed the primary embryonic cortical cultures. Moreover, fluoxetine is cytotoxic at 10 μM even though the clinical dose reaches a max concentration of 34.6 μM in patients.[7] We confirmed the cytotoxicity findings via a 3-(4,5-dimethylthiazol-2-yl)-2,5-diphenyl tetrazolium bromide (MTT) assay **(Fig. 3.2B)**. As expected, cells treated chronically for 72 hours with the traditional antidepressants showed little to no absorbance in the MTT assay, indicating that the cells were mostly dead. A follow-up with the Live or Dead Assay (ThermoFisher) should be conducted to validate this result. Considering the cytotoxicity, I decided to shorten our timepoint to the 1-hour stimulation experiments I previously reported showing psychoplastogens could elicit long-lasting changes in neurite outgrowth following short transient stimulation.[8] 1-hour treatment followed by 71 hours of growth indicated no cell death caused by the traditional antidepressants in the MTT assay **(Fig. 3.2C)**. Thus, I decided to proceed with the 1-hour treatment, 71-hour growth protocol.

7. (a) Hwang, S.; Kim, J.K. Fluoxetine Induces Apoptotic and Oxidative Neuronal Death Associated with The Influx of Copper Ions in Cultured Neuronal Cells. *Chonnam. Med. J.* **2020**, *56*, 20–26.
(b) Karson, C.N.; Newton, J.E.; Livingston, R.; Jolly, J.B.; Cooper, T.B.; Sprigg, J.; Komoroski, R.A. Human brain fluoxetine concentrations. *J. Neuropsychiatry Clin. Neurosci*. **1993**, *5*, 322–329.
8. Ly, C.; Greb, A.C.; Vargas, M.V.; Duim, W.C.; Grodzki, A.C.G.; Lein, P.J.; Olson, D.E. Transient Stimulation with Psychoplastogens Is Sufficient to Initiate Neuronal Growth. *ACS Pharmacol. Transl. Sci.* **2020**, *4*, 452–460.

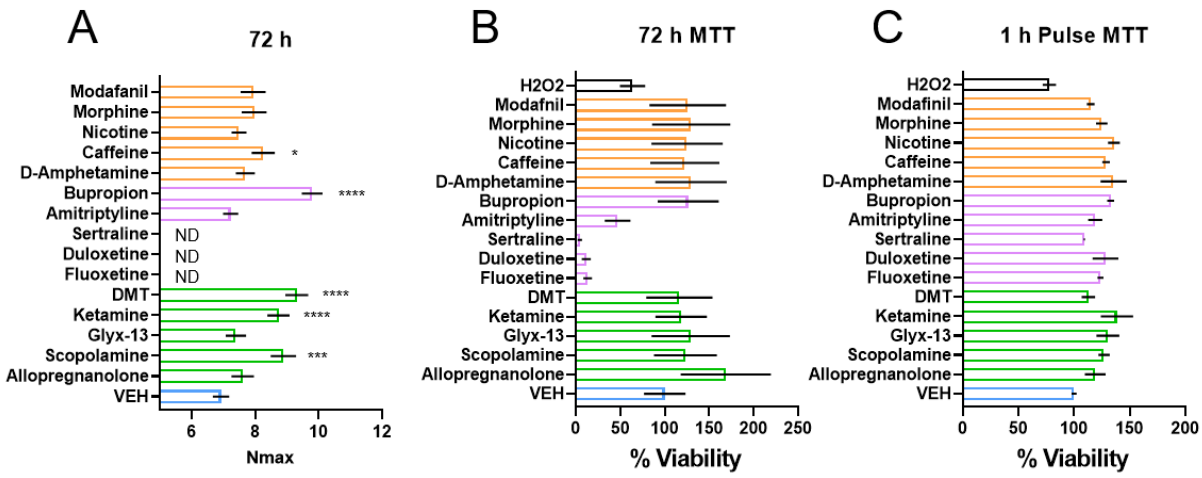

Figure 3.2. Chronic treatment with traditional antidepressants is toxic to neurons. **(A)** Cortical neurons treated with small molecules at DIV3 and assessed at DIV6 for Nmax from the Sholl plots (n = 27–61 neurons). **(B)** Cortical neurons treated at DIV3 and MTT viability assay results were analyzed on DIV6 following 72-hour chronic treatment (n = 6–12 wells). **(C)** Cortical neurons at DIV3 were treated for 1-hour and media was changed to replacement media free of ligands. Cells allowed to grow for 71 hours then MTT viability was conducted (DIV6, n = 3–6 wells). Data are represented as mean ± SEM. *p < 0.05, **p < 0.01, ***p < 0.001, ****p < 0.0001, as compared to VEH control without inhibitor **(A)** following a one-way analysis of variance with a Dunnett's post hoc test. Compounds with ND were not assessed in statistics. VEH = vehicle; DMT = N,N-dimethyltryptamine; MTT = 3-(4,5-dimethylthiazol-2-yl)-2,5-diphenyltetrazolium bromide; H_2O_2 = hydrogen peroxide, 150 μM; Nmax = maximum number of crossings. Green = psychoplastogens (FAD), magenta = traditional antidepressants (SAD), orange = non-antidepressants (NAD).

Next, we tested the ligands **(Fig 3.1)** as our training set in a 1-hour stimulation experiment in DIV3 embryonic cortical cultures. Quantification of the Sholl analysis revealed that all traditional antidepressants and psychoplastogens uniformly increased the Nmax values **(Fig. 3.3A)**. Interestingly, slow-acting antidepressants increase neurite outgrowth at the same dose in the hippocampal cells, albeit at DIV10 and chronically stimulated with ligand for five days.[9] This result suggests that more mature neurons or other

9. Park, S.W.; Lee, J.G.; Seo, M.K.; Lee, C.H.; Cho, H.Y.; Lee, B.J.; Seol, W.; Kim, Y.H. Differential effects of antidepressant drugs on mTOR signalling in rat hippocampal neurons. *Int. J. Neuropsychopharmacol.* **2014**, *17*, 1831–1846.

brain regions may be less susceptible to the cytotoxicity effects of the traditional antidepressants. However, the immature cortical cultures treated chronically rapidly highlights the difference between psychoplastogens and slow-acting antidepressants.

Next, I quantified the area under the curve (AUC) of the Sholl plot **(Fig. 3.3B)**, primary branching **(Fig. 3.3C)**, branch points **(Fig. 3.3D)**, and neurite lengths **(Fig. 3.3E–F)**. As expected, most traditional antidepressants and psychoplastogens increased AUC, primary branching, branch points, and total length values. Furthermore, like the Ly, C. et, al 2018 results, we found no significant increases in longest neurite[10] These phenotypic characterizations of the traditional antidepressants and psychoplastogens indicate that the 1-hour timepoint could not differentiate the two groups of molecules from one another. This result serves as further evidence that the clinical effects of antidepressants may be coming from the rectification of the retraction of neurites in depression.

Subsequently, I hypothesized that the high dose (10 μM) might be eliciting off-target effects. Previously, we reported EC_{50} values for the psychedelics in the Sholl analysis to be ~100 nM.[10] Furthermore, many of these molecules exhibit polypharmacological effects. For example, serotonergic ligands have very similar potencies at many serotonin receptors. Thus, I lowered the dose to 100 nM to avoid off-target effects **(Fig. 3.3G)**. Unfortunately, the result yielded no differentiation between any of the three groups of molecules. Previously, we also observed that ANA-12 (10 μM), a selective inhibitor of TrkB, blocked psychedelic induced neurite outgrowth.[10] I postulated that we could target TrkB as a centralized mechanism for differentiating between psychoplastogens and traditional antidepressants. Unfortunately, ANA-12 blocked all neurite outgrowth **(Fig. 3.3H)**. This result was surprising as we expected ANA-12 to abolish the psychoplastogen-induced neurite outgrowth but not the traditional antidepressants. Upon searching the literature, I found evidence suggesting that the traditional antidepressants were partial agonists at TrkB.[11] Therefore, TrkB-mediated neurite outgrowth was insufficient to separate psychoplastogens from slow-acting antidepressants.

10. Ly, C.; Greb, A. C.; Cameron, L. P.; Wong, J. M.; Barragan, E. V.; Wilson, P. C.; Burbach, K. F.; Soltanzadeh Zarandi, S.; Sood, A.; Paddy, M. R.; Duim, W. C.; Dennis, M. Y.; McAllister, A. K.; Ori-McKenney, K. M.; Gray, J. A.; Olson, D. E. Psychedelics Promote Structural and Functional Neural Plasticity. *Cell Rep.* **2018**, *23*, 3170–3182.
11. (a) Rantamäki, T.; Hendolin, P.; Kankaanpää, A.; Mijatovic, J.; Piepponen, P.; Domenici, E.; Chao, M.V.; Männistö, P.T.; Castrén, E. Pharmacologically diverse antidepressants rapidly activate brain-derived neurotrophic factor receptor TrkB and induce phospholipase-Cgamma signaling pathways in mouse brain. *Neuropsychopharmacology*. **2007**, *32*, 2152–2162.

Next, psychoplastogens, such as ketamine, are thought to elicit their effects through the activation of glutamate receptors, namely α-amino-3-hydroxy-5-methyl-4-isoxazolepropionic acid (AMPA) receptors.[12,13] To test this, I used the AMPAR inhibitor, 6,7-dinitroquinoxaline-2,3-dione (DNQX, 20 μM), to attempt to tease apart traditional antidepressants from psychoplastogens. To our surprise, DNQX (20 μM) inhibited only the psychoplastogens **(Fig. 3.3I)**. We are encouraged by this result as it may indicate that glutamate is critical for the rapid-acting antidepressant effects in the clinic.

Lastly, we thought about modeling depression in our cultures. We know that a hallmark of depression is the retraction of neurites in the prefrontal cortex following chronic stress. Small molecules such as psychoplastogens can rectify these deficits. Thus, the model we decided to investigate involved inducing chronic stress in our primary cortical cultures via treatment with corticosterone. Then, we aimed to rescue the retractions using psychoplastogens. We hypothesized that chronic corticosterone, the endogenous hormone of stress in rats and mice, would cause retraction of neurites and loss of synaptic density in our cultures. Unfortunately, corticosterone did not induce retraction in neurites at DIV6–14 after 3–7 days of chronic treatment.[14] Furthermore, in mature neurons (DIV18) following 24-hour treatments with corticosterone **(Fig. 3.3J)**, I saw an increase in synaptic density. Upon a quick literature search, I discovered that acute stress (and an increase in corticosteroids) induces neurogenesis.[15] Thus, the chronic treatment of corticosterone in culture may need to exceed 2–3 weeks before any signs of retraction. Unfortunately, maintaining cultures beyond DIV20 is very difficult as most neuronal cultures do not survive past DIV21 even under ideal conditions. Therefore, this model for neurite outgrowth may be too difficult to maintain and would not yield robust, reproducible, and rapid results. Synaptic density and the number of dendritic spines in cortical cultures following chronic corticosterone (treated from DIV2–DIV16) may yield a reduction in

(b) Rantamäki, T.; Vesa, L.; Antila, H.; Di Lieto, A.; Tammela, P.; Schmitt, A.; Lesch, K.P.; Rios, M.; Castrén, E. Antidepressant drugs transactivate TrkB neurotrophin receptors in the adult rodent brain independently of BDNF and monoamine transporter blockade. *PLoS One*. **2011**, *6*, e20567.
(c) Casarotto, P.C.; Girych, M.; Fred, S.M.; Kovaleva, V.; Moliner, R.; Enkavi, G.; Biojone, C.; Cannarozzo, C.; Sahu, M.P.; Kaurinkoski, K.; Brunello, C.A.; Steinzeig, A.; Winkel, F.; Patil, S.; Vestring, S.; Serchov, T.; Diniz, C.R.A.F.; Laukkanen, L.; Cardon, I.; Antila, H.; Rog, T.; Piepponen, T.P.; Bramham, C.R.; Normann, C.; Lauri, S.E.; Saarma, M.; Vattulainen, I.; Castrén, E. Antidepressant drugs act by directly binding to TRKB neurotrophin receptors. *Cell.* **2021**, *184*, 1299–1313.
12. Duman, R.S. Pathophysiology of depression and innovative treatments: remodeling glutamatergic synaptic connections. *Dialogues Clin Neurosci.* **2014**, *16*, 11–27.
13. Carbonaro, T.M.; Gatch, M.B. Neuropharmacology of N,N-dimethyltryptamine. *Brain Res. Bull.* **2016**, *126*, 74–88.
14. Data not shown. Alexandra C Greb conducted these experiments.
15. Kirby, E.D.; Muroy, S.E.; Sun, W.G.; Covarrubias, D.; Leong, M.J.; Barchas, L.A.; Kaufer, D. Acute stress enhances adult rat hippocampal neurogenesis and activation of newborn neurons via secreted astrocytic FGF2. *Elife*. **2013**, 2, e00362.

those phenotypes mimicking the loss in structures in depression. Further studies exploring this model could yield additional modifications to the phenotypic assays to small molecules that are psychoplastogens.

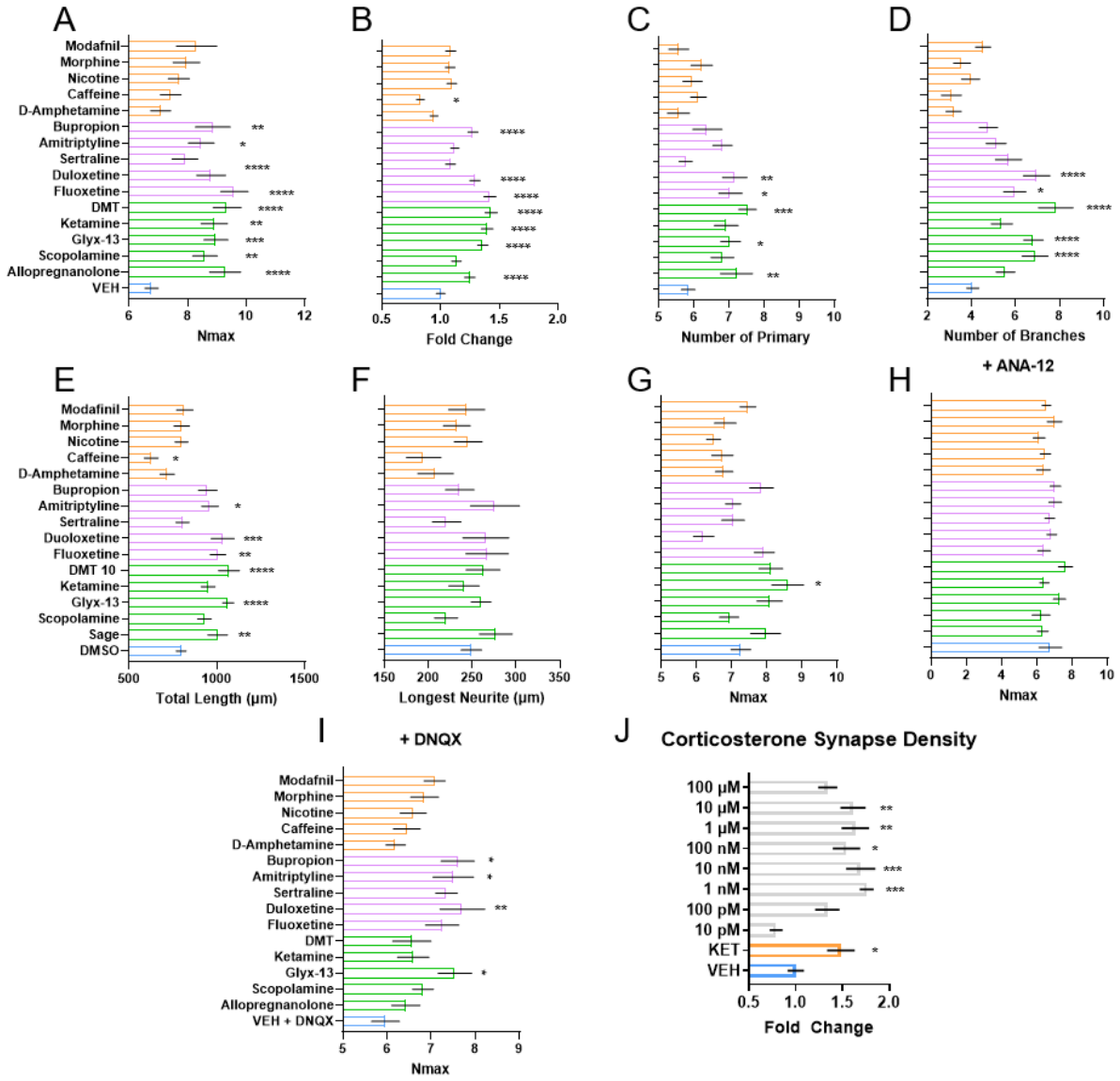

Figure 3.3. Short stimulation with traditional antidepressants does not cause cell death. Neurite outgrowth is an indication of antidepressants. **(A–I)** DIV3 cortical neurons were treated with 10 µM drugs for 1 hour followed by 71 hours of growth. The **(A)** Nmax and **(B)** area under the curve (AUC) were measured using the Sholl analysis plots. The neurons from **(A–B)** were then quantified for their changes in **(C)** the number of primary branches, **(D)** the number of branches points, **(E)** the total length of the neurons, and **(F)** the longest neurite length were measured using the Neurite Tracer plug-in from ImageJ. **(G)** 1-hour stimulation experiment in DIV3 neurons using 100 nM drug showed no changes to the Nmax as compared to VEH.

Inhibition studies on the Nmax using 10 μM dose and cotreatments with **(H)** 10 μM ANA-12 showed abolishment of increases in the Nmax by all compounds and **(I)** 20 μM DNQX was only able to block psychoplastogens. **(J)** DIV18 neurons treated with corticosterone (100 μM–10 pM) for 24 hours and synaptic density was measured. Data are represented as mean ± SEM. *p < 0.05, **p < 0.01, ***p < 0.001, ****p < 0.0001, as compared to VEH control without inhibitor **(A–G, J)** or with inhibitor **(H–I)** following a one-way analysis of variance with a Dunnett's post hoc test. **(A–F)**, n = 21–54 neurons; **(G)**, n = 23–27 neurons; **(H)**, n = 17–27 neurons; **(I)**, n = 24–27 neurons, **(J)** n = 45–52. VEH = vehicle; DNQX = 6,7-dinitroquinoxaline-2,3-dione. Green = psychoplastogens (FAD), magenta = traditional antidepressants (SAD), orange = non-antidepressants (NAD).

Chapter 3.3 Measuring Glutamate Release in Cortical Cultures as a Phenotype of Antidepressants

As AMPAR inhibition blocked the psychoplastogen-induced neurite outgrowth, I hypothesized that glutamate release might be a critical component to measure. First, to measure the amount of glutamate released, I used 90 mM KCl to induce depolarization for 15 minutes.[16] I then collected the buffer and quantified glutamate concentrations using the Promega Glutamate-Glo Assay.[17] Unfortunately, I was unable to quantify the concentrations of glutamate in KCl-depolarized neurons. Furthermore, I attempted to treat with ketamine, as ketamine's mechanism of action is hypothesized to facilitate glutamate release as part of its mechanism of action following inhibition of N-methyl-D-aspartate (NMDA) receptors. However, even at 10 μM ketamine, I was still unable to quantify any changes in glutamate concentration.

As I could not quantify glutamate release in our primary cultures, I hypothesized that this low yield might come from glial cells and interneurons rapidly converting released glutamate to glutamine to prevent excitotoxicity. Thus, I reduced the number of glial cells using 5 μM 1-β-D-arabinofuranosylcytosine (Ara-C or cytosine arabinoside).[16] I treated cells from DIV2 chronically until the day of the experiment at DIV3 and DIV14. Following 15 minutes of treatments, I collected the media to test in the Promega Gluatmate-Glo Assay. Once more, I was unable to observe above baseline levels of glutamate in the culture.[18] Next, the Olson lab attempted to measure glutamate concentrations using iGluSnFr, a genetically encoded fluorescent glutamate sensor that increases fluorescence when glutamate is bound.[19] In primary cortical cultures expressing iGluSnFr, we attempted to measure glutamate release and could not measure any transient glutamate release following treatment with psychoplastogens.[20] The next step would be to utilize

16. Stimulation of cells for 15 minutes was done with depolarizing buffer containing 32 mM NaCl, 90 mM KCl, 2 mM CaCl2, 2 mM MgCl2, 25 mM HEPES, and 30 mM D-Glucose, see **Chapter 3.6.3**.
I adapted the protocol from:
Parker, S. S.; Moutal, A.; Cai, S.; Chandrasekaran, S.; Roman, M. R.; Koshy, A. A.; Khanna, R.; Zinsmaier, K. E.; Mouneimne, G. High Fidelity Cryopreservation and Recovery of Primary Rodent Cortical Neurons. *eNeuro*. **2018**, *5*, ENEURO.0135-18.
17. Promega Glutamate-Glo Assay, J7021. The assay was conducted in white 96-well plates (Fisher Scientific) on BioTek Synergy HTX Plate Reader (Gen5 software).
18. To note, I hypothesized that the reason I was unable to get a change in glutamate was due to the sensitivity of the assay from Promega. Thus, I purchased a kit from Sigma (MAK004) and one from ThermoFisher (A12221) to test the samples collected above. Even with these kits, it seemed the sensitivity was not high enough to measure and quantify the concentrations of glutamate. Next, I tried to increase the density of cells from 6-well plates (3 million cells) to 10 cm (6 million cells) dishes but still could not observe glutamate concentrations above baseline.
19. Marvin, J. S.; Borghuis, B. G.; Tian, L.; Cichon, J.; Harnett, M. T.; Akerboom, J.; Gordus, A.; Renninger, S. L.; Chen, T. W.; Bargmann, C. I.; Orger, M. B.; Schreiter, E. R.; Demb, J. B.; Gan, W. B.; Hires, S. A.; Looger, L. L. An optimized fluorescent probe for visualizing glutamate neurotransmission. *Nat. Methods*. **2013**, *10*, 162–170.
20. This experiment was done by Lindsay P. Cameron in the Olson Lab with Elizabeth K. Unger in the Tian Lab.

HPLC to measure and quantify glutamate secretion. Cell culture media measured in HPLC has been shown to quantify up to 5 μM of glutamate without stimulation using DIV6 or older cell culturing.[21]

21. Macías, W.; Carlson, R.; Rajadhyaksha, A.; Barczak, A.; Konradi, C. Potassium chloride depolarization mediates CREB phosphorylation in striatal neurons in an NMDA receptor-dependent manner. *Brain Res*. **2001**, 890, 222–232.

Chapter 3.4 Clustering Measured Components in a Principal Component Analysis (PCA)

We combined the data I currently had and calculate a "Z-factor" or "Z'" for each component that we had recorded up to this point (cell death, Nmax, the number of primary branches, the number of branch points, the total lengths of the neurites, the longest neurite length, and DNQX inhibited Nmax, **Fig. 3.4A–G**) to use as components in a principal component analysis (PCA). I excluded the data collected from the ANA-12 Nmax experiments as there was no significant difference between the treatment groups. Using RStudio, we could determine and plot a PCA using the 7- components **(Fig. 3.4H)**.[22] From the PCA, we can see that the psychoplastogens (green), traditional antidepressants (magenta), and non-antidepressants (orange) all cluster into different quadrants. The exception here is bupropion, which seems to cluster well with the psychoplastogens (green). We hypothesize that bupropion exhibits psychoplastogenic potential because it is a racemic mixture, and one of the enantiomers may act more like a psychoplastogen, while the other may act as a traditional antidepressant. Previously in our group, we have evidence that one enantiomer of amphetamine is more potent than the other as a psychoplastogen. I found that L-amphetamine increased total BDNF levels whereas D-amphetamine did not; quantified through a BDNF ELISA assay.[23] Thus, we hypothesize that the difference in bupropion may be due to one enantiomer that is active as a psychoplastogen, whereas the other is not. Unfortunately, enantiomerically pure bupropion is not commercially available. Furthermore, an enantioselective synthesis is non-trivial.[24]

22. See **Chapter 3.6.4** for the full PCA script used in RStudio.
23. Data not shown. The fold changes of total BDNF protein (Treatment, Normalized Average, SEM, N, P-value calculated in one-way ANOVA compared to the VEH) is as follows: Vehicle, 1.00, 0.080, 3; L-amphetamine, 1.658, 0.136, 4, 0.0123; D-amphetamine, 0.959, 0.128, 4, 0.9621. For methods, see **Chapter 2.8.2 BDNF ELISA**. This data is also unpublished.
24. I arrived at this conclusion following discussion with the two senior synthetic chemists in our group as of 2021, Lee Dunlap and Guoliang Zhang, in our group.

Thus, in the future, if the enantiomers of bupropion can be separated, it would be interesting to examine the effects of the two compounds.

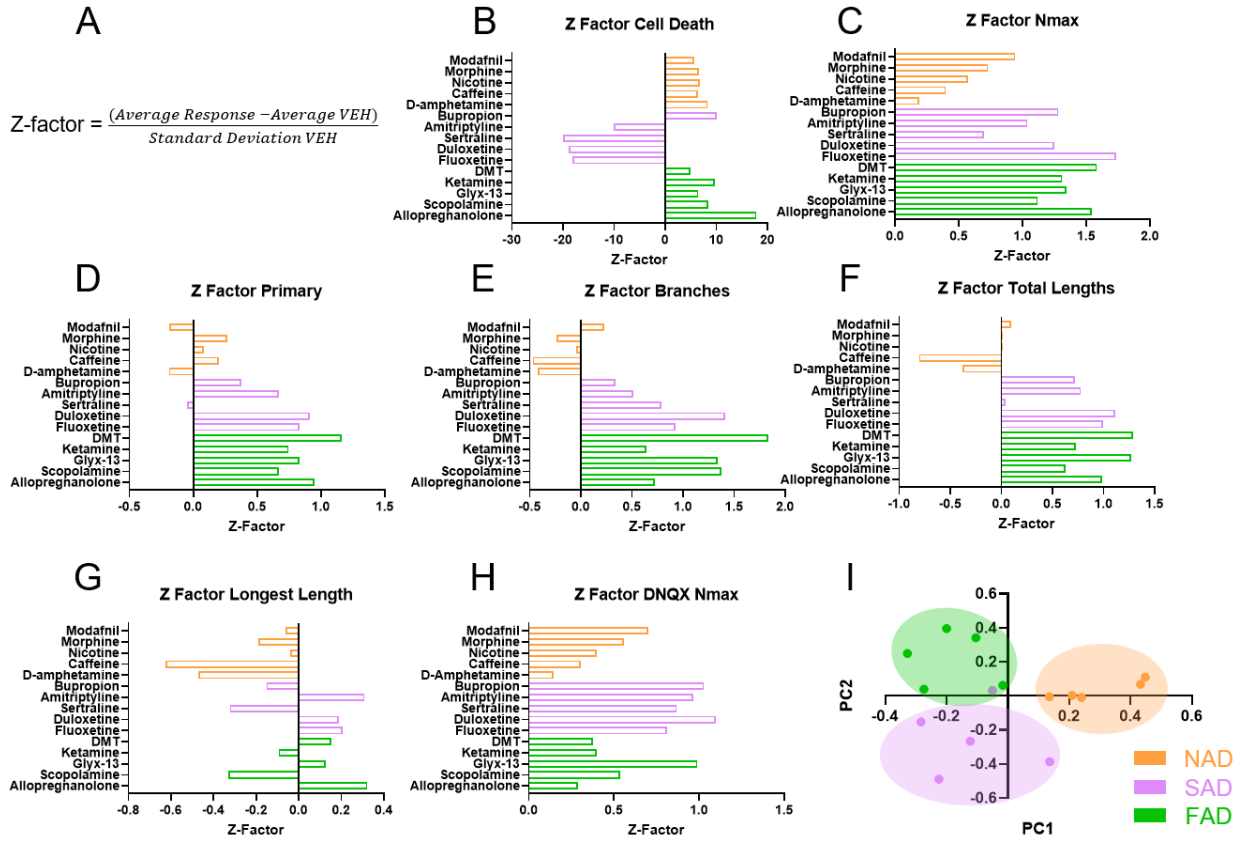

Figure 3.4. Conversion of raw data to Z-factors for principal component analysis (PCA). **(A–H)** Data converted to Z-factor **(A)** and plotted as each component **(B–H)**. **(I)** PCA of **(B–H)** using RStudio to generate the cluster. VEH = vehicle; DNQX = 6,7-dinitroquinoxaline-2,3-dione. Green = psychoplastogens (FAD), magenta= traditional antidepressants (SAD), orange = non-antidepressants (NAD).

Chapter 3.5 Conclusion

Based on the data here, with just the neuritogenesis results alone, we can robustly differentiate between psychoplastogens, traditional antidepressants, and non-antidepressants. The seven components used to generate the PCA establishes clear distinctions between the different classes of compounds. However, I believe that this is a limited approach for the following two reasons. First, most of the separation between psychoplastogens and traditional antidepressants comes from the cell death (MTT assay) component. We observe a distinct difference between the effects of psychoplastogens and traditional antidepressants in the MTT assay. While it would be wise to select molecules that are not cytotoxic as leads, it does not necessarily reflect the neurite outgrowth of cortical neurons. Thus while the MTT assay heavily affects the clustering, I believe we should consider other compounds. Second, the results here are limited strictly to neurite outgrowth. I postulate that the number of dendritic spines and synaptic density would further separate the molecules. Hypothetically, it could be that only psychoplastogens rapidly increase neurite outgrowth, the number of dendritic spines, and synaptic density, whereas traditional antidepressants may be limited to one or two of those phenotypes. For example, bryostatin-1 does not affect neurite outgrowth, reduces the number of dendritic spines, but increases synaptic density.[25] Therefore, additional components are valuable to the assessment of these molecules.

Once we include the number of dendritic spines and synaptic density, we should identify the two most robust components that distinguish psychoplastogens from other small molecules to measure antidepressant potential. The two components identified would accelerate the screening of analogs and small molecules to best cluster them together. Lastly, to validate this system, I would like to screen a small library of compounds to determine a lead compound to move forward with and validate using behavioral paradigms (the forced-swim test and sucrose preference). I believe it would also be interesting to test one molecule from each of the clusters (psychoplastogen, traditional antidepressant, and non-antidepressant) in vivo with a forced-swim test and sucrose preference to confirm their antidepressant potential. Ultimately, in combination with Chapter 4, these assays will become the general pipeline for determining therapeutic

25. Ly, C.; Shimizu, A. J.; Vargas, M. V.; Duim, W. C.; Wender, P. A.; Olson, D. E. Bryostatin 1 Promotes Synaptogenesis and Reduces Dendritic Spine Density in Cortical Cultures Through a PKC-Dependent Mechanism. *ACS Chem. Neurosci.*, **2020**, *11*, 1545–1554.

potential and counter-screen for off-target effects to develop, optimize, and prioritize better-tolerated, fast-acting psychoplastogens.

Chapter 3.6.1 General Methods for Chapter 3

The NIH Drug Supply Program provided modafinil and D-amphetamine hydrochloride. Other chemicals were purchased from commercial sources such as ketamine hydrochloride (KET, Fagron), glyx-13 (Sigma), scopolamine hydrobromide trihydrate (Sigma), 5α-Pregnan-3α-ol-20-one (Allopregnanolone, Sigma), fluoxetine hydrochloride (Sigma), sertraline hydrochloride (Cayman), bupropion hydrochloride (Sigma), (S)-duloxetine hydrochloride (Cayman), amitriptyline hydrochloride (Sigma), ANA-12 (MedChem Express), 6,7-dinitroquinoxaline-2,3-dione (DNQX, Sigma), corticosterone (Sigma), cytosine β-D-arabinofuranoside hydrochloride (Ara-C, Sigma). The fumarate salt of *N*,*N*-dimethyltryptamine (DMT) was synthesized in-house as described previously.[26] All drugs were dissolved in DMSO. All stock solutions were 10 mM except for DNQX (20 mM). The final concentration of ligand was 10 μM and 0.1% DMSO except for the 100 nM dose Nmax **(Fig. 3.3G).** For antagonist studies, DNQX (20 μM) and ANA-12 (10 μM) were used. All antagonist studies were conducted with final concentration of 0.2% DMSO.

Animals

All experimental procedures involving animals were approved by the University of California, Davis Institutional Animal Care and Use Committee (IACUC) and adhered to principles described in the National Institutes of Health Guide for the Care and Use of Laboratory Animals. The University of California, Davis is accredited by the Association for Assessment and Accreditation of Laboratory Animal Care International (AAALAC).

Rat embryonic cortical cultures

Coating media was generated using 2.48g boric acid (BDH) and 3.80g borax (MP) dissolved in 900 mL of water. The mixture was stirred overnight at room temperature to dissolve the solid. The next day, the pH of the solution was adjusted to 8.5 with 1N HCl or 1N NaOH. Next, two bottles of poly-D-lysine hydrobromide

26. Cameron, L. P.; Benson, C. J.; Dunlap, L. E.; Olson, D. E. Effects of N,N-dimethyltryptamine (DMT) on rat behaviors relevant to anxiety and depression. *ACS Chem. Neurosci.* **2018**, *9*, 1582–1590.

(10 mg/ bottle×2) were added. Volume was filled to 1L for a final concentration of 20 µg/mL PDL hydrobromide. The media was then filtered and stored in the dark at 4°C.

Plating media was generated by combining 500 mL Neurobasal Medium (Fisher Scientific), 50 mL HI FBS (Fisher Scientific), 1.25 mL 200mM glutamine (Fisher Scientific), and 5 mL penicillin-streptomycin (Fisher Scientific). The media was then filtered and stored in the dark at 4°C.

HBSS 1X was generated by combining 100 mL 10X HBSS (Fisher Scientific), 20 mL 1M HEPES (Fisher Scientific) 10 mL penicillin-streptomycin (Fisher Scientific) and filling to 1 L with autoclaved water. The HBSS was filtered and stored in the dark at 4°C.

Replacement media (50 mL) was generated by combining 48.5 mL Neurobasal Medium (Fisher Scientific), 1 mL B-27(Fisher Scientific), 125 µL 200mM glutamine (Fisher Scientific), 62.5 µL 10 mM glutamic acid (Fisher Scientific), and 0.5 mL penicillin-streptomycin (Fisher Scientific). The replacement media was then prewarmed to 37°C before use and made fresh.[27]

Feeding media (50 mL) was generated by combining 48.5 mL Neurobasal Medium (Fisher Scientific), 1 mL B-27(Fisher Scientific), 125 µL 200mM glutamine (Fisher Scientific), 0.5 mL penicillin-streptomycin (Fisher Scientific). The feeding media was then prewarmed to 37°C before use and made fresh.[27]

27. When mixing, either invert or allow it to mix in the bead bath over time. Any bubbles generated is due to proteins in B-27 being denatured.

Chapter 3.6.2 General Methods for Chapter 3.2

MTT Assay

MTT assay was conducted as previously described.[28] In brief, embryonic day 18 (E18) primary cortical cultures were plated at 40,000 cells per well in poly-D-lysine-coated 96-well plates (see **Chapter 3.6.1 96-well plates primary cortical cultures**, use black well plates). At DIV3, neurons were treated with compound (see **Chapter 3.6.1** for dilution) either chronically (72 hours) or short stimulation (1-hour treatment followed by removal of media and replaced with drug-free replacement media). 150 μM H_2O_2 was used to induce cell death and all wells contained 0.1% DMSO (VEH).[29] After treatment time had elapsed, 33 μL (working volume is 200 μL) was removed and replaced with 33 μL of a 3 mg/mL MTT solution in Neurobasal (sterile filtered using a 0.45 μm filter and 0.5 mg/mL final concentration of MTT, ThermoFisher). The cells were then incubated in a 37°C incubator at 5% CO_2 for 4 hours. After 4 hours, the media was aspirated and replaced with 50 μL of DMSO. The plate was then incubated at 37°C for 1 hour and then at room temperature for 30 minutes. The absorbance of the plate was then measured at 540 nm on a BioTek Synergy HTX Plate Reader (Gen 5 software).

Tissue Collection

Pregnant Sprague-Dawley dams were euthanized at embryonic day 18 (E18) via CO_2 and cortices of pups were extracted and placed into ice-cold 1X Hanks Buffered Saline Solution (HBSS, ThermoFisher) in a 14 mL culture tube. Afterward, cortices were washed ×3 with sterile 1X HBSS in the tissue culture hood, and then the HBSS was removed until 2 mL of volume remained. 200 μL of 2.5% trypsin (10×) was added and the culture tube was placed in a 37°C bead bath for 10 minutes. After 10 mins, using a 10 mL serological pipette, only cortices were collected and moved into a new, sterile 14 mL culture tube. Cortices were

28. Olson, D. E.; Sleiman, S. F.; Bourassa, M. W.; Wagner, F. F.; Gale, J. P.; Zhang, Y.-L.; Ratan, R. R.; Holson, E. B. Hydroxamate-based Histone Deacetylase Inhibitors Can Protect Neurons from Oxidative Stress by Forming Catalase Mimetic Complexes with Intracellular Iron. *Chem. Biol.* **2015**, *22*, 439-445.
29. Critical notes: H2O2-induced cell death is very rapid as neurons are sensitive to changes in their environment. However, when conducting H2O2-induced cell death change the protocol to Neurobasal only. Feeding and replacement media contains B27. B27 contains supplements, nutrients, and enzymes. In the enzymes, B27 contains catalases that quench your H2O2 before it can induce cell death. Therefore, if your cells are in fresh media containing B27, you will not see sufficient cell death. Therefore, in my data, H2O2 is not complete cell death and there is residual cell activity. Furthermore, I have noticed between there are large variations between replicates, so conduct all experiments within the same 96-well plate to prevent variability.

washed ×3 gently with cold 1X HBSS. Following the last wash, the tube was filled to a total volume of 6 mL with 1X HBSS. Using a 5 mL serological pipette, the cortices were gently pipetted up and down against the bottom of the tube, forcing the tissue out to triturate. Following trituration, 10 µL of cell suspension was mixed with 10 µL of trypan blue stain 0.4% (ThermoFisher) and inserted into a slide for the TC20 automated Cell Counter (BioRad). Cell viability was recorded,[30] and cells were plated.[31]

96-well plates primary cortical cultures

Neurite outgrowth assays were conducted in black 96-well plastic bottom plates using only the center 60 wells. Autoclaved water was added to the remaining 36 wells to protect against evaporation. 96-well plates were coated with coating media overnight at room temperature in the tissue culture (TC) hood with 50 µL.[32] The next day, coating media was aspirated and washed 3× with 100 µL autoclaved water. 200 µL Neurobasal medium was added to each of the 60 center wells. Plates were then put into a water-jacketed incubator at 37°C at 5% CO2 before beginning dissection. The Neurobasal in the 96-well plate was aspirated off. Plating media containing 75,000 cells per mL were generated and placed into a reservoir.[33] For each 96-well plate, generate 15 mL of 75,000 cells per mL. Once complete, the cells were mixed gently and 200 µL of volume per well was pipetted for a final cell density of 15,000 cells per well. Plates were then put back into a water-jacketed incubator at 37°C at 5% CO2. After 16–24 hours, plating media was aspirated and 200 µL replacement media per well was added. At 3 days in vitro (DIV3) cells underwent treatments and were fixed and stained on DIV6 unless otherwise stated.

To conduct treatments in agonist mode, DIV3 cells in 96-well plates first had 20 µL of media removed. Next, DMSO stock solutions were diluted 1:100 in Neurobasal (for 10 µM treatment, stocks were

30. Cell viability following dissection should be greater than 90% (with 90% being the lowest). Generally, the dissection will take a total of 2–3 hours, depending on the number of pups and plates being plated. Furthermore, I have noticed briefly that cell viability went down to 60–70% during dissection but immediately realized that trypan blue was expired and precipitating out of solution. Thus, make sure when doing the trypan blue staining that the trypan blue has no precipitants. See **Figure 1.1.**

31. Cells were diluted directly into the wells containing plating media. Then gently, keeping the plate flat on the TC hood, move the plate away and towards the experimenter, pause at the center, move the plate to the left and the right, pause at the center, and repeat a total of three times. This is to help spread the cells out and equally distribute them. I pause to prevent a circular motion which would force your cells to the edge of the plate instead. Furthermore, make sure the plating media is warm (30°C–37°C). This is critical because cooled plating media will rewarm in the incubator. The rewarming process will cause a convection current that will push cells that have not settled to the edge of the plate.

32. If there is a concern of wells drying out overnight, use 100 µL instead. During the washes use 200 µL autoclaved water instead of 100 µL. The remainder of the procedure is the same.

33. While plating, I will continuously move the reservoir and pipette up and down with the multi-channel pipette every five columns. This method prevents cells from settling on the bottom of the reservoir. Additionally, if I am plating greater than three plates at a time (greater than 45 mL volume of plating media and cells as we use 50 mL reservoirs), I use a new reservoir for every additional set of three plates.

10 mM; for 100 nM treatment, stocks were 100 µM). Then, 20 µL of this solution was added to the well for a 1:10 dilution (final drug concentration = 10 µM, 0.1% DMSO). Finally, plates were gently shaken in the TC hood and placed back into the incubator to incubate for 72 hours. For 1-hour stimulation studies, dilutions and treatments were done the same as above. After 1-hour has elapsed, media was replaced with drug-free replacement media.

To conduct treatments in antagonist mode, DIV3 cells in 96-well plates first had 40 µL of media removed. Next 10 mM DMSO stock solutions of drugs were diluted 1:100 in Neurobasal. After, the corresponding 1000x antagonist was diluted 1:100 in Neurobasal (ANA-12, 10 mM stock, final concentration 10 µM; DNQX, 20 mM stock, final concentration 20 µM). Then, 20 µL of the 1:100 Neurobasal solution of the antagonist was first added to each well. For wells not treated with the antagonist, 1:100 dilution of 100% DMSO in Neurobasal was added. Cells were incubated for 5-10 minutes at 37°C and 5% CO_2. Afterward, 20 µL of 1:100 drugs in Neurobasal solution were then added to each well for a final total concentration of the 10 µM ANA-12 or 20 µM DNQX, 10 µM of drug, and 0.2% DMSO. After 1 hour elapsed, media was replaced with drug-free replacement media.

Fixing, staining, and imaging 96-well plates for neurite outgrowth

After 72 hours total experiment time has elapsed following treatments, plates were removed from the incubator and checked under a light microscope to monitor the health of cells. Following this, in a chemical fume hood, 16% stock paraformaldehyde (PFA, Fisher Scientific) was diluted to 4% PFA in dPBS (1:3 dilution, 10 mL PFA into 30 mL dPBS, total volume 40 mL, 4% final concentration of PFA). The solution was warmed to 37°C. The plates were moved from the incubator to the chemical fume hood and 80% of the working volume (96-well plate = 160 µL) was removed. Next, 50% of the working volume of 4% PFA (96-well plate = 100 µL) was added into each well. The plates were incubated at room temperature without shaking for 20 minutes. After 20 minutes, plates were washed with 2× dPBS (96-well plate = 100 µL) and I proceeded to the staining procedure or stored the plates at 4°C for up to 2 weeks.

To stain, the dPBS was removed and the plates were permeabilized with 0.2% Triton X-100 (Fisher Scientific) in dPBS (50 µL) for 20 minutes at room temperature and without shaking. A 0.2% Triton X-100 was made using 10 mL of dPBS and 200 µL of 10% Triton X-100. Next, a 2% bovine serum albumin (BSA,

VWR) solution in dPBS was made with gentle rocking motions. This solution was not vortexed. Each plate was blocked with BSA for 1 hour at room temperature without shaking (50 µL). Microtubule-associated protein 2 (MAP2, EnCor) chicken IgY antibody 1:10000 was diluted into 2% BSA. After 1 hour elapsed, the blocking BSA was aspirated and 2% BSA containing MAP2 antibody (50 µL) was added. Cells were moved into the 4°C room and gently shaken overnight.

The 16–24 hours later, plates were washed 3× with dPBS. Wash 1x with 2% BSA. A 1:500 dilution of goat anti-chicken IgY secondary antibody Alexa Fluor 488 conjugate (Life Technologies) in 2% BSA was generated. Aspirate the 2% BSA wash and added antibody-containing 2% BSA into each well (50 µL). The plates were incubated at room temperature for 1 hour with gentle shaking in the dark. Afterward, the medium was aspirated off, washed 3× with dPBS, and filled with 100 µL dPBS. The plate was covered foil and kept in the dark and at 4°C until ready to image.

96-well plate image acquisition was done on the Molecular Devices ImageXpress Micro XLS Widefield High-Content Analysis System at 9 sites per well using 20x magnification. Images were analyzed using the Sholl analysis plug-in ImageJ Fiji **(ver. 1.51N)**. First, 0–2 representative neurons were selected per site using the Rectangle Function.[34] Once neurons were selected, a copy of the selected neuron was generated using the duplicate function. After selecting all the neurons for that treatment group, duplicated copies were saved. Once all groups have been completed, I am unblinded to VEH and KET conditions on the plate to adjust brightness and contrast for the plate. This is critical as KET and other psychoplastogens will cause very thin, dim, small neurites to grow that can be missed if image brightness and contrast are not adjusted. Next, brightness and contrast maximum and minimum values are recorded and applied to the image. The images then undergo the Threshold function, converting the images to binary (black and white). From there, the minimum and maximum values of Threshold are adjusted to give the best representation of the original fluorescent image. This value was recorded and was kept the same between all images from the same plate. Finally, images were cleaned using the Paint Brush tool for artifacts in the image, and the

34. This part is very subjective and can take a couple of attempts to get used to what is a good neuron vs what is not. This publication contains examples of what neurons to choose:
Dunlap, L. E.; Azinfar, A.; Ly, C.; Cameron, L. P.; Viswanathan, J.; Tombari, R. J.; Myers-Turnbull, D.; Taylor, J. C.; Grodzki, A. C.; Lein, P. J.; Kokel, D.; Olson, D. E. Identification of Psychoplastogenic N,N-Dimethylaminoisotryptamine (isoDMT) Analogs Through Structure-Activity Relationship Studies. *J. Med. Chem.*, **2020**, *63*, 1142–1155.

center of the neuron was then dotted using the Point function. Images are saved and run through the Batch Process Macro on ImageJ Fiji using the following script:

run("Sholl Analysis...", "starting=0 ending=NaN radius_step=2 #_samples=1 integration=Mean enclosing=1 #_primary=4 infer fit linear polynomial=[Best fitting degree] most semi-log normalizer=Area create background=228 save do");

The Sholl analysis circle radii = 2-pixel increments. All analysis was done by an experimenter blinded to treatment conditions.

For **Figures 3.3C–F** analysis was conducted using the raw images collected above. Simple Neurite Tracer in ImageJ Fiji (**ver. 1.51N**) was used to trace the individual neurons and the pathlengths were exported into Excel and combined to generate the data observed in **Figures 3.3C–F**.

Treating, fixing, staining, and imaging 96-well plates for synaptic density for corticosterone

96-well plates are prepared the same way as above for neurite outgrowth. In brief, E18 embryonic cortical tissue was collected, and primary cortical cultures were plated in plating media at 15,000 cells per well in poly-D-lysine coated black 96-well plates. Next, after 16–24 hours, plating media was removed and replaced with replacement media. On DIV6 and DIV13, cells had 100 µL of media removed and 140 µL of feeding media was added. On DIV18, neurons were then treated with drugs. Dilutions for drugs were done as above in the neurite outgrowth assays. Neurons were treated for 24 hours.

Fixing was done the same as above in the neurite outgrowth section. In a chemical fume hood, 16% stock paraformaldehyde (PFA, Fisher Scientific) was diluted to 4% PFA in dPBS (1:3 dilution, 10 mL PFA into 30 mL dPBS, total volume 40 mL, 4% final concentration of PFA). The solution was warmed to 37°C. Move plates from incubator to chemical fume hood and remove 80% of the working volume (96-well plate = 160 µL). Next, add 50% of the working volume of 4% PFA (96-well plate = 100 µL). Incubate plates at room temperature without shaking for 20 minutes. After 20 minutes, wash the plate with 2× dPBS (96-well plate = 100 µL) and begin staining or store at 4°C for up to 2 weeks.

Following fixing, the dPBS was removed and permeabilized with 0.2% Triton X-100 (Fisher Scientific) in dPBS (50 µL) for 20 minutes at room temperature and without shaking. To generate 0.2%, combine 10 mL of dPBS and 200 µL of 10% Triton X-100. Next, generate a 2% bovine serum albumin (BSA, VWR) solution in dPBS. Do not vortex this mixture, use a gentle rocking motion to mix the solution. Block each plate with BSA for 1 hour at room temperature, without shaking (50 µL). While blocking, a solution containing microtubule-associated protein 2 (MAP2) chicken IgY (EnCor, 1:10,000), guinea pig anti-VGLUT1 (Millipore, 1:1000), and mouse anti-PSD-95 (Millipore, 1:500) antibodies into 2% BSA was made. After 1 hour elapsed, the blocking BSA was aspirated and 2% BSA containing the antibodies (50 µL) was added. Cells were stored in a 4°C room and gently shaken overnight.

The next day (16–24 hours after treatment), plates were washed 3× with dPBS. Wash 1× with 2% BSA. A solution containing goat anti-chicken IgY secondary antibody Alexa Fluor 488 (Life Technologies, 1:500), Cy3 AffiniPure donkey anti-guinea pig IgG (H+L) (Jackson ImmunoResearch Inc, 1:500), and Alexa Fluor 647 AffiniPure donkey anti-Mouse IgG (H+L) (Jackson ImmunoResearch Inc, 1:500) in 2% BSA was generated. This solution into each well (50 µL). The plate was incubated at room temperature for 1 hour with gently shaking in the dark. Afterward, the medium was aspirated off, washed 3× with dPBS, and filled with 100 µL dPBS. Plates were covered with foil and kept in the dark and at 4°C until ready to image.

All images were obtained using a Molecular Devices ImageXpress Micro XLS Widefield High-Content Analysis System at 9 sites per well using 40× magnification. Image analysis was performed using MetaXpress software. Analysis was completed by first using the MAP2 channel to establish a mask of the neuron using thresholds between 0 and 30 µm. Then, the mask of the neuron was expanded by 1 µm. The size of the objects for the presynaptic and postsynaptic fluorescent images was established, and only signals of 0–1.5 µm punctate were used to generate a mask. To measure synaptic density, the presynaptic and postsynaptic masks were overlaid using the logical operation “and” to retain the only signal that colocalized to form the synapse mask. The number of events occurring in this synapse mask was quantified and normalized to the MAP2 channel mask area (number of counts per μm^2). Normalized data were then tested for outliers using the ROUT method in Graphpad Prism (version 8) at Q = 1%. The outlier test was completed to remove artifacts in an unbiased manner.

Chapter 3.6.3 General Methods for Chapter 3.3

Glutamate Assay

Embryonic day 18 (E18) primary cortical cultures were plated at 3 million cells per well in poly-D-lysine-coated 6-well plates (working volume is 2 mL, see **Chapter 3.6.2 96-well plates primary cortical cultures**) or 6 million cells per well in poly-D-lysine coated 10 cm dishes (working volume is 12 mL, culturing and coating conditions are scaled to 12 mL). After 16–24 hours, plating media was removed and replacement media containing 5 μM cytosine β-D-arabinofuranoside hydrochloride (Ara-C)[35] is added and cultured until DIV3 or DIV14 for KCl stimulation to measure glutamate release. For cells grown until DIV14, at DIV6, 50% (1 mL in 6-well plate or 6 mL in 10 cm dishes) of media was removed and 70% (1.4 mL in 6-well plate or 8.4 mL in 10 cm dishes) of feeding media containing 5 μM Ara-C was added. The addition of 70% feeding media is to accommodate loss in media volume due to evaporation in the incubator. At DIV3 and DIV14, media was completely removed and 50% (1 mL in 6-well plate or 6 mL in 10 cm dishes) working volume of a pre-warmed sterile filtered washing solution containing 119 mM NaCl, 2.5 mM KCl, 2 mM CaCl2, 2 mM MgCl2, 25 mM HEPES, and 30 mM D-Glucose in autoclaved deionized water was used to wash the cells gently 3×. On the third wash, 100 μL of this solution was collected to use as the baseline before stimulation. Then, the remaining buffer was removed and added 50% (1 mL in 6-well plate or 6 mL in 10 cm dishes) of the working volume of a pre-warmed sterile filtered depolarization buffer containing 32 mM NaCl, 90 mM KCl, 2 mM CaCl2, 2 mM MgCl2, 25 mM HEPES, and 30 mM D-Glucose in autoclaved deionized water. For cells treated with psychoplastogens, cells were washed with the pre-warmed washing solution. The psychoplastogens are diluted 1:1000 from their 10 mM DMSO stock solutions and added directly onto the cells. Cells were incubated for 15 minutes and the buffer is then collected and prepared for glutamate assay as called for by the manufacturer from Promega (J7021), ThermoFisher (A12221), and Sigma (MAK004). Plate reader used to measure absorbance and bioluminescence on the BioTek Synergy HTX plate reader (Gen5).

35. Schwieger, J.; Esser, K.H.; Lenarz, T.; Scheper, V. Establishment of a long-term spiral ganglion neuron culture with reduced glial cell number: Effects of AraC on cell composition and neurons. *J Neurosci Methods*. **2016**, 268, 106–116.

Chapter 3.6.4 General Methods for Chapter 3.4

Principal component analysis (PCA)

First, install RStudio onto the computer.[36] I currently use RStudio Ver. 1.3.959. Once RStudio is installed, the data of interest is sorted and imported into RStudio using the import function **(Fig. 3.5)**.

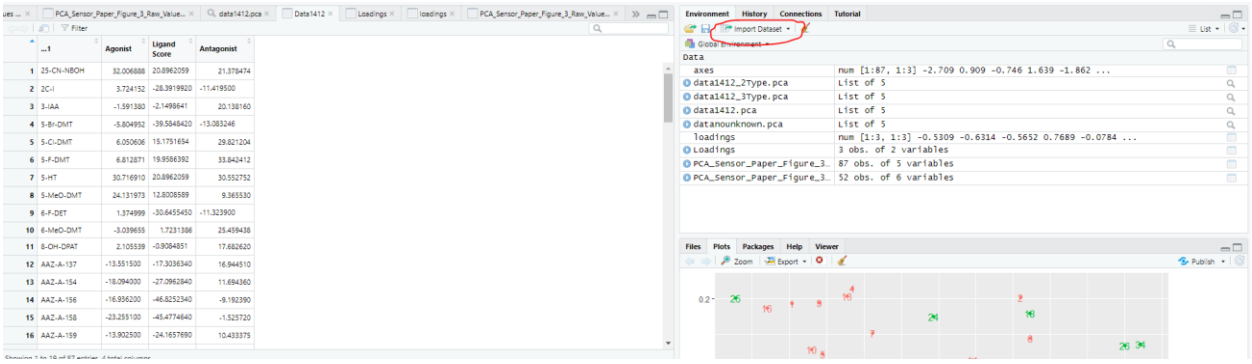

Figure 3.5. Screenshot of RStudio interface illustrating the "Import Data Set."

The imported data should be organized in an Excel sheet. Column A is the treatment name. The following columns should be separated into individual components for the principal component analysis. Furthermore, I use a column to include the "type" function each small molecule may fall into. For example, DMT would be classified as a hallucinogen. This allows for the sorting of the dataset later once the PCA is complete **(Fig. 3.6)**.

36. https://www.rstudio.com/

	Nmax	Primary	Secondary	Total Lengths	Longest Neurite	Cell death	DNQX Inhibited	Type
Allopregnanolone	1.541204	0.947989	0.721537	0.982561	0.32268	17.87647	0.29056	Fast-acting
Scopolamine	1.120006	0.671768	1.373567	0.626879	-0.33068	8.491612	0.536359	Fast-acting
Glyx	1.346945	0.829889	1.339677	1.267559	0.128096	6.477144	0.990415	Fast-acting
Ketamine	1.311283	0.7469	0.640617	0.726372	-0.09496	9.751145	0.396924	Fast-acting
DMT 10	1.582763	1.164065	1.83067	1.288895	0.154604	4.970651	0.376473	Fast-acting
Fluoxetine	1.732739	0.829889	0.926085	0.993268	0.207752	-18.1075	0.809418	Slow-acting
(s)-duloxetine	1.247092	0.914666	1.410167	1.116716	0.189952	-18.8432	1.097002	Slow-acting
Sertraline	0.69855	-0.05056	0.788701	0.037621	-0.3238	-19.9666	0.86975	Slow-acting
Amitriptyline	1.039705	0.671768	0.514569	0.779073	0.309673	-10.0177	0.966282	Slow-acting
Bupropion	1.282105	0.377554	0.342947	0.717775	-0.15205	10.03846	1.029028	Slow-acting
D-amphetamine	0.18956	-0.19151	-0.42258	-0.37693	-0.46965	8.340172	0.145763	Not antidepressant
Caffeine	0.399478	0.201089	-0.47203	-0.80647	-0.62568	6.363539	0.303967	Not antidepressant
Nicotine	0.570421	0.084932	-0.04808	0.01011	-0.04035	6.754382	0.396924	Not antidepressant
Morphine	0.730265	0.264787	-0.23807	0.014607	-0.1896	6.623395	0.559598	Not antidepressant
Modafnil	0.943389	-0.18485	0.226342	0.09623	-0.06083	5.637321	0.70082	Not antidepressant

Figure 3.6. Screenshot of Excel spreadsheet illustrating each component to sort for the PCA.

Once the importing is complete, if this is the first time using RStudio, input the following lines of code into the console:

a) *install.packages("Rcpp", dependencies = TRUE)*

b) *install.packages("devtools")*

c) *install.packages("backplot")*

d) *install.packages("tidyverse")*

e) *install.packages("ggfortify")*

Next, run the following lines of code in order:

a. *Library(devtools)*

b. *Library(ggplot2)*

c. *Library(ggfortify)*

d. *"file name for PCA" <- prcomp("file name from Excel imported"[,c("column numbers you want analyzed")], center = TRUE,scale.= TRUE)*

   i. Example:

   data1412_2Type.pca <-

   prcomp(PCA_Sensor_Paper_Figure_3_Raw_Values_for_R [,c(2:8)])

e. *Autoplot("PCA file name), label = T, data = "file name from Excel imported", colour = "column title that sorts your drugs", frame = TRUE)*

   i. Example:

   autoplot(data1412_2Type.pca, label=T, data= PCA_Sensor_Paper_Figure_3_Raw_Values_for_R, colour ="Type")

Finally, a plot will appear on the console. This plot can be exported by saving the graph using the "Save" function. In my data set, I used the column "Type" to separate and color code the specific dots in the plot to easily distinguish between treatment groups and whether there was any clustering.[37] However, I prefer to export the data and use Prism to plot my data. Thus, the last line of code I use to export the data is as follows:

"PCA file name"$x

For example: data1412_2Type.pca$x

37. Be careful of the spelling of "colour" as it is an easy mistake to overlook when writing this line of code into the console.

Chapter 4 PsychLight: A Psychedelic-inspired Serotonin 2A Biosensor[1]

Chapter 4.1 Introduction

G-protein coupled receptors (GPCRs) represent about 30% of all FDA-approved medications.[2] These medications only target about 10% of the known GPCRs, making GPCRs attractive targets for therapeutics.[3] Many of these drugs target the intracellular signaling pathways mediated through heterotrimeric G proteins, arrestins, and/or other effectors.[4] Biased agonism, otherwise known as functional selectivity, activates or deactivates distinct signaling pathways of GPCRs through the stabilization of distinct conformations. These conformations can be recorded, calculated, and modeled to determine the o each structure represents as a model for a drug discovery platform.[5]

Despite decades of efforts to elucidate the critical functions of GPCRs to better target therapeutics, current methodologies assessing these functions overlook the myriad of dynamic ranges in signaling that GPCRs engage. For example, radioligand binding assays are efficient at determining target engagement with high temporal kinetics, allosteric modulation, and suitable for all GPCR classes. However, the radioligand binding assay falls short as it does not examine the function of ligands (agonist, partial agonist, antagonist, or inverse agonist) at the receptor. Ca^{2+} flux, inositol trisphosphate (IP3) release, cyclic adenosine monophosphate (cAMP) release, and bioluminescence resonance energy transfer (BRET) or Förster resonance energy transfer (FRET) β-Arrestin recruitment assays can determine the function of a ligand at the GPCR of interest but offers no information on binding affinity.[6] Therefore, to determine the

---

1. The data in this chapter is published in the following publication:
Dong, C.; Ly, C.; Dunlap, L. E.; Vargas, M. V.; Sun, J.; Hwang, I.-W.; Azinfar, A.; Oh, W. C.; Wetsel, W. C.; Olson, D. E.; Tian, L. Psychedelic-Inspired Drug Discovery Using an Engineered Biosensor. *Cell*, **2021**, *184*, 2779–2792.
2. Hauser, A.S.; Attwood, M.M.; Rask-Andersen, M.; Schiöth, H.B.; Gloriam, D.E. Trends in GPCR drug discovery: new agents, targets and indications. *Nat. Rev. Drug Discov.* **2017**, *16*, 829–842.
3. (a) Fang, Y.; Kenakin, T.; Liu, C. Editorial: Orphan GPCRs As Emerging Drug Targets. *Front. Pharmacol.* **2015**, *6*, 295.
(b) Kroeze, W.K.; Sheffler, D.J.; Roth, B.L. G-protein-coupled receptors at a glance. *J. Cell Sci.* **2003**, *116*, 4867–4869.
4. Kenakin, T.; Miller, L.J. Seven transmembrane receptors as shapeshifting proteins: the impact of allosteric modulation and functional selectivity on new drug discovery. *Pharmacol. Rev.* **2010**, *62*, 265–304.
5. (a) Roth, B.L.; Irwin, J.J.; Shoichet, B.K. Discovery of new GPCR ligands to illuminate new biology. *Nat. Chem. Biol.* **2017**, *13*, 1143–1151.
(b) Shonberg, J.; Lopez, L.; Scammells, P.J.; Christopoulos, A.; Capuano, B.; Lane, J.R. Biased agonism at G protein-coupled receptors: the promise and the challenges--a medicinal chemistry perspective. *Med. Res. Rev.* **2014**, *34*, 1286–1330.
6. (a) Tan, L.; Yan, W.; McCorvy, J.D.; Cheng, J. Biased Ligands of G Protein-Coupled Receptors (GPCRs): Structure-Functional Selectivity Relationships (SFSRs) and Therapeutic Potential. *J. Med. Chem.* **2018**, *61*, 9841–9878.
(b) Cvijic, M.E.; Sum, C.S.; Alt, A.; Zhang, L. GPCR profiling: from hits to leads and from genotype to phenotype. *Drug Discov. Today Technol.* **2015**, *18*, 30–37.
(c) Flanagan, C.A. GPCR-radioligand binding assays. *Methods Cell Biol.* **2016**, *132*, 191–215.

potency of ligands at the receptor, we collaborated with the Tian lab at UC Davis to engineer a biosensor that could characterize both phenotypes of ligands in a single assay.

While there are hundreds of GPCRs, the serotonin 2A (5-HT2A) receptor is of interest to our group as it is associated with depression, hallucinations, and psychosis.[7] Several key psychedelics are currently in clinical trials for the treatment of depression, such as lysergic acid diethylamide (LSD),[8] psilocybin,[9] and 5-methoxy-*N*,*N*-dimethyltryptamine (5-MeO-DMT Previously, we have shown that classic psychedelics can promote neural plasticity.[10] Furthermore, research has shown that changes in structural plasticity in the prefrontal cortex may be the basis of the therapeutic response of antidepressants in the clinic. Therefore, we postulate that the therapeutic effects of psychedelics are not necessarily dependent on their hallucinogenic potential.[11] Non-hallucinogenic analogs have been tested and exhibit similar therapeutic potential compared to their hallucinogenic counterpart, albeit currently only in rodents.[12] To explore the therapeutic potential of non-hallucinogenic analogs **(Fig. 4.1A)**, I tested these molecules in my neurite outgrowth assay **(Fig. 4.1B–G)** and discovered all of the tryptamine analogs (black) and two of the ergoline analogs (magenta) increased neurite arborization in our cortical cultures. Then I tested one tryptamine and one ergoline in my dendritic spine number assay and observed increases in the number of dendritic spines following treatment with ligand **(Fig. 4.1H)**. Moreover, sub-hallucinogenic doses elicit antidepressant potential suggesting the hallucinogenic side effects can be decoupled from the therapeutic effects.[13] Thus, the analogs of the hallucinogens become attractive lead compounds to develop better-tolerated, fast-acting therapeutics for depression. Lastly, 5-HT2AR antagonists and inverse agonists, such as clozapine and

(d) Zhang, R.; Xie, X. Tools for GPCR drug discovery. *Acta. Pharmacol. Sin*. **2012**, *33*, 372–384.
7. (a) Nichols, D.E. Hallucinogens. *Pharmacol. Ther*. **2004**, *101*, 131–181.
(b) Savitz, J.B.; Drevets, W.C. Neuroreceptor imaging in depression. *Neurobiol. Dis*. **2013**, 52, 49–65.
8. clinicaltrials.gov/ct2/show/NCT03866252
9. Psilocybin recently failed to meet its primary outcomes in phase 2 clinical trials. Secondary outcomes not corrected for multiple comparisons indicated that results favored psilocybin over escitalopram as an antidepressant. For more information see the following: Carhart-Harris, R.; Giribaldi, B.; Watts, R.; Baker-Jones, M.; Murphy-Beiner, A.; Murphy, R.; Martell, J.; Blemings, A.; Erritzoe, D.; Nutt, D.J. Trial of Psilocybin versus Escitalopram for Depression. *N. Engl. J. Med.* **2021**, *384*, 1402–1411.
10. Ly, C.; Greb, A.C.; Cameron, L.P.; Wong, J.M.; Barragan, E.V.; Wilson, P.C.; Burbach, K.F.; Soltanzadeh Zarandi, S.; Sood, A.; Paddy, M.R.; Duim, W.C.; Dennis, M.Y.; McAllister, A.K.; Ori-McKenney, K.M.; Gray, J.A.; Olson, D.E. Psychedelics Promote Structural and Functional Neural Plasticity. *Cell Rep.* **2018**, 23, 3170–3182.
11. Olson, D. E. The Promise of Psychedelic Science. *ACS Pharmacol. Transl. Sci*. **2021**, 4, 413–415.
12. (a) Dunlap, L.E.; Azinfar, A.; Ly, C.; Cameron, L.P.; Viswanathan, J.; Tombari, R.J.; Myers-Turnbull, D.; Taylor, J.C.; Grodzki, A.C.; Lein, P.J.; Kokel, D.; Olson, D.E. Identification of Psychoplastogenic *N*,*N*-Dimethylaminoisotryptamine (isoDMT) Analogues through Structure-Activity Relationship Studies. *J. Med. Chem.* **2020**, *63*, 1142–1155.
(b) Cameron, L. P.; Tombari, R. J.; Lu, J.; Pell, A. J.; Hurley, Z. Q.; Ehinger, Y.; Vargas, M. V.; McCarroll, M. N.; Taylor, J. C.; Myers-Turnbull, D.; Liu, T.; Yaghoobi, B.; Laskowski, L. J.; Anderson, E. I.; Zhang, G.; Viswanathan, J.; Brown, B. M.; Tjia, M.; Dunlap, L. E.; Rabow, Z. T.; Fiehn, O.; Wulff, H.; McCorvy, J. D.; Lein, P. J.; Kokel, D.; Ron, D.; Peters, J.; Zuo, Y.; Olson, D. E. A Non-Hallucinogenic Psychedelic Analogue with Therapeutic Potential. *Nature*, **2021**, *589*, 474–479.
13. Cameron, L.P.; Benson, C.J.; DeFelice, B.C.; Fiehn, O.; Olson, D.E. Chronic, Intermittent Microdoses of the Psychedelic N,N-Dimethyltryptamine (DMT) Produce Positive Effects on Mood and Anxiety in Rodents. *ACS Chem. Neurosci*. **2019**, *10*, 3261–3270.

risperidone, have antipsychotic properties that make them effective therapeutics to manage psychosis.[14] Hence, an in vitro assay that can determine the potency and pharmacological activities of novel small molecules would help to better characterize lead compounds as next-generation therapeutics at the 5-HT2AR. Current assays measuring hallucinogenic potential requires a rodent behavioral model to distinguish this functional off-target effect—head-twitch response (HTR)[12a] or drug discrimination (DD).[15]

Here, we describe a medium-throughput hallucinogenic potential assay using an engineered human 5-HT2AR biosensor (psychLight). PsychLight differentiates between known hallucinogens and non-hallucinogens using a conformation-dependent fluorescent output. Furthermore, we screened, characterized, and identified two previously unknown hallucinogens and a previously unknown non-hallucinogen in a small library screen (83 compounds). These results were then validated using HTR. Lastly, we identified a potential therapeutic using our neurite outgrowth assay and screened with psychLight for its hallucinogenic potential. We then confirmed the hallucinogenic potential (HTR) and therapeutic potential (FST and sucrose preference) in vivo.

14. Sullivan, L. C.; Clarke, W. P.; Berg, K. A. Atypical antipsychotics and inverse agonism at 5-HT2 receptors. *Curr. Pharm. Des.* **2015**, *21*, 3732–3738.
15. Glennon, R.A.; Young, R.; Jacyno, J.M.; Slusher, M.; Rosecrans, J.A. DOM-stimulus generalization to LSD and other hallucinogenic indolealkylamines. *Eur. J. Pharmacol.* **1983**, *86*, 453–459.

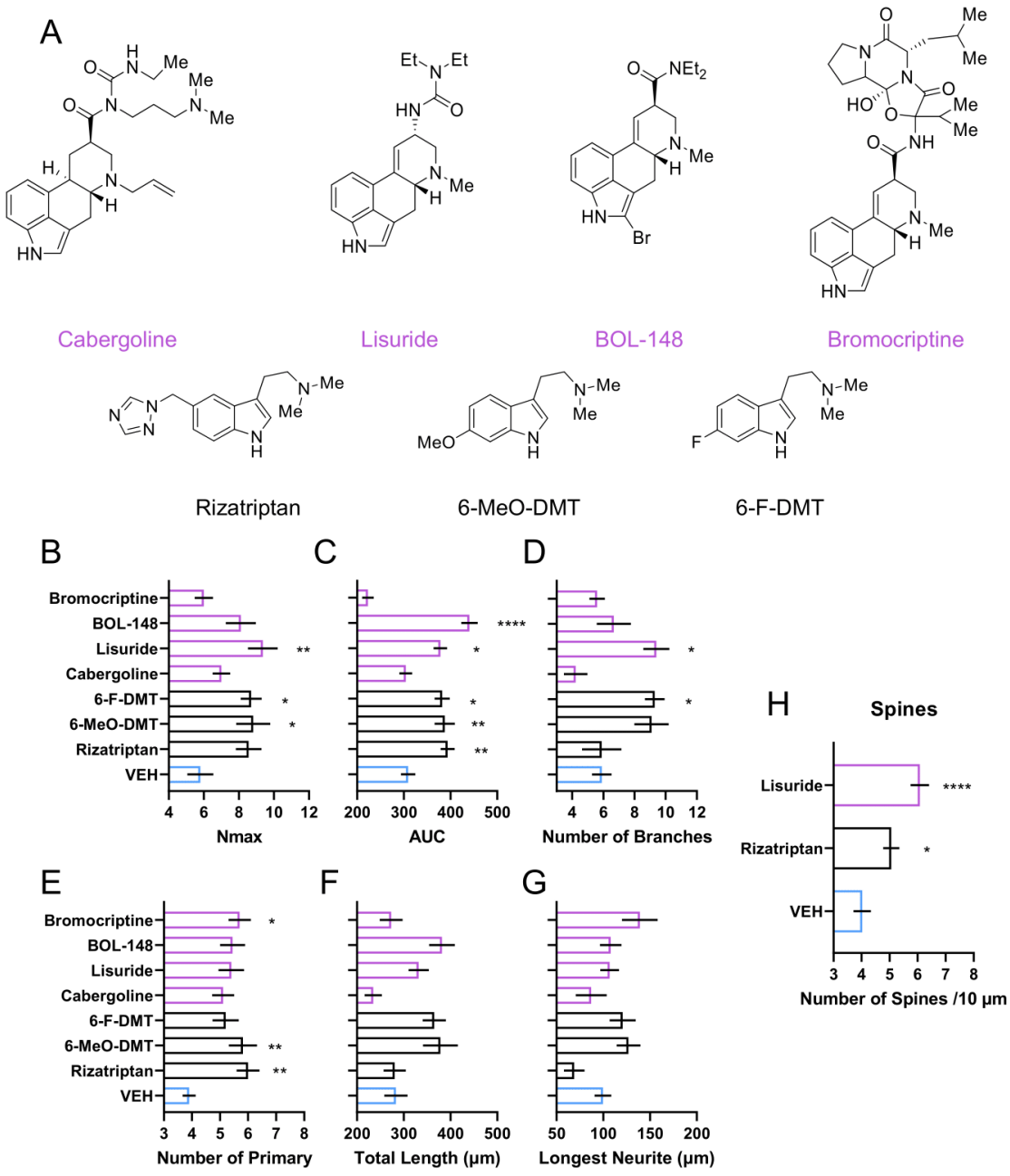

Figure 4.1.[16] Examples of potential non-hallucinogenic congeners that promote neurite outgrowth and the increase in the number of dendritic spines. **(A)** Structures of non-hallucinogenic analogs.[17] **(B–G)** Sholl

16. This data has not been published.
17. Cabergoline, lisuride, BOL-148, and bromocriptine are all non-hallucinogenic analogs of LSD. Rizatriptan, 6-MeO-DMT, and 6-F-DMT are analogs of DMT. While it has been shown that 6-MeO-DMT does not have hallucinogenic potential in HTR (see footnotes 14a and 18). In clinical trials, rizatriptan had infrequent (1/101 patients) induced hallucination.
See: Seeburger, J.L.; Cady, R.K.; Winner, P.; MacGregor, A.; Valade, D.; Ge, Y.; Zhang, Y.; Hustad, C.M.; Strickler, N.; Schaefer, E.; Connor, K.M.; Ho, T.W. Rizatriptan for treatment of acute migraine in patients taking topiramate for migraine prophylaxis. *Headache*. **2012**, 52, 57–67.

analysis characterization and quantification of **(B)** Nmax, **(C)** area under the curve (AUC), **(D)** the number of branches, **(E)** the number of primary neurites, **(F)** the total length of neurites, and **(G)** the longest neurite measured. **(H)** The number of dendritic spines quantified following lisuride and rizatriptan treatments. Data represented as mean ± S.E.M. **(B–G)** n= 9–11; **(H)** n=18–20. For **(B–H)**, a one-way analysis of variance with a Dunnett's post hoc test was utilized as compared to the VEH control. *p < 0.05, **p < 0.01, ***p < 0.001, ****p < 0.0001. BOL-148 = 2-bromo-lyseric acid diethylamide; 6-F-DMT = 6-fluoro-N,N-dimethyltryptamine; 6-MeO-DMT = 6-methoxy-N,N-dimethyltryptamine; VEH = vehicle.

6-F-DMT has been thought to be non-hallucinogenic as 6-F-DET (6-fluoro-N,N-diethyltryptamine) has been shown to not substitute for LSD in DD.
See: Helsley, S.; Fiorella, D.; Rabin, R.A.; Winter, J.C. A comparison of N,N-dimethyltryptamine, harmaline, and selected congeners in rats trained with LSD as a discriminative stimulus. *Prog. Neuropsychopharmacol Biol. Psychiatry*. **1998**, 22, 649–663.
No HTR or DD data exists for 6-F-DMT describing its hallucinogenic potential.

Chapter 4.2 Characterization of PsychLight.

The 5-HT2A biosensor was developed and engineered by the Tian lab by replacing the third intracellular loop (IL3) of the human 5-HT2AR with a circularly permuted green fluorescent protein (cpGFP, **Fig. 4.2A**). Following optimizations, we named the best variant psychLight1. In human embryonic kidney 293T (HEK293T) cells, psychLight1 was expressed on the cell surface. However, in neurons, we observed predominately intracellular expression of psychLight1 **(Fig. 4.2B)**. The intracellular expression of wild-type 5-HT2AR in neurons is well known.[18] Unfortunately, due to this, our psychLight1 construct in neurons was unable to produce a robust increase of fluorescence signal following serotonin (5-HT) treatment because 5-HT is not cell membrane permeable and requires the serotonin transporter (SERT). The SERT is not expressed on cortical neurons where a large population of the 5-HT2AR is localized.[19] As we wanted to use psychLight in neurons, we needed to localize the expression to the cell surface to optimize the fluorescent signal and potentially measure binding of hallucinogenic drugs to the 5-HT2ARs in vivo to correlate with behavior. Therefore, Chunyang Dong of the Tian Lab incorporated an ER export motif (FCYENEV) to the C-terminus of psychLight1, which yielded a variant (psychLight2) with improved membrane expression in both HEK293T cells and neurons **(Fig. 4.2B)**.

18. (a) Weber, E.T.; Andrade, R. Htr2a Gene and 5-HT(2A) Receptor Expression in the Cerebral Cortex Studied Using Genetically Modified Mice. *Front Neurosci.* **2010**, *4*, 36.
(b) Gelber, E.I.; Kroeze, W.K.; Willins, D.L.; Gray, J.A.; Sinar, C.A.; Hyde, E.G.; Gurevich, V.; Benovic, J.; Roth, B.L. Structure and function of the third intracellular loop of the 5-hydroxytryptamine2A receptor: the third intracellular loop is alpha-helical and binds purified arrestins. *J Neurochem.* **1999**,*72*, 2206–2214.
(c) Xia, Z.; Hufeisen, S.J.; Gray, J.A.; Roth, B.L. The PDZ-binding domain is essential for the dendritic targeting of 5-HT2A serotonin receptors in cortical pyramidal neurons in vitro. *Neuroscience.* **2003**, *122*, 907–920.
(d) Schmid, C.L.; Raehal, K.M.; Bohn, L.M. Agonist-directed signaling of the serotonin 2A receptor depends on beta-arrestin-2 interactions in vivo. *Proc Natl Acad Sci U S A*. **2008**, *105*, 1079–1084.
19. (a) Blackburn, K.J.; French, P.C.; Merrills, R.J. 5-hydroxytryptamine uptake by rat brain in vitro. *Life Sci*. **1967**, *6*, 1653–1663.
(b) Xu, T.; Pandey, S. C. Cellular localization of serotonin(2A) (5HT(2A)) receptors in the rat brain. *Brain Res. Bull*. **2000**, *51*, 499–505.
(c) Zhou, FC.; Sari, Y.; Zhang, JK. Expression of serotonin transporter protein in developing rat brain. *Brain Res Dev Brain Res.*, **2000**, *1*, 33–45.
(d) Lebrand, C.; Cases, O.; Wehrlé, R.; Blakely, RD.; Edwards, RH.; Gaspar P. Transient developmental expression of monoamine transporters in the rodent forebrain. *J. Comp. Neurol.* **1998**, *4*, 506–524.

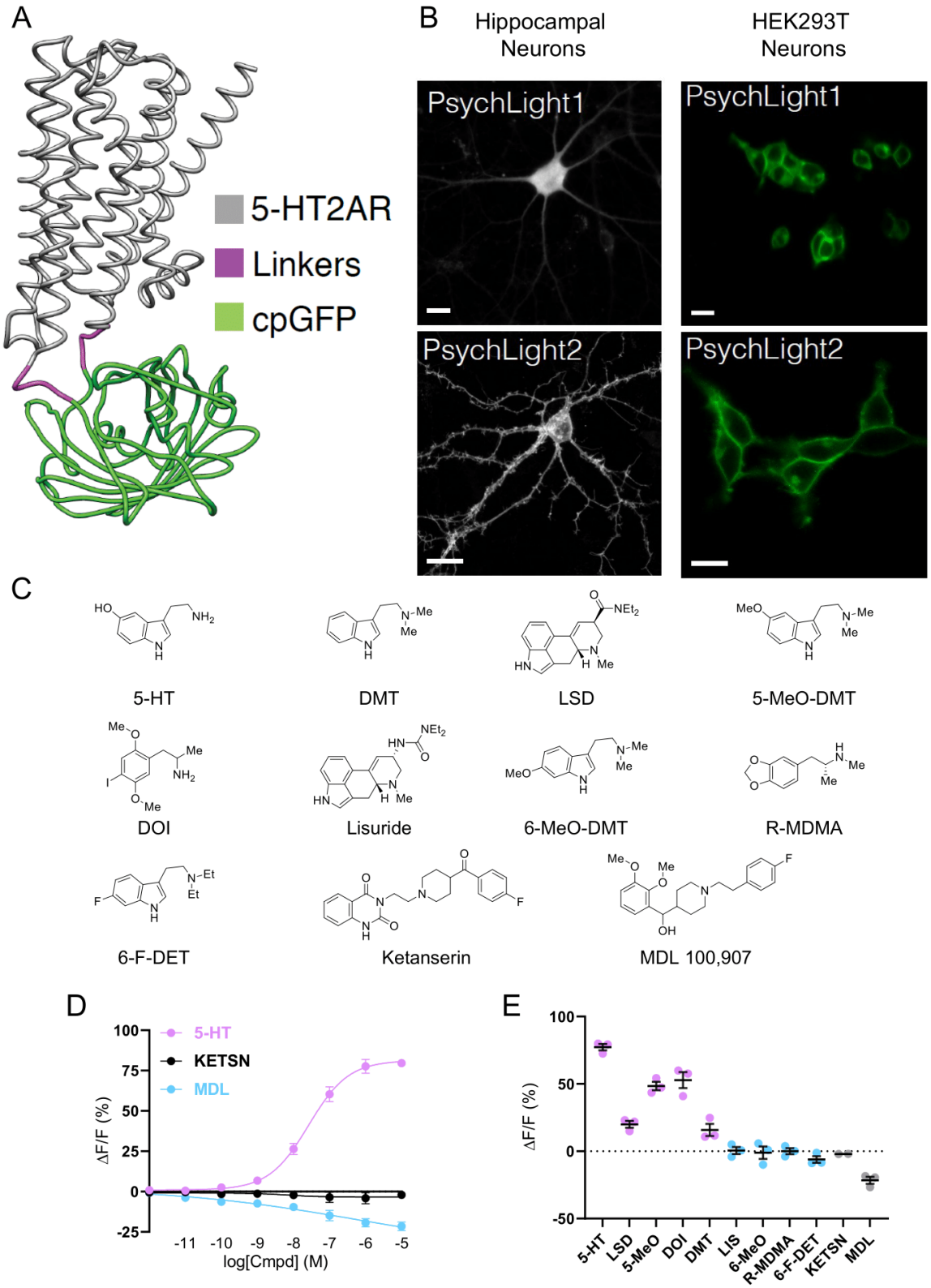
A
5-HT2AR
Linkers
cpGFP
B
Hippocampal Neurons
HEK293T Neurons
PsychLight1
PsychLight1
PsychLight2
PsychLight2
C
5-HT
DMT
LSD
5-MeO-DMT
DOI
Lisuride
6-MeO-DMT
R-MDMA
6-F-DET
Ketanserin
MDL 100,907
D
5-HT
KETSN
MDL
ΔF/F (%)
log[Cmpd] (M)
E
ΔF/F (%)
5-HT
LSD
5-MeO
DOI
DMT
LIS
6-MeO
R-MDMA
6-F-DET
KETSN
MDL

Figure 4.2. Development of a fluorescent sensor based on the 5-HT2A receptor. **(A)** Simulated structure of psychLight consisting of the serotonin 2A (5-HT2A) receptor (gray), a linker (magenta), and a cpGFP (green). **(B)**. Representative images of cultured hippocampal neurons and HEK293T cells transiently expressing psychLight1 and psychLight2. Scale bars = 20 μm. **(C)** Structures of known hallucinogens and non-hallucinogens used in this study. **(D)** PsychLight1-expressing HEK293T cells respond to ligands in a dose-dependent manner. **(E)** PsychLight1 is activated by hallucinogenic 5-HT2A agonists (magenta) and not non-hallucinogenic congeners (blue) or antagonists (gray). 5-HT = serotonin; DMT = N, N-dimethyltryptamine; LSD = lysergic acid diethylamide; 5-MeO-DMT = 5-meothxy-N, N-dimethyltryptamine; DOI = 2,5-dimethoxy-4-iodoamphetamine; 6-MeO-DMT = 6-meothxy-N, N-dimethyltryptamine; R-MDMA = (R)-3,4-methylenedioxymethamphetamine; 6-F-DMT = 6-fluoro-N, N-diethyltryptamine.

Next, we characterized the biosensor using the endogenous ligand, serotonin (5-HT), and known antagonists, ketanserin (KETSN) and MDL 100,907 (MDL) (**Fig. 4.2D**) in agonist mode. The agonist mode assay compares the baseline fluorescence to the resulting fluorescence after treatment with a drug of interest. We began with a dose-response and found that 5-HT elicited a response (EC_{50} = 26.3 nM, **Fig. 4.2D**) from the psychLight, whereas the two antagonists did not. This result suggested that we measured the differences in ligand-induced conformational changes: agonists induced a conformation leading to an increase in fluorescence while antagonists produced a conformation leading to a decrease in fluorescence. Furthermore, the EC_{50} observed for 5-HT was comparable to the K_i and EC_{50} values measured in radioligand binding assays[20] and Ca^{2+} flux assays.[21] Subsequently, we tested known hallucinogen and non-hallucinogen congeners of different structural classes **(Fig. 4.2C)** and were surprised to observe that only the known hallucinogens (10 μM) caused a conformation change in psychLight that lead to an increase in fluorescence **(Fig. 4.2E)**. We chose the hallucinogenic ligands (DMT, LSD, 5-MeO-DMT, and DOI) because they induce hallucinations in humans.[22] Immediately, we began conducting dose responses for each

20. Psychoactive Drug Screening Program (PDSP)
21. Toro-Sazo, M.; Brea, J.; Loza, M.I.; Cimadevila, M.; Cassels, B.K. 5-HT2 receptor binding, functional activity and selectivity in N-benzyltryptamines. *PLoS One*. **2019**, *14*, e0209804.
22. (a) Benes, H.; Deissler, A.; Rodenbeck, A.; Engfer, A.; Kohnen, R. Lisuride treatment of restless legs syndrome: first studies with monotherapy in de novo patients and in combination with levodopa in advanced disease. *J. Neural. Transm. (Vienna)*. **2006**, 113, 87–92.
(b) Dunlap, L.E.; Andrews, A.M; Olson, D.E. Dark Classics in Chemical Neuroscience: 3,4-Methylenedioxymethamphetamine. *ACS Chem. Neurosci*. **2018**, 9, 2408–2427.

hallucinogenic and non-hallucinogenic pair in transfected HEK293T cells expressing psychLight1. We observe that all hallucinogenic molecules in humans increased the fluorescence signal of the sensor **(Fig. 4.3A)**. The EC_{50}s calculated paralleled those determined by radioligand binding assays **(Fig. 4.3B)**.[23] Interestingly, the potencies of psychLight correlated well ($r^2 = 0.9$) with the potencies of hallucinogens in humans, but not the maximal response (E_{max}) of psychLight **(Fig. 4.3C)**.

In contrast to known hallucinogens, analogs that were not hallucinogenic in humans did not increase the fluorescence of psychLight1. To determine whether molecules were binding, we conducted our assay in antagonist mode. In antagonist mode, we imaged the baseline of our transfected HEK293T cells expressing psychLight1. Next, we loaded 100 nM 5-HT into the wells to induce an increase in fluorescence. Finally, we slowly perfused solutions containing an increasing concentration of non-hallucinogenic ligands (lisuride [LIS] and 6-methoxy-N, N,dimethyltryptamine [6-MeO-DMT]) and 100 nM 5-HT to maintain the 5-HT concentration in our dish. We found that as we increased the concentrations of LIS and 6-MeO-DMT, we began to see a reduction in fluorescence **(Fig. 4.3D)**. This result indicated that the non-hallucinogenic ligands were competing off 5-HT bound to psychLight1 and induced a different confirmational motif that reduced the fluorescence.

At first, we had hypothesized that hallucinogenic and non-hallucinogenic ligands that were agonists at the 5-HT2AR would induce similar increases in fluorescence from psychLight. We postulated this because radioligand binding assays and functional assays of the hallucinogenic and non-hallucinogenic agonists exhibit similar responses. For example, LSD and LIS are equipotent at [35S]GTPγS binding, PI hydrolysis, and Ca^{2+} mobilization **(Fig. 4.3E)**.[24,25] DMT, 5-MeO-DMT, and 6-F-DET also have similar potencies at PI hydrolysis.[24,25] These data suggest all five molecules are potent 5-HT2AR agonists and are

(c) Halberstadt, A.L.; Chatha, M.; Klein, A.K.; Wallach, J.; Brandt, S.D. Correlation between the potency of hallucinogens in the mouse head-twitch response assay and their behavioral and subjective effects in other species. *Neuropharmacology*. **2020**, *167*, 107933.
(d) Kalir, A.; Szara, S. SYNTHESIS AND PHARMACOLOGICAL ACTIVITY OF FLUORINATED TRYPTAMINE DERIVATIVES. *J. Med. Chem*. **1963**, *6*, 716–719.
23. McKenna, D.J.; Peroutka, S.J. Differentiation of 5-hydroxytryptamine2 receptor subtypes using 125I-R-(-)2,5-dimethoxy-4-iodo-phenylisopropylamine and 3H-ketanserin. *J. Neurosci.* **1989**, *9*, 3482–3490.
24. Rabin, R.A.; Regina, M.; Doat, M.; Winter, J.C. 5-HT2A receptor-stimulated phosphoinositide hydrolysis in the stimulus effects of hallucinogens. *Pharmacol. Biochem. Behav*. **2002**, *72*, 29–37.
25. Cussac, D.; Boutet-Robinet, E.; Ailhaud, M.C.; Newman-Tancredi, A.; Martel, J.C.; Danty, N.; Rauly-Lestienne, I. Agonist-directed trafficking of signalling at serotonin 5-HT2A, 5-HT2B and 5-HT2C-VSV receptors mediated Gq/11 activation and calcium mobilisation in CHO cells. *Eur. J. Pharmacol*. **2008**, *594*, 32–38.

indistinguishable from one another. Yet, LIS[26] and 6-F-DET[17] produce no behavioral phenotype indicating hallucinogenic potential in rodents. Taken together, this highlights the ability of psychLight to differentiate between hallucinogenic and non-hallucinogenic congeners that traditional GPCR assays cannot detect. This quantifiable difference is one of the strengths of psychLight.

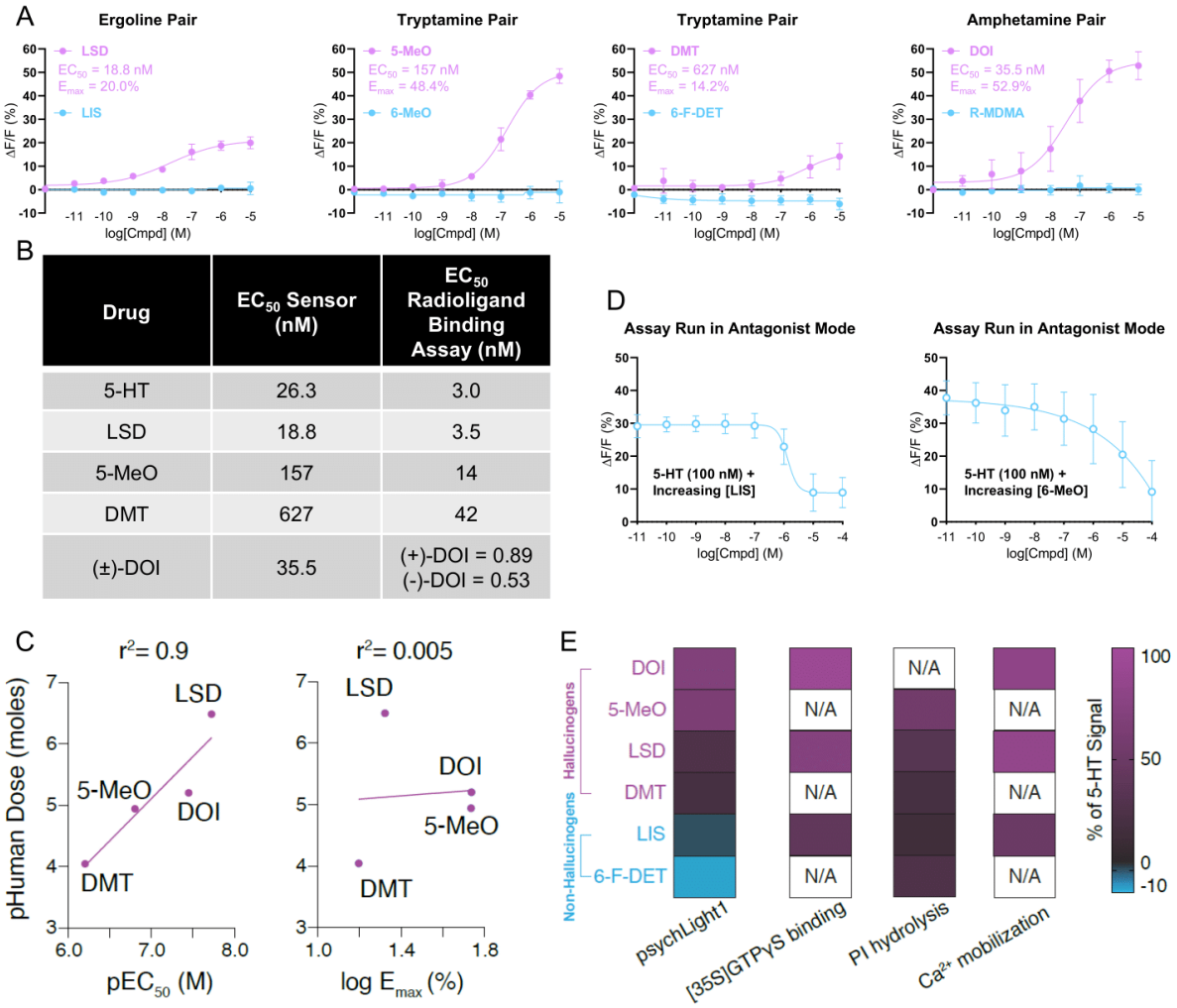

Figure 4.3. Differentiating between hallucinogens and non-hallucinogens in vitro. **(A)** Ergoline, two tryptamines, and an amphetamine hallucinogen and non-hallucinogen pairs were tested in HEK293T expressing psychLight1 on a confocal microscope. Only known hallucinogenic ligands activated the biosensor (n = 3 cells from 3 passages). **(B)** List of EC_{50} of agonists tested in **(A)** compared to radioligand

26. González-Maeso, J.; Weisstaub, N.V.; Zhou, M.; Chan, P.; Ivic, L.; Ang, R.; Lira, A.; Bradley-Moore, M.; Ge, Y.; Zhou, Q.; Sealfon, S.C.; Gingrich, J.A. Hallucinogens recruit specific cortical 5-HT(2A) receptor-mediated signaling pathways to affect behavior. *Neuron*. **2007**, *53*, 439–452.

binding assay with [H]^{3}-DOI.[23] **(C)** PsychLight1 EC_{50} values, but not E_{max} values, correlate with hallucinogen potencies in humans. **(D)** Lisuride and 6-MeO-DMT were tested in antagonist mode where 5-HT concentrations were kept at 100 nM through the entire experiment and the concentrations of lisuride and 6-MeO-DMT were varied in a dose response manner to determine binding from lisuride and 6-MeO-DMT. **(E)** PsychLight1 E_{max} values differentiate hallucinogens and non-hallucinogens, but other measures of 5-HT2AR activation (e.g., phosphoinositide (PI) hydrolysis, Ca^{2+} mobilization, [^{35}S]GTPγS binding) do not. Data represented by the heatmap with a double color gradient from values above 0 (magenta to black) and data below 0 (black to blue). Data are normalized to 5-HT values within each experiment. Data for PI hydrolysis, Ca^{2+} mobilization, and [^{35}S]GTPγS binding were obtained from previous reports.[24,25] PI hydrolysis data for 6-F-DET were estimated based on graphical data presented in.[24] N/A indicates that the data are not available. LSD = lysergic acid diethylamide; LIS = lisuride; 5-MeO = 5-MeO-DMT = 5-methoxy-N,N-dimethyltryptamine; 6-MeO = 6-MeO-DMT = 6-methoxy-N,N-dimethyltryptamine; DMT = N,N-dimethyltryptamine; 6-F-DET = 6-fluoro-N,N-diethyltryptamine; DOI = 2,5-dimethoxy-4-iodoamphetamine; (R)-MDMA = 3,4-methylenedioxymethamphetamine; 5-HT = serotonin.

After observing the response in vitro, we sought to correlate psychLight with a behavioral assay. We chose the HTR because it has been shown to correlate well with hallucinogenic 5-HT2AR ligand-induced activation.[27] Furthermore, we used the hallucinogen 5-methoxy-N,N-dimethyltryptamine (5-MeO), as we have previously shown it produces robust HTR.[12a] Three weeks after the mice were injected with AAV9.hSynapsin1.psychLight2 into the prelimbic cortex **(Fig. 4.4A)**, 50 mg/kg of 5-MeO (i.p.) was administered and psychLight2 activation was measured via fiber photometry. We observed a sharp increase in fluorescence response and an increase in HTR at the same time following 1 minute after drug injection. The fluorescence positively correlated with the increased HTRs over several minutes until psychLight2 stabilized and remained elevated while head twitch frequency decreased **(Fig 4.4B)**. Lastly, saline (VEH) and ketanserin (KETSN, 10 mg/kg, i.p.) induced no HTR and there was no fluorescence observed following administration **(Fig. 4.4C)**. This result suggests that the sensor is sensitive enough to measure conformational changes in 5-HT2A following a hallucinogenic treatment (5-MeO) treatment in vivo.

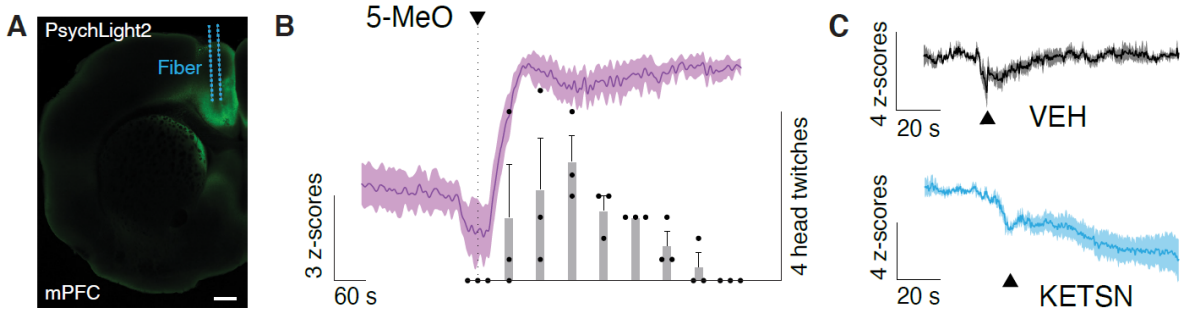

Figure 4.4. PsychLight is activated in vivo by hallucinogenic drugs. **(A)** Representative image of expression of psychLight2 in the prelimbic cortex near the site of fiber implantation. Scale bar = 500μm. **(B)** Averaged-trial traces of psychLight2 responses shown as z-score following injection of 50 mg/kg 5-MeO-DMT (magenta, i.p). The number of head-twitch response (bars) were also recorded and binned as 1-minute intervals (n = 3 mice). **(C)** Averaged-trial traces of psychLight2 responses following the injection of saline (VEH, black, n = 3 mice) or ketanserin (KETSN, 10 mg/kg i.p., blue, n = 3 mice). VEH = saline; KETSN =

27. Hanks, J.B.; González-Maeso, J. Animal models of serotonergic psychedelics. *ACS Chem. Neurosci.* **2013**, *4*, 33–42.

ketanserin; 5-MeO = 5-methoxy-N,N-dimethyltryptamine; mPFC = media prefrontal cortex. **(A)** Image was taken by Chunyang Dong.

Next, we wanted to optimize the assay from a confocal format to a higher throughput format using a widefield high content microscope. First, we compared psychLight1 and psychLight2 responses on the confocal and widefield imager, respectively **(Fig 4.5A–B)**. While we observed similar trends in 5-HT activation of the psychLight, we saw a reduction in signal between confocal analyzed images compared to the widefield images (from ~80% ΔF/F confocal to ~40% ΔF/F widefield). This result might be due to an increased background as we transitioned from a laser on the confocal to a LED filter cube on the widefield imager. However, this reduction in signal was not detrimental to the assay as we could still measure hallucinogenic potential. However, we did observe some differences in baseline fluorescence between transfections. To stabilize the assay, we generated a HEK293T cell line stably expressing psychLight2 (PSYLI2). We then tested PSYLI2 cells for their robustness in a 96-well plate format using 5-HT and KETSN at 10 μM in agonist mode **(Fig. 4.5B)** to generate a Z-factor (Z').[28] The calculated Z-factor = 0.6, suggesting that the assay is robust and reproducible. **Figure 4.5D–E** are representative images of PSILI2 cells in both agonist **(Fig. 4.5D)** and antagonist modes **(Fig. 4.5E).**

28. Zhang, J.H.; Chung, T.D.; Oldenburg, K.R. A Simple Statistical Parameter for Use in Evaluation and Validation of High Throughput Screening Assays. *J. Biomol. Screen*. **1999**, *4*, 67–73.

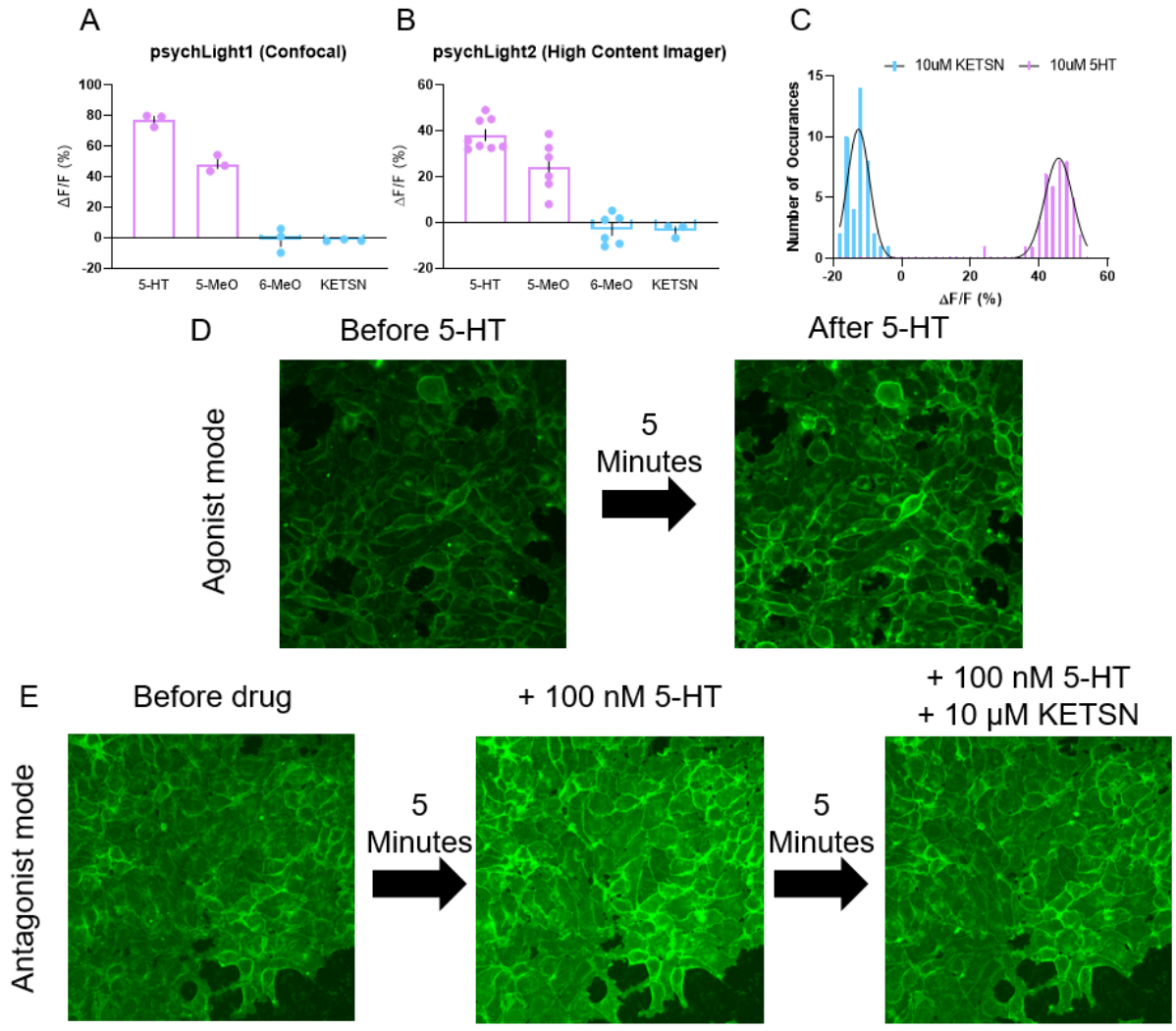

Figure 4.5. Optimizing low-throughput assay to medium-throughput. Control compounds tested on **(A)** psychLight1 using a confocal microscope compared to **(B)** psychLight2 using a wide-field microscope. HEK293T cells stably expressing psychLight2 (PSYLI2 cell line) were imaged on wide-field microscope and data was compiled to generate a Z' = 0.6 **(C)** for the assay (n = 42). **(D)** Representative images at 40x magnification of PSYLI2 cells in agonist mode. A before and after image were taken with 5 minutes incubation period in between each image following 5-HT addition. Images illustrate increase of fluorescence following 5-HT addition indicating ligand-receptor interactions. **(E)** Representative images at 40x magnification of PSYLI2 cells in antagonist mode. A before, after 5-HT 100 nM, and after 5-HT 100 nM + KETSN image was taken. 5 minutes incubation time between each image. Images illustrate reduction of

fluorescence following drug addition, indicating ligand-receptor interactions. 5-HT = serotonin; 5-MeO = 5-methoxy-*N*,*N*-dimethyltryptamine; 6-MeO = 6-methoxy-*N*,*N*-dimethyltryptamine; KETSN = ketanserin.

With a robust and reproducible assay in hand, we began screening a small library of tryptamines with varying degrees of methylation **(Fig 4.6A)**. We saw a decrease in fluorescence as methylation increased, indicating PSYLI2 cells were sensitive enough to discern minute modifications on the tryptamine scaffold **(Fig 4.6B)**. We then screened a medium library of compounds (eighty-three compounds) that consisted of known hallucinogens, known non-hallucinogens, known non-2A ligands, and unknown small molecules (both commercially available and lab-made) **(Fig. 4.7)**, in agonist and antagonist modes **(Fig. 4.6C–D)**. Next, to categorize compounds that are hallucinogenic from non-hallucinogenic molecules, we generated an artificial ligand score. Non-hallucinogens were unlikely to increase the fluorescence signal of the sensor in either agonist or antagonist mode. Therefore, we combined these two modes **(Fig. 4.6E)** and observed that hallucinogenic and non-hallucinogenic ligands tended to have positive (red) and negative (blue) ligand scores, respectively. For example, LSD and lisuride have calculated ligand scores of 23.0 and -42.3, respectively.[29] Furthermore, non-serotonergic hallucinogens and dissociatives such as ketamine, phencyclidine, and salvinorin A exhibited near-zero (black) ligand scores. Subsequently, agonist (x-axis) and antagonist mode (y-axis) data of known hallucinogenic (red), non-hallucinogenic (blue), and non-binding 5-HT2AR ligands (black) tested were plotted on a Cartesian coordinate system **(Fig. 4.6F)**.

Lastly, we noticed two small molecules known to be 5-HT2A antagonists gave a positive response at 10 μM: 2-bromo-LSD (BOL-148) and bromocriptine. We suspected that they were pan-assay interference compounds (PAINS)[30] as both molecules contained the 2-bromoindole scaffold. We conducted a dose-response in both PSYLI2 cells and a fluorescence plate reader and confirmed that the two molecules were PAINS **(Fig. 4.5G–H)**. Moving forward, I believe any molecule determined to be a hallucinogen in this assay should have a dose-response conducted to verify the results. Furthermore, using a plate reader will help to assess the autofluorescence from any potential positive hit.

29. See **Chapter 4.7.4** for calculations of the ligand score.
30. Baell, J.; Walters, M.A. Chemistry: Chemical con artists foil drug discovery. *Nature*. **2014**, 513, 481–483.

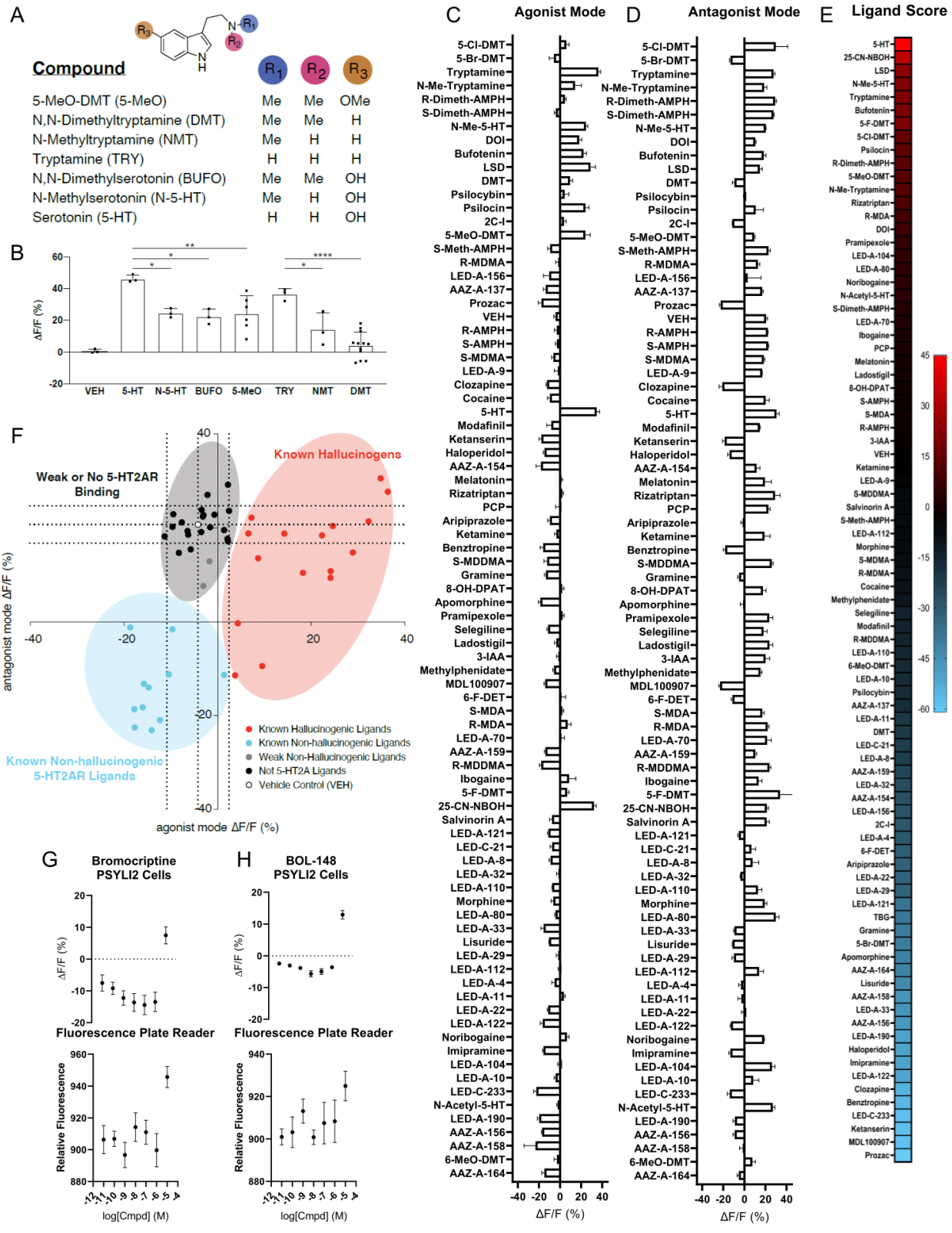
A
Compound
R1
R2
R3
5-MeO-DMT (5-MeO) Me Me OMe
N,N-Dimethyltryptamine (DMT) Me Me H
N-Methyltryptamine (NMT) Me H H
Tryptamine (TRY) H H H
N,N-Dimethylserotonin (BUFO) Me Me OH
N-Methylserotonin (N-5-HT) Me H OH
Serotonin (5-HT) H H OH
B
ΔF/F (%)
VEH
5-HT
N-5-HT
BUFO
5-MeO
TRY
NMT
DMT
C
Agonist Mode
D
Antagonist Mode
E
Ligand Score
F
Weak or No 5-HT2AR Binding
Known Hallucinogens
Known Non-hallucinogenic 5-HT2AR Ligands
antagonist mode ΔF/F (%)
agonist mode ΔF/F (%)
Known Hallucinogenic Ligands
Known Non-hallucinogenic Ligands
Weak Non-Hallucinogenic Ligands
Not 5-HT2A Ligands
Vehicle Control (VEH)
G
Bromocriptine
PSYLI2 Cells
Fluorescence Plate Reader
Relative Fluorescence
log[Cmpd] (M)
H
BOL-148
PSYLI2 Cells
Fluorescence Plate Reader
Relative Fluorescence
log[Cmpd] (M)

Figure 4.6. Screen with psychLight-based pharmacology assay. **(A)** Structure of tryptamine hallucinogens and their related analogs. **(B)** Agonist mode of compounds from **(A)** indicating PSYLI2 cells can differentiate with small differences in methylation at 10 μM (n = 3–12 wells). **(C–D)** Small library screen of known hallucinogens, non-hallucinogens, and unknown compounds in **(C)** agonist and **(D)** antagonist mode (n = 3 wells, **C–D**). **(E)** Heat map of ligand score calculated. Ligand scores greater than 0 indicate increased hallucinogenic potential and ligand scores less than 0 indicate non-hallucinogenic ligands. **(F)** A series of hallucinogenic and non-hallucinogenic compounds with known 5-HT2AR affinities were tested in agonist (x-axis) and antagonist mode (y-axis). Dotted lines represent 1 standard deviation from the VEH control (white). Hallucinogenic (red), non-hallucinogenic (blue) 5-HT2A ligands, and non-binding ligands (black) shown. Dots indicate averaged ΔF/F values (n = 3 passages). **(G–H)** Confirmed PAINS tested on PSYLI2 and fluorescence plate reader for **(G)** bromocriptine (10 μM) and **(H)** BOL-148 (10 μM).

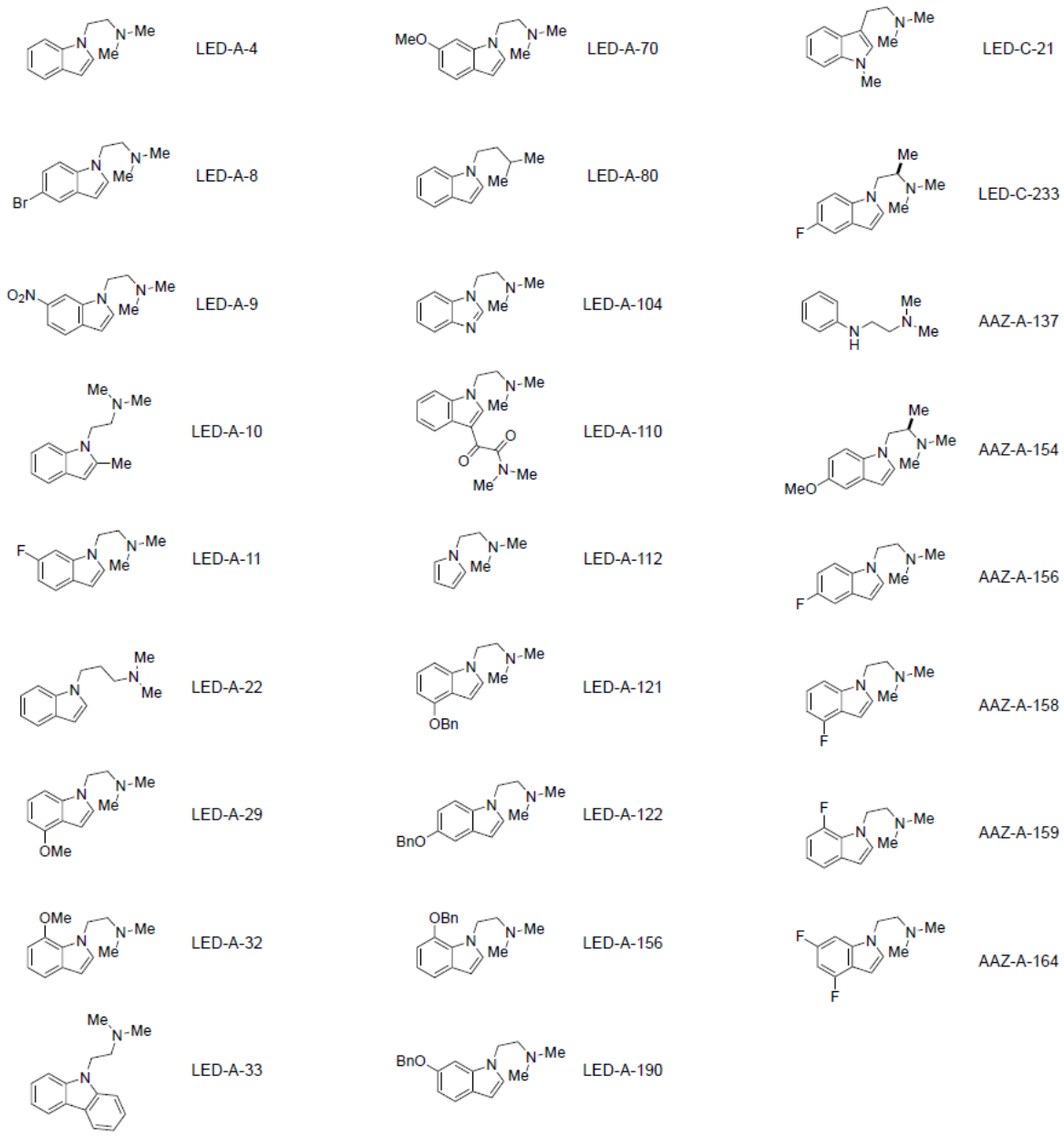

Figure 4.7. Structures of unknown small molecules synthesized in house by Lee E. Dunlap and Arya Azinfar.

Chapter 4.4 PsychLight Predicts Hallucinogenic Potential.

We next assessed the sensor's ability to detect and predict the hallucinogenic potential of a ligand. In the small library screen **(Fig. 4.6C–E)**, thirty-four small molecules were unknown. Of the thirty-four, we found the 5-substituted-halo-DMTs most interesting (**Fig. 4.8A**). By assessing the agonist mode results, 5-F-DMT and 5-Cl-DMT were predicted to be hallucinogenic, while the larger 5-Br-DMT was predicted to not be **(Fig. 4.8B)**. We then took the 5-halo-DMTs into a HTR to confirm the predictions made by the sensor **(Fig. 4.8C–D)**. As predicted, 5-F-DMT and 5-Cl-DMT both produced robust HTRs, while 5-Br-DMT failed to produce HTR at all doses **(Fig. 4.8C)**. Interestingly, locomotion and HTR was not correlated, as evidenced by reduced locomotion induced by all drugs at 50 mg/kg (**Fig. 4.8D**). This result further highlights the capacity for psychLight to detect minute functional differences between compounds with high degree of similarity.

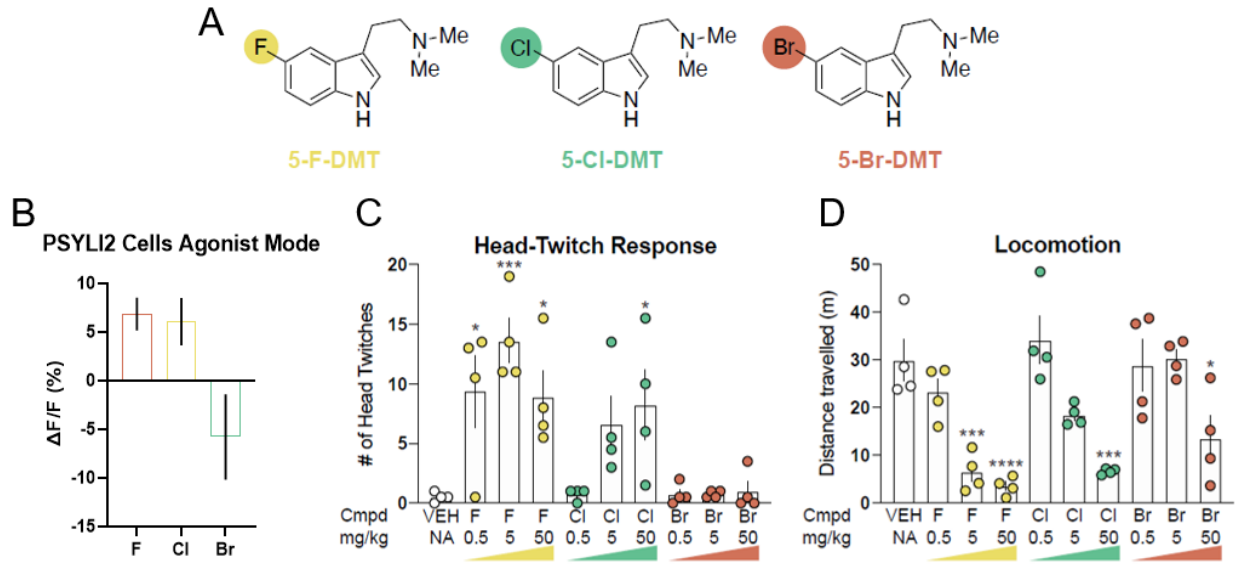

Figure 4.8. PsychLight predicts hallucinogenic potential. **(A)** Structure of 5-halo-DMT derivatives. **(B)** Agonist mode PSYLI2 cells tested with 5-halo substituted DMTs (n = 3 wells). **(C)** 5-F-DMT and 5-Cl-DMT produce head twitches whereas 5-Br-DMT does not (n = 4 mice). **(D)** All 5-halo-DMT produce a dose-dependent decrease in locomotion (n = 4 mice). Data are represented as mean ± SEM., ****p<0.0001, ***p<0.001, and *p<0.05, vs. the vehicle control. For **(C–D)**, a one-way ANOVA with a Dunnett's post hoc

test. Lee E. Dunlap (LED) and Chunyang Dong (CD) conducted the injection. LED and I quantified the HTR. LED calculated locomotion.

Chapter 4.5 AAZ has Antidepressant Potential and is a Non-hallucinogenic 5-HT2AR Ligand

---

Finally, I wanted to identify a novel non-hallucinogenic 5-HT2AR ligand that had therapeutic potential. My colleague, Lee E. Dunlap, designed and synthesized the molecule AAZ-A-154 (AAZ, **Fig. 4.9A**). The inspiration behind the development of AAZ starts with the isoDMT core scaffold. IsoDMT was previously shown to be a non-hallucinogenic isomer of DMT and the 6-methoxy substituted isoDMT introduced hallucinogenic potential. Furthermore, the 5-methoxy substitution did not. Next, Lee and I noticed that the R(-)- and S(+)-amphetamines had differential effects in our embryonic cortical cultures. The R(-)-amphetamine seemed to promote increases in total brain-derived neurotrophic factor (BDNF) levels but not the S(+)-amphetamine.[31] Lee used the 5-MeO-isoDMT scaffolded as we knew it was non-hallucinogenic. Lee then introduced a stereocenter on the 2-position of the ethylamine chain by inserting a methyl group. From this, we developed AAZ.

Next, we tested AAZ in agonist and antagonist mode in the PSYLI2 cells and observed that the assay predicted AAZ was a non-hallucinogenic ligand of the 5-HT2AR. We followed up with a Schild regression analysis—this pharmacological analysis determines the type of interaction observed on a receptor of interest with AAZ—which revealed AAZ's functions as a competitive antagonist of psychLight **(Fig. 4.9B)**. To further assess the hallucinogenic potential of AAZ in vivo, we performed HTR experiments across multiple doses in mice. As predicted, AAZ did not produce a HTR even up to 100 mg/kg **(Fig. 4.9C)**. A high dose of AAZ does hinder locomotion **(Fig. 4.9D)**, indicating that the compound is still impacting behavior without producing hallucinogenic effects.

31. See **Chapter 3.4**, footnote 24.

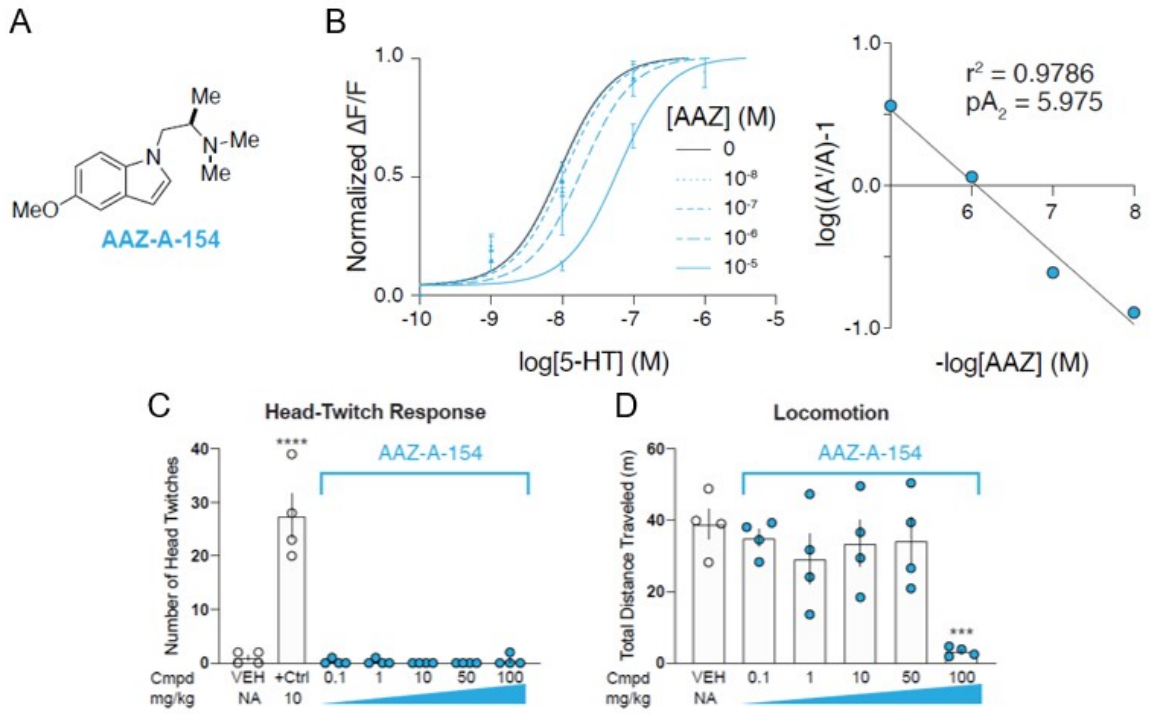

Figure 4.9. AAZ increases neuritogenesis through a 5-HT2AR dependent mechanism and is not predicted to be hallucinogenic. **(A)** Structure of AAZ (AAZ). **(B)** A Schild's regression analysis and a pA_2 with AAZ reveals to be a competitive antagonist (n = 3 wells). **(C)** Head-twitch response assay in mice to confirm AAZ's non-hallucinogenic potential (n = 4 mice). **(D)** AAZ's effects also showed no effect in locomotion (n = 4 mice). Data are represented as mean ± SEM., ****p<0.0001, ***p<0.001, and *p<0.05, vs. the vehicle control. For **(C–D)**, a one-way ANOVA with a Dunnett's post hoc test. +Ctrl = 5-MeO-DMT; VEH = saline; AAZ = AAZ-A-154. Maxemiliano Vargas and LED conducted the behavioral assays listed here.

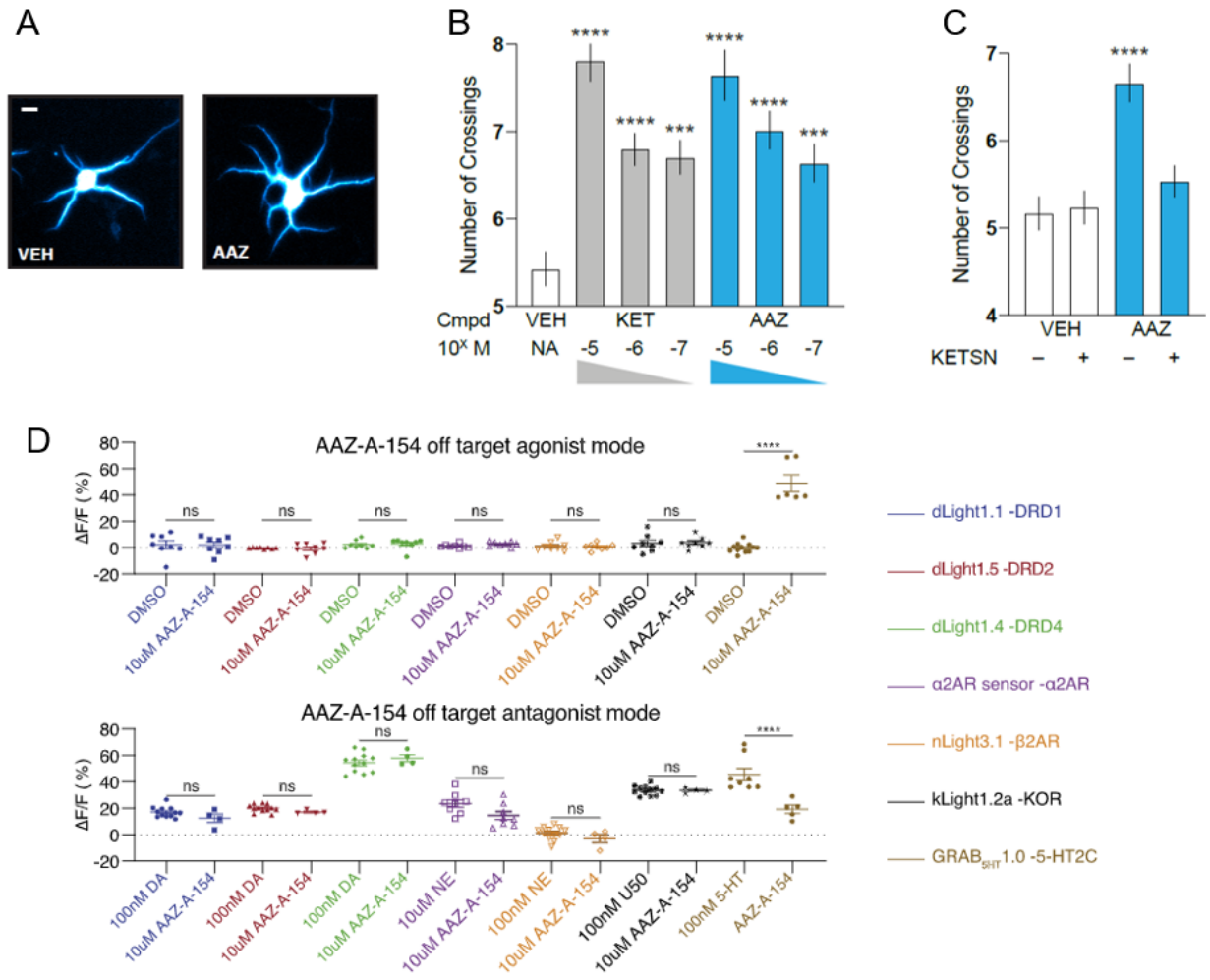

Figure 4.10. 5-HT2A and 5-HT2C receptors may be responsible for AAZ's mechanism of action. **(A)** Representative images of DIV6 neurons treated with VEH and AAZ (10 μM). Scale bar = 20 μm. **(B)** Dose-dependently increases the amount of neuritogenesis equal to that of KET (n = 51–60 neurons). **(C)** Ketanserin (10 μM) co-treatment with AAZ (1 μM) abolishes the neuritogenesis (n = 39–58). **(D)** Data from agonist and antagonist mode of 7 receptor-based sensors (Agonist mode: 0.1% DMSO or 10μM AAZ-A-154 was added; Antagonist mode: 0.1% DMSO or 10uM AAZ-A-154 was added in the presence of 100 nM dopamine (DA), norepinephrine (NE), U-50488 (U50) or serotonin (5-HT). Data are represented as mean ± SEM., ****p<0.0001, ***p<0.001, and *p<0.05, vs. the vehicle control. For **(B–C)**, a one-way ANOVA with a Dunnett's post hoc test, **(D)** one-way ANOVA. Tukey's multiple comparisons test. dlight = dopamine light; DRD1 = dopamine receptor D1; DRD2 = dopamine receptor D2; DRD4 = dopamine receptor D4; nLight =

norepinephrine light; α2AR = alpha 2-adrenoceptor; β2AR = beta 2-adrenoceptor; KOR = kappa opioid receptor; $GRAB_{5\text{-}HT}$ = GPCR-Activation-Based 5-HT; 5-HT2C = serotonin 2C.

Recently, we showed that 5-HT2A ligands promote structural plasticity in a 5-HT2A-dependent manner.[10] Thus, given the similar structure to many psychoplastogens,[10,32] we tested the ability of AAZ to promote neuritogenesis in embryonic rat cortical cultures. Using Sholl analysis, we demonstrated AAZ treatments increased Nmax comparably to ketamine (KET, **Fig. 4.10.A–B**). This result suggests that AAZ is a potential psychoplastogen. We then blocked the plasticity-promoting effects of AAZ with ketanserin (KETSN, **Fig. 4.10C**). A caveat to this study is the concentration of ketanserin (1 μM) that we used blocked the effects of AAZ in Nmax **(Fig. 4.9C)**. This dose of ketanserin is high enough to block serotonin 2C (5-HT2C) receptors. Thus we cannot rule out the possibility that the mechanism of action of AAZ inducing neurite outgrowth is 5-HT2C dependent. Furthermore, we tested AAZ in other genetically encoded GPCR biosensors available in the Tian lab: dopamine receptor D1 (DRD1), D2 (DRD2), D4 (DRD4),[33] alpha-2 adrenergic receptor (α2AR), beta-2 adrenergic receptor (β2AR), kappa opioid receptor (KOR),[34] and 5-HT2C (Grab 5-HT2C).[35] We found that AAZ activated the 5-HT2C biosensor **(Fig. 4.10D)**. AAZ did not activate any of the other biosensors in both agonist and antagonist modes. The ketanserin blocking studies may indeed be inhibiting the neurite outgrowth phenotype through the 5-HT2CR rather than the 5-HT2AR or that it might be a combination of both receptors as ketanserin is 100-fold more potent at 5-HT2AR compared to 5-HT2CR (IC_{50} 5-HT2CR = 130 nM; IC_{50} 5-HT2AR = 2–3 nM).[20]

Next, we tested AAZ in the forced swim test (FST, **Fig. 4.11A**) and found a reduction in immobility time–a behavioral response commonly produced by other known psychoplastogens[13,36] and antidepressants such as ketamine.[37] In these studies, we utilized C57BL/6J mice, as this strain does not respond robustly to traditional antidepressants such as selective serotonin reuptake inhibitors (SSRIs) or

32. Olson, D. E. Psychoplastogens: A Promising Class of Plasticity-Promoting Neurotherapeutics *J. of Exp. Neurosci.* **2018**, *12*, 1–4.
33. Patriarchi, T.; Cho. J.R.; Merten, K.; Howe, M.W.; Marley, A.; Xiong, W.H.; Folk, R.W.; Broussard, G.J.; Liang, R.; Jang, M.J.; Zhong, H.; Dombeck, D.; von Zastrow, M.; Nimmerjahn, A.; Gradinaru, V.; Williams, J.T.; Tian, L. Ultrafast neuronal imaging of dopamine dynamics with designed genetically encoded sensors. *Science*. **2018**, *360*, eaat4422.
34. KOR sensor from the Tian lab has yet to be published. It was designed similarly to D1–D4 receptors from the Tian lab.
35. Wan, J.; Peng, W.; Li, X.; Qian, T.; Song, K.; Zeng, J.; Deng, F.; Hao, S.; Feng, J.; Zhang, P.; Zhang, Y.; Zou, Y.; Pan, S.; Zhu, J.J.; Jing, M.; Xu, M.; Li, Y. A genetically encoded GRAB sensor for measuring serotonin dynamics in vivo. *BioRxiv.* **2020**.
36. Nakamura, K.; Ikoma, Y.; Kimura, K.; Nakada, Y.; Kobayashi, S.; Yamaguchi, M.; Nakagawa, H. [Effects in animal models of depression of lisuride alone and upon coadministration with antidepressants]. *Nihon Yakurigaku Zasshi*. **1989**, 94, 81–89. Japanese.
37. Li, N.; Lee, B.; Liu, R.J.; Banasr, M.; Dwyer, J.M.; Iwata, M.; Li, X.Y.; Aghajanian, G.; Duman, R.S mTOR-dependent synapse formation underlies the rapid antidepressant effects of NMDA antagonists. *Science*. **2010**, 329, 959–964.

tricyclics,[38] thus highlighting the similarity between AAZ and next-generation antidepressants like ketamine. Moreover, AAZ produced both rapid (30 min) and long-lasting (1 week) antidepressant-like effects after a single administration **(Fig. 4.11A)**.

38. Hascoët, M.; Bourin, M. "The Forced Swimming Test in Mice: A Suitable Model to Study Antidepressants." *Neuromethods*, **2009**, *42*, 85–118.

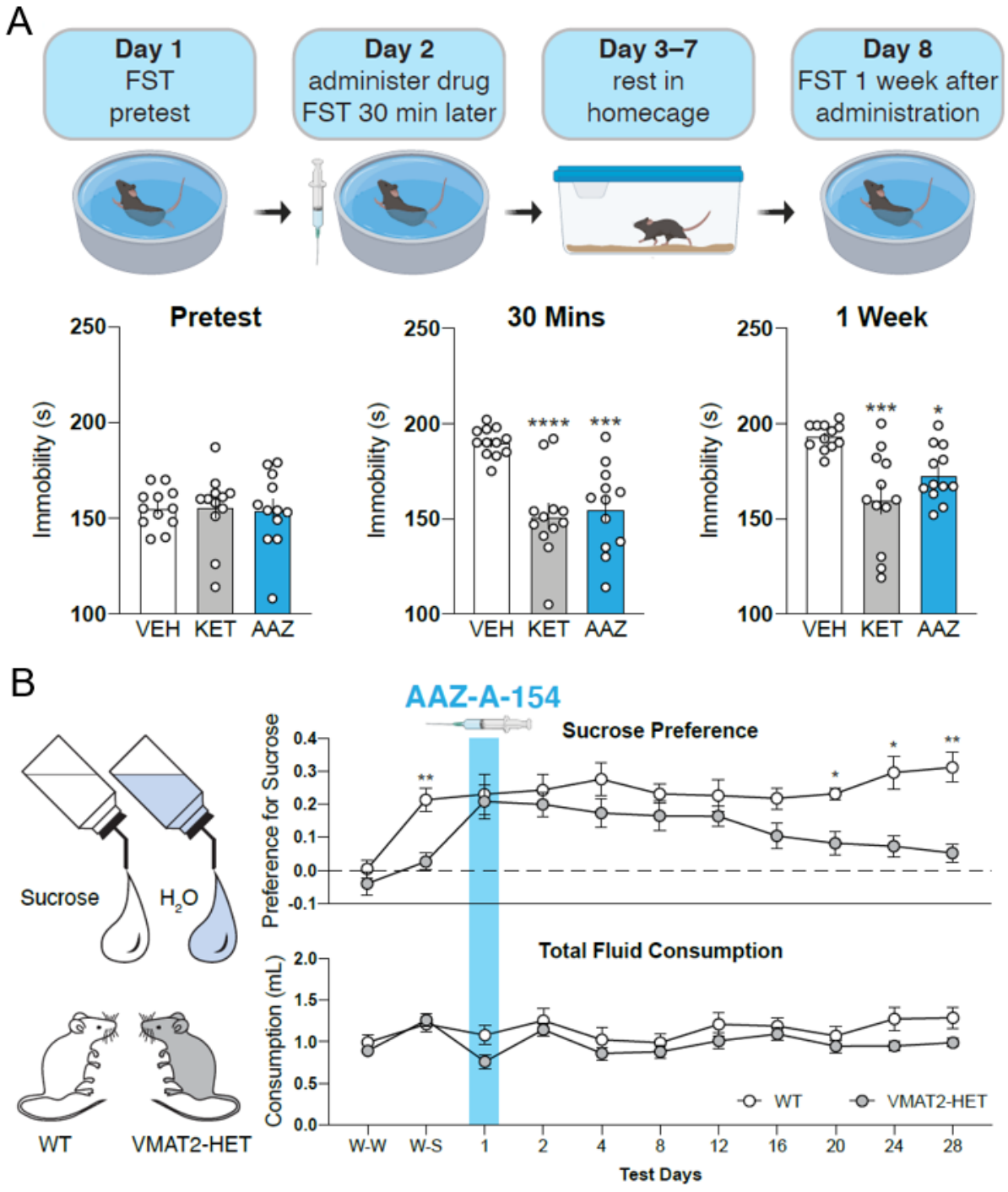

Figure 4.11. Characterization of AAZ as an antidepressant. **(A)** Schematic of force swim test (FST). AAZ (20 mg/kg) produces fast (30 min) and long-lasting (1 week) antidepressant like effects in the FST comparable to ketamine (n = 12 mice). *p<0.05, ***p<0.001, and ****p<0.0001. For **(A)**, a one-way ANOVA with a Dunnett's post hoc test **(B)** Sucrose preference test reveals that AAZ (15 mg/kg) reduces anhedonia

in VMAT2-HET mice for at least 12 days. Water-water pairing = W-W, water-sucrose (1%) pairing = W-S. When given the choice between water and a 1% sucrose solution (W-S), only WT mice displayed a sucrose preference. Total fluid consumption was not different between genotypes at any time point. n= 11 mice/genotype; data are represented as means and SEMs, *p<0.05 and **p<0.01, WT vs. VMAT2-HET, repeated measures ANOVA with Bonferroni corrected pair-wise comparisons. KET = ketamine; AAZ = AAZ-A-154. William C. Wetsel supervised the behavioral assays conducted here.

To determine if AAZ could reduce anhedonia, we used VMAT2 heterozygous (VMAT2-HET) mice.[39] Pharmacological inhibition of VMAT2 precipitates depressive-like behaviors in humans[40] and VMAT2-HET mice display several depressive phenotypes. These include a reduced preference for a 1% sucrose solution over water alone. The wild-type (WT) animals displayed a strong preference for the sucrose solution while at the beginning, the VMAT2-HET mice did not **(Fig. 4.11B)**. However, immediately following a single administration of AAZ, the VMAT2-HET mice exhibited a sucrose preference that was indistinguishable from WT controls. This anti-anhedonic effect after a single administration of AAZ persisted for at least 16 days before the treated VMAT2-HET animals began to display reduced sucrose preference **(Fig. 4.11B)**. Notably, the change in sucrose preference observed for the VMAT2-HET mice cannot be attributed to differential fluid consumption since both genotypes drank about the same volumes of liquids across the entire experiment **(Fig. 4.11B)**. Moreover, the effects of AAZ cannot be ascribed to increasing sucrose palatability, as AAZ did not modify sucrose preference in the WT animals **(Fig. 4.11B)**. Overall, these results suggest that psychLight has applications to identifying both hallucinogenic and beneficial, non-hallucinogenic ligands of the 5-HT2AR.

This cellular assay is the first example of an in vitro assay to predict the hallucinogenic potential of small molecules. To date, the most common ways to conduct these screens are through very laborious behavioral assays, such as DD[15] and HTR.[12a] As psychLight fluorescence is activated by ligand-induced conformational changes specific to serotonergic hallucinogens, this sensor reports the hallucinogenic

39. Fukui, M.; Rodriguiz, R.M.; Zhou, J.; Jiang, S.X.; Phillips, L.E.; Caron, M.G.; Wetsel, W.C. Vmat2 heterozygous mutant mice display a depressive-like phenotype. *J. Neurosci.* **2007**, *27*, 10520–10529.
40. Freis, E.D. Mental depression in hypertensive patients treated for long periods with large doses of reserpine. *N Engl J Med*. **1954**, *251*, 1006–1008.

potential of ligands even with structural similarities. Gonzalez-Maeso and co-workers have demonstrated that hallucinogenic and non-hallucinogenic 5-HT2AR ligands induce distinct immediate early gene expression patterns[26] and may differentially activate 5-HT2AR–mGluR2 heterodimers[26,41] However, these results have yet to be developed into a reliable cellular assay capable of differentiating between hallucinogenic and non-hallucinogenic congeners across a wide range of chemical structures.[42] With psychLight, the hallucinogenic potential of 5-HT2A ligands can be rapidly assessed in cells through a direct fluorescence readout. The activation of psychLight in living animals is temporally correlated with hallucinogen-induced HTR, providing further confirmation that the sensor detects conformational changes induced by hallucinogens. We predict that this assay will be easily adapted to a 384-well format and will complement additional orthogonal GPCR assays (e.g., Ca^{2+} flux, G protein activation, β-arrestin activation, cAMP production, etc.). Additional protein engineering efforts will help to improve the dynamic range of psychLight and increase the sensor's sensitivity to further minimize false-negative results.

41. González-Maeso, J.; Ang, R.L.; Yuen, T.;Chan, P.; Weisstaub, N.V.; López-Giménez, J.F.; Zhou, M.; Okawa, Y.; Callado, L.F.; Milligan, G.; Gingrich, J.A.; Filizola, M.; Meana, J.J.; Sealfon, S.C. Identification of a serotonin/glutamate receptor complex implicated in psychosis. *Nature*. **2008**, *452*, 93–97.

42. Initially, I attempted to use these early immediate gene differences in LSD and LIS to establish a high-throughput genetic screen to identify hallucinogens from non-hallucinogens. However, I was unable to replicate the data in footnote 41. González-Maeso, J.; et al. observed that LSD and LIS both increased *c-fos*, but only LSD increased the immediate early gene *early growth response-1* (*egr-1*) and *egr-2*. When I attempted to recapitulate this experiment using cortical cultures just as Javier did, I could not get the same response. I saw no change in *egr-1* or *egr-2*. I did see *c-fos*, but it was not significant.

Chapter 4.6 Conclusion

In summary, the engineering of psychLight and the establishment of the PSYLI2 cell line opens the door to many overlooked scaffolds as potential serotonergic agonists and therapeutics for depression. Furthermore, using psychLight, we identify non-hallucinogenic 5-HT2AR antagonists (such as clozapine or apomorphine)[43] and non-hallucinogenic biased agonists (e.g. lisuride). In 2020, there has been a substantial amount of research published regarding non-hallucinogenic analogs from the Olson Lab (isoDMT[12a] and tabernanthalog[12b]) and these non-hallucinogenic congeners are unique in that they retain their therapeutic effects without the side effects. Here, we describe AAZ as a novel non-hallucinogenic analog of psychedelics and a psychoplastogen that produces long-lasting antidepressant effects (>2 weeks) in FST and sucrose preference following a single administration.

Looking forward, I believe it would be interesting to revisit the importance of conformational changes in determining the functional selectivity at the 5-HT2AR. Ideally, cryogenic electron microscopy (cryo-EM) of psychLight or wild-type 5-HT2AR in the presence of a hallucinogen, non-hallucinogenic agonist, and non-hallucinogenic antagonist would be used to generate a crystal structure of the respective motifs. Then, using the structural data acquired, conduct docking studies to identify novel scaffolds for each of the conformations and validate each molecule's potential in PSYLI2 cells and HTR. Finally, I would test these synthetic molecules for their potential as therapeutics in structural plasticity and ultimately, validate these next-generation therapeutics in rodents.

43. Newman-Tancredi, A.; Cussac, D.; Quentric, Y.; Touzard, M.; Verrièle, L.; Carpentier, N.; Millan, M.J. Differential actions of antiparkinson agents at multiple classes of monoaminergic receptor. III. Agonist and antagonist properties at serotonin, 5-HT(1) and 5-HT(2), receptor subtypes. *J. Pharmacol. Exp. Ther.* **2002**, *303*, 815–822.

Chapter 4.7.1 Experimental Section for Chapter 4

Drugs

The NIH Drug Supply Program provided lysergic acid diethylamide hemitartrate, psilocin, psilocybin, 2-(4-Iodo-2,5-dimethoxyphenyl)ethan-1-amine hydrochloride (2C-I) , 2-bromo-lysergic acid diethylamide tartrate (BOL-148), ibogaine hydrochloride, noribogaine, cocaine hydrochloride, salvinorin A, and phencyclidine hydrochloride (PCP). Other chemicals were purchased from commercial sources such as serotonin hydrochloride (5-HT, Fisher, 50-120-7920), ketanserin (KETSN, ApexBio, 50-190-5332), ketamine hydrochloride (KET, Fagron, 803647), morphine sulfate (Mallinckrodt, Inc., 0406-1521-53), lisuride maleate (LIS, Tocris, 40-5210), bromocriptine mesylate (Tocris, 04-275-0), (±)-2,5-dimethoxy-4-iodoamphetamine hydrochloride (DOI, Cayman, 13885), imipramine hydrochloride (Cayman, 15890), modafinil (Cayman, 15417), (±)-threo-methylphenidate hydrochloride (Cayman, 11639), indole 3-aceitic acid (3-IAA, ACROS, AC12216-0250), gramine (ACROS, AC12018-0100), N-acetylserotonin (ACROS, AC22693-1000), melatonin (ACROS, AC12536-2500), tryptamine (TRY, ACROS, AC15798-0050), N-methyltryptamine (NMT, ACROS, AC151751000), MDL 100907 (MDL, Sigma, M3324-5MG), haloperidol (Sigma, H1512), clozapine (Sigma, C6305), aripiprazole (Sigma, SML0935), fluoxetine hydrochloride (Sigma, F132-10MG), rizatriptan benzoate (Sigma, SML0247-10MG), benztropine mesylate (Sigma, SML0847-500MG), (±)-8-hydroxy-2-(dipropylamino)tetralin hydrobromide (8-OH-DPAT, Sigma, H8520-25MG), R-(-)-apomorphine hydrochloride hemihydrate (Sigma, A4393-100MG), pramipexole hydrochloride (Sigma, PHR1598-500MG), selegiline hydrochloride (Sigma, M003-250MG), ladostigil tartrate (Sigma, SML2263-5MG), RuBi-5-HT (Tocris, 3856) escitalopram oxalate (ESC, Tocris, 4796), L-glutamic acid (GLU, Sigma, G1251-500G), γ-aminobutyric acid (GABA, A5835-25G), dopamine hydrochloride (DA, Sigma, H8502-25G), and norepinephrine bitartrate (NE, 1468501). For cellular experiments, the VEH is dimethyl sulfoxide (DMSO, ACROS, AC327182500). For *in vivo* experiments, VEH = USP grade saline (0.9%, VWR, 68099-103). The remaining compounds used in these studies were synthesized in house and judged to be pure based on NMR and UHPLC-MS. Lee E. Dunlap and Arya Azinfar synthesized all the LED and AAZ compounds listed in **Figure 4.7**. I will not be including the synthesis as I did not participate in the synthesis.

Animals

All experimental procedures involving animals were approved by the Institutional Animal Care and Use Committee (IACUC) at the University of California, Davis, the University of Colorado School of Medicine, or Duke University, and adhered to principles described in the National Institutes of Health Guide for the Care and Use of Laboratory Animals. The University of California, Davis, the University of Colorado School of Medicine, and Duke University are accredited by the Association for Assessment and Accreditation of Laboratory Animal Care International (AAALAC).

Chapter 4.7.2 Experimental Section for Chapter 4.1

Tissue Culture

Coating media was generated using 2.48g boric acid (BDH) and 3.80g borax (MP) dissolved in 900 mL of water. The mixture was stirred overnight at room temperature to dissolve the solid. The next day, the pH of the solution was adjusted to 8.5 with 1N HCl or 1N NaOH. Next, two bottles of poly-D-lysine (PDL) hydrobromide (10 mg/ bottle×2) were added. Volume was filled to 1L for a final concentration of 20 µg/mL PDL hydrobromide. The media was then filtered and stored in the dark at 4°C.

Plating media was generated by combining 500 mL Neurobasal Medium (Fisher Scientific), 50 mL HI FBS (Fisher Scientific), 1.25 mL 200mM glutamine (Fisher Scientific), and 5 mL penicillin-streptomycin (Fisher Scientific). The media was then filtered and stored in the dark at 4°C.

HBSS 1X was generated by combining 100 mL 10X HBSS (Fisher Scientific), 20 mL 1M HEPES (Fisher Scientific) 10 mL penicillin-streptomycin (Fisher Scientific) and filling to 1 L with autoclaved water. The HBSS was filtered and stored in the dark at 4°C.

Replacement media (50 mL) was generated by combining 48.5 mL Neurobasal Medium (Fisher Scientific), 1 mL B-27(Fisher Scientific), 125 µL 200mM glutamine (Fisher Scientific), 62.5 µL 10 mM glutamic acid (Fisher Scientific), and 0.5 mL penicillin-streptomycin (Fisher Scientific). The replacement media was then prewarmed to 37°C before use and made fresh.[44]

Feeding media (50 mL) was generated by combining 48.5 mL Neurobasal Medium (Fisher Scientific), 1 mL B-27(Fisher Scientific), 125 µL 200mM glutamine (Fisher Scientific), 0.5 mL penicillin-streptomycin (Fisher Scientific). The feeding media was then prewarmed to 37°C before use and made fresh.[44]

44. When mixing, either invert or allow it to mix in the bead bath over time. Any bubbles generated is due to proteins in B-27 being denatured.

Tissue Collection

Pregnant Sprague-Dawley dams were euthanized at embryonic day 18 (E18) via CO_2 and cortices of pups were extracted and placed into ice-cold 1X Hanks Buffered Saline Solution (HBSS, ThermoFisher) in a 14 mL culture tube. Afterward, cortices were washed 3× with sterile 1X HBSS in the tissue culture hood and removed HBSS until 2 mL of volume remained. 200 µL of 2.5% trypsin (10X, Fisher Scientific) was added and the culture tube was placed in a 37°C bead bath for 10 minutes. After 10 minutes, using a 10 mL serological pipette, only cortices were collected and moved into a new, sterile 14 mL culture tube. Cortices were washed 3× gently with cold 1X HBSS. Following the last wash, the tube was filled to a total volume of 6 mL with 1X HBSS. The cells were triturated using a 5 mL serological pipette to pipette up and down against the bottom of the tube. Following trituration, 10 µL of cell suspension was mixed with 10 µL of trypan blue stain 0.4% (ThermoFisher). Cell counting and viability was quantified on a slide for the TC20 automated Cell Counter (BioRad). Cell viability was recorded,[45] and cells are plated.[46] For specific sections of cell culture, please see the related figures.

General neurite outgrowth cell culturing in 24-well plates

For **Figures 4.1B–G** neurite outgrowth was conducted in a low-throughput manner assay 24-well plastic bottom plates (VWR) using the center 8 wells. This was conducted using methods previously described. In brief, 24-well plates were coated with 250 µL of coating media overnight at room temperature. The next day, plates were washed 3× with 500 µL autoclaved water. After the last wash, 500 µL of plating media was added to each of the center 8 wells and autoclaved water was added to the remaining outer wells to reduce evaporation. The plates were placed into a 37°C and 5% CO2 water-jacketed incubator prior to dissection. After dissection (see **Tissue Collection** above), 50,000 cells per well were added to each well and returned to the incubator. After 16–24 hours, plating media was aspirated and 500 µL of

45. Cell viability following dissection should be greater than 90% (with 90% being the lowest). Generally, the dissection will take a total of 2–3 hours, depending on the number of pups and plates being plated. Furthermore, I have noticed briefly that cell viability went down to 60–70% during dissection but immediately realized that trypan blue was expired and precipitating out of solution. Thus, make sure when doing the trypan blue staining that the trypan blue has no precipitants. See **Figure 1.1.**

46. Cells were diluted directly into the wells containing plating media. Then gently, keeping the plate flat on the TC hood, move the plate away and towards the experimenter, pause at the center, move the plate to the left and to the right, pause at the center, and repeat a total of three times. This is to help spread the cells out and equally distribute them. I pause to prevent a circular motion which would force your cells to the edge of the plate instead. Furthermore, make sure the plating media is warm (30°C–37°C). This is critical because cooled plating media will rewarm in the incubator. The rewarming process will cause a convection current that will push cells that have not settled to the edge of the plate.

prewarmed replacement media was added to each well. Cells were ready to be treated at 3 days in vitro (DIV3).

General dendritic spine cell culturing in 24-well plates

For **Figures 4.1H** dendritic spine experiments were conducted in a low-throughput assay using 24-well plastic bottom plates (VWR). First, 12 mm circular 1.5 mm thick coverslips (Fisher Scientific) were briefly dipped in 70% ethanol and flame sterilized using an ethanol flame. After, coverslips and a pair of tweezers were covered with foil and were autoclaved on the dry cycle for 30 minutes. Once coverslips were sterilized, autoclaved, and cooled, they were sprayed with 70% ethanol and placed into the tissue culture (TC) hood. The tweezers were sprayed with 70% ethanol and wiped down for any residue that might have accumulated during the flame sterilization. Next, a single coverslip was added into each of the center 8 wells on a 24-well plate. These wells and coverslips were coated with coating media overnight at room temperature in the TC hood with 500 µL. The coverslips were gently pressed down to ensure it was completely submerged in the coating media. The next day, coating media was aspirated and washed 3× with 500 µL autoclaved water. After the last wash was aspirated, 500 µL plating media was added to each of the 8 center wells. Autoclaved water was added to the remaining 16 wells to protect against evaporation. Plates were then put into a water-jacketed incubator at 37°C at 5% CO2 before beginning dissection. 24-well plates are plated at 35,000 cells per well. Plates were then put back into a water-jacketed incubator at 37°C at 5% CO2. After 16–24 hours, plating media was aspirated and 500 µL replacement media per well was added. On DIV6 and DIV13, 250 µL of the culture media in the well was removed and 350 µL of prewarmed feeding media was added. Cells were treated on DIV18–20.

Fixing procedure for 24-well plates

After treatments are complete, cells were fixed and stained. To fix cells, the plates were removed from the incubator and checked under a light microscope and returned to the incubator. Following this, in a chemical fume hood, 16% stock paraformaldehyde (PFA, Fisher Scientific) was diluted to 4% PFA in dPBS

(1:3 dilution, 10 mL PFA into 30 mL dPBS, total volume 40 mL, 4% final concentration of PFA).[47] The solution was warmed to 37°C. The plates were then removed from incubator and into the chemical fume hood where 80% of the working volume per well (400 µL) was removed. Next, a 50% working volume of 4% PFA (250 µL) was added per well.[48] The plates were incubated at room temperature without shaking for 20 minutes. After 20 minutes, the plates were washed with 3× dPBS (500µL) and filled with dPBS (500 µL). The cells were then either immediately stained or stored at 4°C until ready to begin staining procedure (viable up to 2 weeks).

Staining for neurite outgrowth assays in 24-well plates

To stain, the dPBS was removed and the cells were permeabilized with a 0.2% Triton X-100 (Fisher Scientific) in dPBS (250 µL) solution for 20 minutes at room temperature without shaking. This 0.2% Triton X-100 solution was generated by combining 9.8 mL of dPBS and 200 µL of 10% Triton X-100. Next, a 2% bovine serum albumin (BSA, VWR) solution in dPBS was generated by dissolving 0.2g of BSA in 10 mL of dPBS.[49] Each well was blocked with 2% BSA for 1 hour at room temperature without shaking (250 µL). During the blocking, microtubule-associated protein 2 (MAP2, EnCor) chicken IgY antibody 1:10,000 was diluted into fresh 2% BSA. After 1 hour has elapsed, the blocking 2% BSA was aspirated and the 2% BSA solution containing MAP2 antibody was added (250 µL) and the plates were incubated overnight at 4°C. The next day (16–24 hours), plates were washed 3× with dPBS (500 µL) and 1× with fresh 2% BSA. A 1:500 dilution of goat anti-chicken IgY secondary antibody Alexa Fluor 488 conjugate (Life Technologies) in 2% BSA was generated. This 2% BSA solution containing the Alexa Fluor 488 was added into each well (250 µL). The plate was covered with foil and incubated at room temperature for 1 hour with gentle shaking. After 1 hour, the plates were washed 3× with dPBS (500 µL) and filled with dPBS after the last wash (500 µL). The plates were covered with foil and kept in the dark at 4°C until I was ready to image.

47. From experience, this 4% PFA solution can be freeze-thawed to up to 5 times. To avoid this, make 5 mL aliquots to freeze to prevent multiple freeze thaws. Next, I do not recommend leaving the 4% PFA in the bead bath at 37°C as PFA can polymerize and not fix your cells. Furthermore, when making the 4% PFA dilutions from 16%, use dPBS and not Neurobasal. Neurobasal contains amino acids that will crosslink with the PFA and render it inactive. Lastly, when fixing, do not exceed 25 minutes incubation and do not fix at 4°C. Fixing beyond 25 minutes will cause additional crosslinking that may occlude the epitope for your antibody. Fixing cells at 4°C causes your cells to contract and will affect the morphology of your cells. Neurites will retract as well during this. Lastly, I do recommend fixing using prewarmed 4% PFA at 37°C to avoid any retraction or contractions that may occur.
48. Neurons are extremely sensitive to changes in environment. Therefore, we retain 20% of the media to prevents the neurons from contracting and changing the morphology.
49. Do not vortex this solution, use a gentle rocking motion to mix the solution together. The vortex will denature the BSA.

Imaging and analysis for neurite outgrowth on 24-well plates.

24-well plate image acquisition was done on the Leica inverted epifluorescence microscope at 40x magnification. Images were then analyzed using the Simple Neurite Tracer and Sholl analysis plug-ins from ImageJ Fiji (version 1.51N). In brief, neurons captured on epifluorescence microscopy were traced using the Simple Neurite Tracer plug-in. The initial neurite was set to the start at the center of the soma to establish an epicenter for the Sholl analysis plug-in to build concentric circles from. Next, neurites were traced by hand and the "paths" of each trace were saved. Once fully traced, the traces were analyzed through the Sholl analysis plug-in and the data was output to Excel for further averaging between treatments. Sholl analysis circle radii = 2 μm increments. All images were taken and analyzed by an experimenter blinded to treatment conditions.

Staining for dendritic spines assays in 24-well plates

To stain, the dPBS was removed and the cells were permeabilized with a 0.2% Triton X-100 (Fisher Scientific) in dPBS (250 μL) solution for 20 minutes at room temperature without shaking. This 0.2% Triton X-100 solution was generated by combining 9.8 mL of dPBS and 200 μL of 10% Triton X-100. Next, a 2% bovine serum albumin (BSA, VWR) solution in dPBS was generated by dissolving 0.2g of BSA in 10 mL of dPBS.[49] Each well was blocked with 2% BSA for 1 hour at room temperature without shaking (250 μL). During the blocking, microtubule-associated protein 2 (MAP2, EnCor) chicken IgY antibody 1:10,000 was diluted into fresh 2% BSA. After 1 hour has elapsed, the blocking 2% BSA was aspirated and the 2% BSA solution containing MAP2 antibody was added (250 μL) and the plates were incubated overnight at 4°C. The next day (16–24 hours), plates were washed 3× with dPBS (500 μL) and 1× with fresh 2% BSA. A 1:500 dilution of goat anti-chicken IgY secondary antibody Alexa Fluor 568 conjugate (Life Technologies) in 2% BSA was generated. This 2% BSA solution containing the phalloidin conjugated to Alexa Fluor 488 (Life Technologies) and anti-chicken Alexa Fluor 568 was added into each well (250 μL). The plate was covered with foil and incubated at room temperature for 1 hour with gentle shaking. After 1 hour, the plates were washed 3× with dPBS (500 μL) and filled with dPBS after the last wash (500 μL). The plates were covered with foil and kept in the dark at 4°C until I was ready to mount.

Mounting procedures

To mount, I used ProLong Gold Antifade Mountant (Thermofisher) and added a single drop onto a microscope slide (Fisher Scientific) using a P200 micropipette. Once the ProLong Gold was dropped onto the microscope slide, the dPBS in the well was aspirated and the coverslip was removed using a pair of tweezers. The coverslip was inverted onto the coverslip. The slides were then stored at room temperature for 24 hours to allow the ProLong Gold to cure. After 24 hours, the coverslip was sealed using clear nail polish. The slides were stored in a microscope slide box and kept in the dark at 4°C until I was ready to image.

Imaging and quantification of dendritic spines

Coverslips were imaged on a Nikon N-SIM Structured Illumination Super-resolution Microscope with a 100x/NA 1.49 objective, 100 EX V-R diffraction grating, and an Andor iXon3 DU-897E EMCCD. Specifically, secondary dendrites were taken and images were recollected and reconstructed using “2D-SIM” mode (no out of focus light removal; the reconstruction used three diffraction grating angles each with three translations). Dendritic spines were counted manually by an experimenter blinded to the treatment conditions.

Transient Transfection of PsychLight1[50]

HEK293T cells were grown in **growth media** (DMEM supplemented with 10% fetal bovine serum [FBS] and 1% penicillin-streptomycin [P/S]). Cells were transfected with Effectene (Qiagen) according to the manufacturer's instructions. In brief, the day before, plates were coated in coating buffer (35 mm coverslip petri dish working volume 5 mL, 24-well plates = 2 mL, and 96-well plates = 100 µL) at room temperature in the tissue culture hood. The next day, plates were washed 3x with water (35 mm coverslip petri dish = 5 mL, 24-well plates = 1 mL, 96-well plates = 200 µL). Next, HEK293T cells around 40–80% confluency were washed 1x with prewarmed dPBS and trypsin-EDTA (0.05%) was added (T-75 flask = 500 µL of trypsin). Cells were then incubated in a 37°C, 5% CO_2 incubator for 3 minutes. Then cells were collected using 4.5 mL of **growth media**. Cells were spun down at 300G for 3 minutes. Cells are spun down and resuspended in **growth media**. Transfection done is as regular or reverse transfection[51]:

Regular transfection: HEK293T cells were plated in **growth media** (35 mm coverslip petri dish = $4.0x10^4$ cells per well; 24-well plate = $8.0x10^4$ cells per well; 96-well plate = $2.0x10^4$ cells per well) on PDL-coated plates. After 24 hours, **growth media** containing Effectene Transfection reagent was added to transfect the cells 24 hours prior to each experiment (35 mm coverslip petri dish, 0.4 µg per well of DNA; 24-well plate, 0.2 µg per well of DNA; 96-well plate, 0.1 µg per well of DNA).[50] After 6 hours of incubation, the transfection media was removed and was replaced with fresh **growth media**. The cells were allowed to grow for another 18 hours and were imaged the next day.

50. See Qiagen's Effectene Transfection Reagent Handbook. Page 9 for seeding density and page 14 DNA and volumes of other reagents from the kit (it is listed out exactly there for each plate size). For regular transfection, use the highest concentration of cells as recommended on page 9. If doing reverse transfection, use double the amount of the highest concentration of cells as recommended on page 9 based on what size plate you are using.

51. **Regular transfection (traditional)**: The cells are first plated and allowed to adhere. Once the cells adhere, transfection is conducted the following day. The procedure typically takes 48 hours. Forward transfection has some variability in delivery of DNA depending on pipettor used to each well.
Reverse transfection: The cells are transfected in the culture tube and plated all together. Once the cells adhere, media is exchanged for fresh growth media. The procedure typically takes 24 hours (saves a day). Because reverse transfection requires cells to be mixed with the transfection reagent and DNA prior to plating, the cells will generally be exposed to the same amount of DNA and have a more uniform expression of the protein of interest.

Reverse transfection: HEK293T cells had Effectene Transfection reagent mixed with the cells in **growth media** and plated at the appropriate densities (35 mm coverslip petri dish = $8.0x10^4$ cells per well with 0.8 µg per well of DNA; 24-well plate = $1.6x10^5$ cells per well with 0.4 µg per well of DNA; 96-well plate = $4.0x10^4$ cells per well with 0.2 µg per well of DNA)[52] on PDL-coated plates. After 6 hours later, transfection media was removed, and fresh **growth media** was added to each well. The cells were allowed to grow for another 18 hours and were imaged the following day.

Prior to imaging, cells were washed with Hank's Balanced Salt Solution (HBSS) supplemented with 2 mM $MgCl_2$ and 2 mM $CaCl_2$. All images were collected in HBSS containing Mg^{2+} and Ca^{2+} at ambient conditions.

Confocal Microscopy Experiments

Dose-response experiments were performed using an Automate Perfusion System. HEK293T cells were grown on 12 mm coverslips and transfected with psychLight1. The coverslips were then placed into a coverslip holder and washed with 5 mL of HBSS containing 2 mM $MgCl_2$ and 2 mM $CaCl_2$. Cells were perfused first with 5 mL of 0.1% DMSO, then drugs in ascending concentrations from 1 pM to 10 µM were added, with the concentration of DMSO being held constant at 0.1%. Images were recorded using a 465 nm laser and a 40x oil objection (0.55 N.A.) on a Zeiss 710 confocal microscope. Analysis was performed by taking 3 ROIs on the cell membrane using ImageJ (ver. 1.51J) and calculating the mean intensity for each ROI across the time-points. Finally, the ΔF/F was calculated using the average of the baseline (0.1% DMSO) and the average intensity between each dosage over the average of the baseline.

For the competition studies described in **Fig. 4.3D**, HEK293T cells were prepared as described above; however, the cells were first exposed to 5 mL of 0.2% DMSO. Next, 100 nM 5-HT in 0.2% DMSO was introduced to the cells followed by ascending concentrations of the drug (from 1 pM to 10 µM) in a solution of 100 nM 5-HT, with the concentration of DMSO kept constant at 0.2%. Analysis was performed by taking 3 ROIs on the cell membrane using ImageJ and calculating the mean intensity for each ROI

52. The cell density was doubled because regular transfection allows the cells to double overnight before conducting the transfection. Reverse transfection does not have the additional 24 hours of cell growth prior to transfection and so we double up the number of cells to accommodate for that.

across the time-points. Finally, the ΔF/F was calculated using the average of the baseline (0.2% DMSO) and the average intensity between each dosage over the average of the baseline.

Chapter 4.7.4 Experimental Section for Chapter 4.3

Head-twitch Response with Fiber Photometry

Three animals were used for experiments measuring sensor activity in the prelimbic cortex. A 10-minute baseline was recorded prior to compound administration (50 mg/kg 5-MeO and 4 mg/kg KETSN, i.p.) in a 5 mL/kg volume using 0.9% saline as the vehicle. To calculate the ΔF/F time series, a linear fit was applied to the 405 nm signals and aligned to the 465 nm signals. The fitted 405 nm signal was subtracted from 465 nm channels, and then divided by the fitted 405 nm signal to yield ΔF/F values. The number of head twitches were counted in 1-minute intervals by 2 observers blinded to the treatment conditions and the results were averaged (Pearson's correlation coefficient between 2 observers = 0.96).

High-Content Imaging Experiments

Glass bottom 96-well plates (P96-1.5H-N, Cellvis)[53] were coated with 50 µg/mL of poly-D-lysine (Sigma, P6407-5MG) and 10 µg/mL of laminin (Sigma, L2020) overnight in an incubator (37°C, 5% CO_2).[54] Plates were washed with Dulbecco's PBS (dPBS, ThermoFisher, 14190-250) and PSYLI2 cells[55] were suspended in DMEM (Fisher, 11995073) containing 10% FBS (Fisher, 26-140-079) with 5% P/S (Fisher, 15140-163) and plated at a density of 40,000 cells/well 24 hours prior to each experiment. Stock solutions of drugs in DMSO (10 mM) were diluted 1:100 in imaging media distributed across an empty 96-well plate (treatment plate) in triplicate following a randomized plate map. Once the treatment plate was generated, 200 µL of warmed (37°C) imaging media consisting of 1X HBSS (Fisher, 14175103) containing 0.5 M $MgCl_2$ (Sigma, M8266-1KG) and 0.5 M $CaCl_2$ (Sigma, C5670-50G) was used to wash cells grown in a separate

53. Currently, we have conducted experiments comparing plastic bottom and glass bottom 96-well plates as a means to cut costs. However, plastic bottom plates generally have additional background fluorescence. This background fluorescence can be brighter than the signal from the PSYLI2 cells and therefore, is recommended to go with glass-bottom plates as to have as little background noise as possible. This is especially true because the majority of the signal comes from the cell membrane and the intracellular portion of the cell is generally has no fluorescence.

54. The laminin procedure was only used in the Tian lab. In brief, laminin and PDL were dissolved in dPBS and sterile filtered prior to use. Now when we conduct this experiment, we do not include laminin anymore in our coating buffer. We no longer use it because there is no difference between PDL coating alone or with laminin. Therefore, we now conduct overnight incubations at room temperature in the back of the TC hood. Furthermore, we now use autoclaved water to wash the plates rather than dPBS now. There was no significant difference was found between dPBS wash versus autoclaved water wash.

55. One T-75 flask (ThermoFisher) of PSYLI2 cells on average yields roughly 12 million cells when at 90%–100% confluency. This single T-75 flask yields four full 96-well plates and residual cells to continue passage to maintain the cell line.

96-well plate (assay plate) 3×.[56] Wells were filled with an appropriate volume of imaging media for the respective experiment (*vide infra*).

Agonist Mode

For agonist mode experiments, 180 µL of imaging media were added to each well of the assay plate. Wells were then imaged on a Lecia DMi8 using Leica Application Suite X (V3.6.0.20104) at 40x (N.A. = 0.6) with 5 regions of interest (ROI) taken per well using the default 5 ROI pattern for each well with no bias to location and no overlap of the ROIs (exposure = 350 ms, LED power = 80%). Next, 20 µL from the treatment plate was transferred to the assay plate containing a 1:1000 dilution of drug (10 µM as the final concentration in 0.1% DMSO). As positive, negative, and neutral controls, 5-HT (10 µM), ketanserin (10 µM), and DMSO (0.1%) were used, respectively. All final concentrations of drugs were 10 µM (0.1% DMSO) in agonist mode unless stated otherwise. After 5 minutes of incubation, the same sites were re-imaged using the same settings.

Once imaging was complete,[57] the images were exported, and analyzed using a MATLAB script written by Chunyang Dong. See below for MATLAB script. In short, segmentation was performed on individual images and a mask highlighting the membrane of the HEK293T cells was generated. Pixel intensities were obtained from the mask-highlighted area and exported into Excel. The ΔF/F values for each well were calculated using the following equation:

$$\frac{(average\ after\ drug - average\ before\ drug)}{average\ before\ drug\ (baseline)}$$

These values were then used to obtain the triplicate mean (N = 3).

Antagonist Mode

For antagonist mode experiments, 160 µL of imaging media was added to each well of the assay plate. Wells were imaged on a Lecia DMi8 using Leica Application Suite X (V3.6.0.20104) at 40x (N.A. =

56. It is critical that washing is completed very gently. PSYLI2 (and HEK293T) cells lift off glass bottom plates very easily. When I conducted washes, I manually aspirated using a multichannel pipette and was very gentle in the addition of imaging media for the washes.
57. The PSYLI2 cells are robust and can survive perfectly fine in imaging buffer at room temperature and ambient conditions for up to 2 hours.

0.6) with 5 regions of interest (ROI) taken per well using the default 5 ROI pattern for each well with no bias to location and no overlap of the ROIs (exposure = 350 ms, LED power = 80%). A 100 µM 5-HT stock solution in DMSO was diluted 1:100 in imaging buffer. Next, 20 µL of this solution was added to the assay plate for a final concentration of 111 nM 5-HT (0.1% DMSO). The same 5 ROIs were imaged after 5 min of incubation. Next, 20 µL from the treatment plate was transferred to the assay plate for a final 1:1000 dilution of drug (10 µM drug, 100 nM 5-HT, 0.2% DMSO). All final concentrations of drugs were 10 µM with 100 nM 5-HT (0.2% DMSO) in antagonist mode unless stated otherwise. After 5 minutes of incubation, the same sites were re-imaged using the same settings.

Once imaging was complete, the images were exported, and analyzed using the same MATLAB script. See below for MATLAB script. In short, segmentation was performed on individual images and a mask highlighting the membrane of the HEK293T cells was generated. Pixel intensities were obtained from the mask highlighted area and exported into Excel. Then the ΔF/F values for each well were calculated using the following equation:

$$\frac{(average\ after\ drug - average\ before\ 5HT\ )}{average\ before\ 5HT\ (baseline)}$$

These values were then used to obtain the triplicate average (N = 3). All imaging and incubation (both agonist and antagonist mode) were performed at ambient atmosphere and temperature.

MATLAB script (ver. 2020b):[58]

```
%This script uses the Canny method for edge detection. Put all your images
%in one folder. Images must be in .tif file format. Please name images by
%their well number


clear all
%Opens up a dialogue box to choose files
[file, path] = uigetfile('*.tif', 'Select All Image Files', 'MultiSelect','on');
%Adjust fudge factor so threshold for edge detection is more or less strict
```

58. This script is specifically for Windows. For Macs, check the Github site here (https://github.com/lintianlab/psychLight) for the Mac version (Chunyang Dong wrote the original script on a Mac and thus the unconverted version is there for Macs). I do not know whether this script works on any other version of MATLAB besides **ver. 2020b**.

```
fudgeFactor = 1.5;
conn = 8;
%Index each file and obtain mask of image
for i = 1:numel(file)
    img(:,:,:,i) = imread(fullfile(path,file{i}));
    [~, threshold] = edge(img(:,:,i), 'Canny');
    BW(:,:,i) = edge(img(:,:,i), 'Canny',threshold*fudgeFactor);
    %Dilate image
    se90 = strel('line',5, 90);
    se0 = strel('line', 5, 0);
    BWsdil(:,:,i) = imdilate(BW(:,:,i), [se90 se0]);
    %Remove small objects
    BWC(:,:,i) = bwareaopen(BWsdil(:,:,i), 300);
   %To view the binary mask and corresponding original image use
   %imshowpair(BW(:,:n),img(:,:,n), 'montage') where n is the index of the
   %image you want to view. To view final mask replace BW with BWC.

   %Quantify the intensity values in the masked area
   test = BWC(:,:,i);
   y = test;
   zed = img(:,:,i);
   gamma = img(:,:,i);
   z = zed;
   z(y == 0) = 0;
   % set temp to all values in ROI that aren't zero (not part of the mask)
   temp = z(z~=0);
   %Calculate intensity of regions in the mask: https://www.mathworks.com/help/images/measuring-
regions-in-grayscale-images.html
```

```
  mean_intensity(:,i) = mean(temp);
  median_intensity(:,i) = median(temp);
  total_intensity(:,i) = sum(temp);
  %Calculate the ROI area
  ROIarea(:,i) = sum(sum(gamma.*z));

end
mean_intensity = mean_intensity';
median_intensity = median_intensity';
total_intensity = total_intensity';
ROIarea = ROIarea';
File = file';
%Export data to excel or txt file
T = table(File, mean_intensity, median_intensity, total_intensity, ROIarea);
s = path;
%Remove special characters or file will not save properly
s = strrep(s, ' ', '_');
s = strrep(s, ':', '_');
s = strrep(s, '\', '_');
disp(s);
filename = string([s, '.xls']);
disp(filename);
%Saves table to excel file where s is the file name
writetable(T, filename);
%s(~isstrprop(s,':\')) = '';
```

Calculation of the Ligand Score

Compounds unlikely to bind to the sensor should produce minimal to no response in either agonist or antagonist mode. Therefore, a ligand score was calculated as:

$$(\Delta F/F)_{\text{Compound Agonist Mode}} - [(\Delta F/F)_{\text{VEH Antagonist Mode}} - (\Delta F/F)_{\text{Compound Antagonist Mode}}]$$

The black heatmap value indicating no effect was set to the value calculated for the vehicle control (i.e., -4.2). The maximal red and blue values were set to those calculated for a prototypical agonist (i.e., LSD, Ligand Score = 21) and antagonist (i.e., MDL100907, Ligand Score = -58), respectively.

Schild Regression Analysis

A treatment plate was prepared by pre-mixing various concentrations of a non-hallucinogenic compound with increasing concentrations of 5-HT 10-fold above the final concentration. During imaging, 180 µL of imaging media were added to each well of the assay plate. Wells were then imaged on a Lecia DMi8 using Leica Application Suite X (V3.6.0.20104) at 40x (N.A. = 0.6) with 5 regions of interest (ROI) taken per well using the default 5 ROI pattern for each well with no bias to location and no overlap of the ROIs (exposure = 350 ms, LED power = 80%). Next, 20 µL from the treatment plate was transferred to the assay plate for a final 1:1000 dilution of drug. All final drug treatments contained 0.1% DMSO. After 5 min of incubation, the same sites were re-imaged using the same settings. The data analysis method was the same as in agonist and antagonist mode.

Fluorescence Plate Reader

A 96-well plate (UV transparent) was prepared with 100mL of increasing concentration of BOL-148 and bromocriptine from 10^{-12} to10^{-5} M together with vehicle control. The plate was read by Tecan Microplate Reader Sparkâ with excitation wavelength 465 nm (bandwidth 20 nm), emission wavelength 518 nm (bandwidth 20 nm), gain of 120, 5 ROI per well, total 30 flashes per well, and read at z-position 30000 mm from bottom of the plate. All settings controlled by Spark Control software, V2.3.

Chapter 4.7.5 Experimental Section for Chapter 4.4

For the dendritogenesis conducted using cultured E18 cortical neurons, timed-pregnant Sprague Dawley rats were obtained from Charles River Laboratories (Wilmington, MA). For full culturing details, see above in **Chapter 4.7.1.**

General neurite outgrowth cell culturing in 96-well plates

For **Figures 2.4A–B, 2.5D,** and **2.12B–I**, neurite outgrowth assay was conducted in a medium-throughput assay using black 96-well plastic bottom plates (Corning) using the center 60 wells. 96-well plates were coated with 100 µL of coating media overnight at room temperature. The next day, plates were washed 3× with 200 µL autoclaved water. After the last wash, 200 µL of Neurobasal was added to each of the center 60 wells and autoclaved water was added to the remaining outer wells to reduce evaporation. The plates were placed into a 37°C and 5% CO2 water-jacketed incubator prior to dissection. After dissection (see Tissue Collection above), the Neurobasal was aspirated and 200 µL of a 75,000 cell per mL diluted in plating media (final cell density of 15,000 cells per well) and returned to the incubator. After 16–24 hours, plating media was aspirated and 200 µL of prewarmed replacement media was added to each well. Cells were ready to treat at DIV3.

Fixing procedure for 96-well plates

After treatments are complete, cells were fixed and stained. To fix cells, the plates were removed from the incubator and checked under a light microscope and returned to the incubator. Following this, in a chemical fume hood, 16% stock paraformaldehyde (PFA, Fisher Scientific) was diluted to 4% PFA in dPBS (1:3 dilution, 10 mL PFA into 30 mL dPBS, total volume 40 mL, 4% final concentration of PFA). The solution was warmed to 37°C. The plates were then removed from incubator and into the chemical fume hood where 80% of the working volume per well (160 µL) was removed. Next, a 50% working volume of 4% PFA (100 µL) was added per well. The plates were incubated at room temperature without shaking for 20 minutes. After 20 minutes, the plates were washed with 3× dPBS (200 µL) and filled with dPBS (200 µL). The cells

were then either immediately stained or stored at 4°C until ready to begin staining procedure (viable up to 2 weeks).

Imaging and analysis for neurite outgrowth on 96-well plates.

96-well plate image acquisition was done on the Molecular Devices ImageXpress Micro XLS Widefield High-Content Analysis System at 9 sites per well using 20x magnification. Images were analyzed using the Sholl analysis plug-in ImageJ Fiji (version 1.51N). First, 0–2 representative neurons were selected per site using the "rectangle" function.[59] Once neurons were selected, a copy of the selected neuron would be generated using the "duplicate" function. After selecting all the neurons for that treatment group, duplicated copies were saved. Once all groups were completed, I was unblinded to VEH and KET plate controls[60] on the plate and adjusted "brightness and contrast" that was used for the rest of the plate.[61] Next, these "brightness and contrast" "maximum" and "minimum" values were recorded and applied to the images within the same plate. The images then were converted to a binary image using the "threshold" function. From there, the "minimum" and "maximum" values of the threshold were adjusted obtain the best binary image that represented the respective fluorescent image. These values were recorded. All "brightness and contrast" and "threshold" were kept the same between all images from the same plate. Finally, images were cleaned using the "paint brush" tool for artifacts in the image, and the center of the neuron was then dotted using the "point" function. Images were saved and ran through the "batch process macro" on ImageJ Fiji using the following script:

59. This part is very subjective and can take a couple of attempts in order to get used to what is a representative neuron. We select neurons that are not overlapping with other neurons in the field of view (FOV). We search for pyramidal-like neurons and avoid bipolar neurons (neurons that only have two neurites growing on opposite sides of one another). Furthermore, I look at the FOV as a whole to determine the average neurite per soma and select the best representative(s) in that FOV. If the FOV has a very sparse number of neurons (generally less than 10 per FOV), I will opt to skip that FOV as the small sample size can skewer the results. Neurons that are alone generally have longer neurites and less branching, neurons that are clustered together will have more branching and shorter neurites. Finding a neuron that is far enough away from each other while still having neighbors nearby for neurotrophic support will offer the best representative neuron.
This publication for examples:
Dunlap, L. E.; Azinfar, A.; Ly, C.; Cameron, L. P.; Viswanathan, J.; Tombari, R. J.; Myers-Turnbull, D.; Taylor, J. C.; Grodzki, A. C.; Lein, P. J.; Kokel, D.; Olson, D. E. Identification of Psychoplastogenic N,N-Dimethylaminoisotryptamine (isoDMT) Analogs Through Structure-Activity Relationship Studies. *J. Med. Chem.*, **2020**, *63*, 1142–1155.
60. The ketamine (positive control) and vehicle (negative control) here are plate controls that are not used for publication. I use these as quality controls for my plates to ensure that the experiment worked and confirm the data obtained is robust. The edge wells (columns 2 and 11, 6 wells total per condition) are used as controls because these wells have the largest potential for variability due to plate effects and evaporation of media. I rotate ketamine and vehicle between the columns to prevent any bias during selection of neurons.
61. This is critical as ketamine and other psychoplastogens will cause very thin, dim, small neurites to grow that can be missed if image brightness and contrast are not adjusted.

run("Sholl Analysis...", "starting=0 ending=NaN radius_step=2 #_samples=1 integration=Mean enclosing=1 #_primary=4 infer fit linear polynomial=[Best fitting degree] most semi-log normalizer=Area create background=228 save do");

Sholl analysis circle radii = 2-pixel increments. All analysis was done by blinded to treatment conditions except for VEH and KET plate controls.

Forced Swim Test (FST)

Male and female C57BL/6J mice (9–10 weeks old at time of experiment, n = 6 of each sex per condition) were obtained from The Jackson Laboratory and housed 4–5 mice of the same sex/cage in a UCD vivarium following an IACUC approved protocol. After 1 week in the vivarium, each mouse was handled for approximately 1 minute by a male experimenter for 3 consecutive days prior to the first FST. All experiments were conducted by the same male experimenter who performed the initial handling. During the FST, mice underwent a 6-minute swim session in a clear Plexiglas cylinder (40 cm tall, 20 cm in diameter) filled with 30 cm of 24 ± 1ºC water. Fresh water was used for every mouse. After handling and habituation to the experimenter, drug-naïve mice first underwent a pretest swim to induce a depressive-like phenotype more reliably in subsequent FST sessions. Immobility scores for all mice were determined after the pre-test and mice were assigned to treatment groups to generate groups with similar mean immobility scores used in the following two FST sessions. The next day, the animals received injections (i.p.) of AAZ (20 mg/kg), ketamine (3 mg/kg) as the positive control, or vehicle (saline). After 30 minutes, the animals were subjected to the FST, dried with a towel, and then returned to their home cages. One week later, the FST was performed to assess the sustained effects of the drugs. All FSTs were performed between the hours of 0800 and 1300 hour. The experiments were divided into two cohorts either of all males or females and conducted on different days. Experiments were video-recorded and manually scored offline by an experimenter blinded to treatment conditions. Immobility time—defined as passive floating or remaining motionless with no activity other than that needed to keep the mouse's head above water—was scored for the last 4 minutes of the 6 minutes trial.

Head-Twitch Response (HTR) and Locomotion Assays

The HTR assay was performed as described previously[12a] using both male and female C57BL/6J mice (2 male and 2 female = 4 total per treatment). The mice were obtained from The Jackson Laboratory (Sacramento, C.A.) and were approximately 8-weeks old at the time of the experiments. Compounds were administered (5 mL/kg, i.p.) using 0.9% saline as the vehicle. After injection, animals were placed into an empty cage (8" x 13" x 5") and HTRs were videotaped, scored later by two blinded observers, and the results were averaged (interpersonnel kappas, Pearson correlation coefficient > 0.91). Locomotion was assessed using AnyMaze automated tracking software.

Sucrose Preference

Adult male and female wild-type (WT) and VMAT2 heterozygous (VMAT2-HET) mice were used for these experiments,[62] and they were housed in a humidity- and temperature-controlled room on a 14:10 hour light:dark cycle. Mice were housed individually 48 hours prior to the experiment with *ad libitum* access to chow and water. For each day's experiment, bottles were prepared with water or a 1% sucrose solution and these were weighed just prior to the test. Two hours prior to the beginning of the dark cycle, the home-cage water bottle was removed. One hour after onset of the dark cycle, a pair of bottles was placed into the home-cage. The mouse was given 2 hours to drink, after which the bottles were removed and weighed immediately. Approximately 1-hour later, the home-cage water bottle was returned. This procedure was repeated daily with the water-water (W-W) pairing until the mouse showed stable drinking volumes over 3 consecutive days without any side-bias. Once criterion was achieved, the mouse was presented with the water-sucrose (W-S) pairing. The next day (day 1), mice were administered an acute injection of AAZ (15 mg/kg, i.p.) and 5 minutes later were given the W-S pairing (i.e., day 1). Subsequent W-S pairings were presented on days 2 and 4, and then at 4-day intervals. Preference for the sucrose bottle was calculated as the volume of sucrose consumed minus the volume of water consumed, divided by the total volume of liquid consumed. Preference scores approaching "0" indicated no preference for sucrose or water, whereas positive scores signified a preference for sucrose and negative scores denoted a preference for water.

62. Fukui, M.; Rodriguiz, R.M.; Zhou, J.; Jiang, S.X.; Phillips, L.E.; Caron, M.G.; Wetsel, W.C. Vmat2 heterozygous mutant mice display a depressive-like phenotype. *J Neurosci*. **2007**, *27,* 10520–10529.